

817439
2
1007



This is to certify that the
thesis entitled

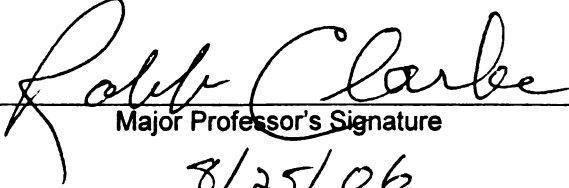
**THE INFLUENCE OF WATER CONTENT IN
HYDRATED SUPERABSORBENT POLYMER ON
DIELECTRIC PROPERTIES, ANTENNA RADIATED
POWER, AND RFID TAG READABILITY**

presented by

Xuebing Zhang

has been accepted towards fulfillment
of the requirements for the

M.S. degree in Packaging


Major Professor's Signature

8/25/06
Date

PLACE IN RETURN BOX to remove this checkout from your record.
TO AVOID FINES return on or before date due.
MAY BE RECALLED with earlier due date if requested.

DATE DUE	DATE DUE	DATE DUE

**THE INFLUENCE OF WATER CONTENT IN HYDRATED
SUPERABSORBENT POLYMER ON DIELECTRIC PROPERTIES, ANTENNA
RADIATED POWER, AND RFID TAG READABILITY**

By

Xuebing Zhang

A THESIS

Submitted to
Michigan State University
in partial fulfillment of the requirements
for the degree of

MASTER OF SCIENCE

School of Packaging

2006

ABSTRACT

THE INFLUENCE OF WATER CONTENT IN HYDRATED SUPERABSORBENT POLYMER ON DIELECTRIC PROPERTIES, ANTENNA RADIATED POWER AND RFID TAG READABILITY

By Xuebing Zhang

The performance and stability of RFID systems in a supply chain relies on the readability of passive RFID transponders. This thesis presents research on correlation and influence of readability on passive RFID transponders and water content in products simulated by hydrated superabsorbent polymer (SAP).

High water absorbable SAP provided a wide range of simulation options, from 45% to 95% water. The dielectric property in terms of permittivity of the hydrated SAP samples was characterized and differentiated by S-parameter measurement using a HP8510C network analyzer with a WR340 waveguide. Moreover, radiated power measurement and a readability survey using Alien® 915 MHz squiggle RFID tags with the same SAP specimens were performed with an R&S® NRP-Z22 power sensor with LabVIEW® program and Alien® RFID Gateway software.

The research results showed that the weight percent of water content in saturated SAP affected permittivity. The dielectric constant, $\text{Re}(\epsilon_r)$ and water content have a nearly linear relationship. The loss factor, $\text{Im}(\epsilon_r)$ showed complicated fluctuations and sudden declines in some frequency ranges. High water concentration in the SAP mixtures indicated high power loss and low readability. More than 75% water content in the samples usually attained near 0% readability. Reader antenna style, position and transponder orientation showed different influence on readability and power loss with the same saturated samples. This research shows that product content and packaging operations are challenges to successful implementation of RFID system in supply chain.

t
a
I
t
T
re
T
su
Es
My
ext
in r

ACKNOWLEDGEMENTS

I am indebted to Dr Robert Clarke, my major advisor and committee chair, for all his guidance and support during the thesis preparation and all throughout my masters program in the School of Packaging, MSU. Dr Clarke has generously given his time to discuss with me and to provide his knowledge and patience, which have been invaluable to this research and my life.

I would like to thank Dr. Leo Kempel and Dr. Ed Rothwell for their contribution at material characterization in this research as well. Without their participation and guidance, all measurements of material characterization are impossible.

I would like to thank Mr. Andrew Eric Bogle and Mr. Steve Cossmann, who contributed their time, experience, work and patient and cooperation in this research.

Thanks to Dr. Bruce Harte as a committer member providing advices and guiding for this research and preparation of the thesis.

Thanks to Mr. Bill Lindsay at Grain Processing Corporation who provided superabsorbent polymer for this research.

Especially, I want to thank my son Yifan Andrew Zhang, My parents Zhongde, Huinong, My brother Xuefei, their love and support is always the source of power which I am get exhausted. In addition, I would like to thank to Dr. Weijuan Ni, who provided many help in my master program.



TABLE OF CONTENTS

LIST OF TABLES	VIII
LIST OF FIGURES	IX
KEY TO ABBREVIATIONS.....	XV
LIST OF PRINCIPAL LETTER SYMBOLS.....	XVIII
CHAPTER 1 INTRODUCTION.....	1
1.1 OVERVIEW	1
1.2 RFID PUZZLES.....	2
1.3 RESEARCH ASPECTS	3
1.4 RESEARCH GOALS	4
1.5 THESIS SUMMARY.....	5
CHAPTER 2 LITERATURE REVIEW.....	6
2.1 AUTOMATIC IDENTIFICATION TECHNOLOGIES	6
2.2 BRIEFLY HISTORY OF RFID.....	6
2.3 RFID SYSTEM COMPONENTS.....	7
2.3.1 <i>Transponder</i>	7
2.3.2 <i>Interrogator</i>	9
2.3.3 <i>Computer and Backbone Software</i>	10
2.4 BASIC PRINCIPLES.....	10
2.4.1 <i>Frequency Allocation</i>	10
2.4.2 <i>Near Field and Far Field</i>	11
2.4.3 <i>Read Range and Power Assumption</i>	13
2.4.4 <i>Modulation</i>	14
2.5 ELECTROMAGNETIC PROPERTIES	15
2.5.1 <i>Dipole Moment and Molecular Polarity</i>	15
2.5.2 <i>Dielectric Permittivity</i>	16
2.5.3 <i>Loss Tangent</i>	18
2.5.4 <i>Dielectric Absorption</i>	18
2.6 WATER CONTENT IN FOODS.....	19
2.6.1 <i>Water Activity</i>	19

2.6.2	<i>Water Forms</i>	20
2.6.3	<i>Dielectric Properties</i>	21
2.6.4	<i>Gel Structure and Food Biopolymers</i>	22
2.7	SUPERABSORBENT POLYMER	23
2.7.1	<i>History of Superabsorbent</i>	23
2.7.2	<i>Structure and Properties</i>	24
2.7.3	<i>Mechanism of Water Absorption</i>	25
2.8	PREVIOUS RESEARCH	25
2.8.1	<i>RFID Application</i>	25
2.8.2	<i>Material Characterization</i>	27
2.8.3	<i>Material</i>	27
2.9	RELEVANCY	27
	CHAPTER 3 METHODOLOGY	29
3.1	INTRODUCTION	29
3.2	PRODUCT SIMULATION	31
3.3	MEASUREMENT DESCRIPTION	32
3.4	SUPERABSORBENT SPECIFICATIONS	33
3.5	SPECIMEN PREPARATION	33
3.6	DETERMINATION OF WATER CONTENT	34
3.7	S-PARAMETER MEASUREMENT	35
3.8	POWER MEASUREMENT	36
3.9	READABILITY SURVEY	36
	CHAPTER 4 MATERIAL CHARACTERIZATION	38
4.1	MATERIAL CHARACTERIZATION	38
4.2	MEASUREMENT EQUIPMENT	39
4.2.1	<i>Vector Network Analyzer</i>	39
4.2.2	<i>Waveguide</i>	39
4.3	EXPERIMENTAL SETUP	40
4.4	CALIBRATION PROCESSING	41
4.5	MEASUREMENT CALIBRATION	42
4.6	CALIBRATION OF NETWORK ANALYZER	43
4.6.1	<i>One-path 2-Port Calibration</i>	43
4.6.2	<i>Full 2-port and TRL Calibrations</i>	44
4.6.3	<i>Full 2-Port Calibration</i>	44
4.6.4	<i>TRL Calibration</i>	44
4.6.5	<i>TRL Calibration Procedure</i>	45

4.7 S-PARAMETERS MEASUREMENT PROCEDURE	46
4.8 VALIDATION OF MEASUREMENTS	47
4.9 EXTRACTION PROCESS	48
CHAPTER 5 POWER MEASUREMENT AND READABILITY SURVEY	51
5.1 INTRODUCTION	51
5.2 EXPERIMENTAL EQUIPMENT	52
5.2.1 Power Sensor	52
5.2.2 Calibration	53
5.2.3 2-Wire Folded Dipole Antenna	55
5.2.4 RFID Equipment	55
5.2.5 Virtual Power Meter Configuration	56
5.2.6 LabVIEW Programming	57
5.3 RECEIVING ANTENNA PLACEMENT	58
5.4 ALUMINUM SHIELDING	59
5.5 MEASUREMENT DEVIATION	60
5.6 POWER MEASUREMENT PROCEDURE	63
5.7 READABILITY SURVEY	64
5.8 ANTENNA ORIENTATION	65
CHAPTER 6 RESULTS AND DISCUSSION	67
6.1 S-PARAMETERS	67
6.2 VALIDATION	80
6.3 PERMITTIVITY	85
6.4 LOSS FACTOR	93
6.5 LOSS TANGENT	95
6.6 POWER MEASUREMENT	99
6.6.1 Antenna Style	100
6.6.2 Shielding	102
6.6.3 Circular Antenna	103
6.6.4 Linear Antenna	106
6.7 CRITICAL POWER	108
6.8 READABILITY SURVEY	109
6.8.1 Readability Decaying Model in Open-air	109
6.8.2 Tag Orientation	110
6.8.3 Water Content	111

CHAPTER 7 CONCLUSIONS	116
7.1 MATERIAL CHARACTERIZATION	116
7.2 RECEIVED RADIATED POWER	117
7.3 READABILITY	117
7.4 LIMITATIONS OF THIS RESEARCH.....	118
7.5 FUTURE RESEARCH	119
7.6 SUMMARY CONCLUSION	120
APPENDIX A S-PARAMETERS IN SATURATED SAP (90%)	122
APPENDIX B EXPERIMENTAL PERMITTIVITY AND PERMEABILITY	125
APPENDIX C GLOSSARY	126
REFERENCES	128

Tabl

Tab

Tab
and

Tab

Tab

Tab

Tab

Tab

Tab

LIST OF TABLES

Table 2.1 EPC tags classes.....	9
Table 2.2 Near field and far field regions.....	12
Table 2.3 Dielectric properties of foodstuffs and other packaging materials at 2.45GHz and 68°F	22
Table 4.1 WR340 waveguide characteristics.....	40
Table 5.1 Power measurement range	53
Table 5.2 Descriptive statistics of measurement deviation.....	61
Table 6.1 Correlations of water concentration and sample relative permittivity.....	90
Table 6.2 Average shielding power loss (dB).....	102
Table 6.3 Half decaying rate of readability and least power in free space	108

LIST OF FIGURES

Figure 2.1 UHF 915 MHz RFID transponder, reader, and antenna.....	8
Figure 2.2 RFID signal propagation and backscattering	9
Figure 2.3 Attenuation of magnetic strength vs. distance in near field region	11
Figure 2.4 FSK and PSK digital signal modulation.....	15
Figure 2.5 Orientation of atoms and direction of the electric dipole relative in H ₂ O.....	16
Figure 2.6 Complex permittivity and loss tangent	18
Figure 2.7 Hydrated superabsorbent polymer sample, with more than ten times of its weight of water absorbed by the SAP particles	23
Figure 2.8 Crosslinking structure in a superabsorbent polymer	24
Figure 3.1 Dimension of 2-wire folded dipole antenna	30
Figure 3.2 Hydrated SAP mixtures in the sample window.....	32
Figure 4.1 HP-8510C Network Analyzer and panel block	39
Figure 4.2 WR340 waveguide components and cross section	40
Figure 4.3 VNA and WR340 waveguide set-up	42
Figure 4.4 Waveguide sample holder	43
Figure 4.5 WR340 standard calibration line section.....	45
Figure 4.6 SAP specimens in the wrap.....	46
Figure 4.7 Transmission and reflection of signals: side view of waveguide with specimen layer.....	47

Figure 4.8 FORTRAN extractor: input the initial values and extract permittivity and permeability	48
Figure 5.1 Default data acquisition interface for power sensor	52
Figure 5.2 Average power measurement	54
Figure 5.3 Two-wire folded half-wavelength dipole antenna of power sensor	55
Figure 5.4 Alien Squiggle ALL-9338 RFID tag	56
Figure 5.5 Program interface of virtual power meter for R&S® NRP-Z22 power sensor	57
Figure 5.6 LabVIEW diagram of virtual power meter	58
Figure 5.7 Experimental setup of power measurement and readability survey	59
Figure 5.8 Periodical fluctuation of discrete average power reading	60
Figure 5.9 Stable average power in measurement	61
Figure 5.10 Continuous decline or incline deviation in power measurement.....	62
Figure 5.11 Undulation in power measurement.....	62
Figure 5.12 Comparison of measurement accuracy.....	63
Figure 5.13 Hydrated SAP specimen, dipole antenna connected with power meter and reader antenna in the other side of sample window	64
Figure 5.14 Power sensor and receiving antenna in one side, mobile reader antenna in the other side.....	65
Figure 5.15 Alien RFID Gateway for readability survey	65
Figure 5.16 Polarization losses in a linear reader antenna.....	66
Figure 6.1 The diagram of incident waves (a1, a2), reflected waves (b1, b2) and S-parameters in a typical two-port network	68

I
F
F
F
Fi
Fig
Fig
Fig
Fig
Fig
Fig
Figure
Figure

Figure 6.2 Comparison of S11 in SAP specimen with 70% water content	70
Figure 6.3 Comparison of S22 in SAP specimen with 55% water content	70
Figure 6.4 Comparison of S21 in SAP specimen with 80% water content	71
Figure 6.5 Comparison of S12 in SAP specimen with 60% water content	72
Figure 6.6 Comparison of experimental S11 (real) in SAP mixtures (12 mm)	72
Figure 6.7 Comparison of experimental S11 (real) in SAP mixtures (7 mm)	73
Figure 6.8 Comparison of experimental S11 (img) in SAP mixtures (12 mm)	73
Figure 6.9 Comparison of experimental S11 (img) in SAP mixtures (7 mm)	74
Figure 6.10 Comparison of experimental S22 (real) in SAP mixtures (12 mm)	74
Figure 6.11 Comparison of experimental S22 (real) in SAP mixtures (7 mm)	75
Figure 6.12 Comparison of experimental S22 (img) in SAP mixtures (12 mm)	75
Figure 6.13 Comparison of experimental S22 (img) in SAP mixtures (7 mm)	76
Figure 6.14 Comparison of experimental S12 (real) in SAP mixtures (12 mm)	76
Figure 6.15 Comparison of experimental S12 (real) in SAP mixtures (7 mm)	77
Figure 6.16 Comparison of experimental S12 (img) in SAP mixtures (12 mm)	77
Figure 6.17 Comparison of experimental S12 (img) in SAP mixtures (7 mm)	78
Figure 6.18 Comparison of experimental S21 (real) in SAP mixtures (12 mm)	78
Figure 6.19 Comparison of experimental S21 (real) in SAP mixtures (7 mm)	79
Figure 6.20 Comparison of experimental S21 (img) in SAP mixtures (12 mm)	79
Figure 6.21 Comparison of experimental S21 (img) in SAP mixtures (7 mm)	80

Figure 6.22 Comparison of loss factors in SAP samples (55%).....	81
Figure 6.23 Comparison of loss factors in SAP samples (60%).....	82
Figure 6.24 Comparison of loss factors in SAP samples (65%).....	82
Figure 6.25 Comparison of loss factors in SAP samples (70%).....	82
Figure 6.26 Comparison of loss factors in SAP samples (75%).....	83
Figure 6.27 Comparison of loss factors in SAP samples (80%).....	83
Figure 6.28 Comparison of loss factors in SAP samples (85%).....	84
Figure 6.29 Comparison of loss factors in SAP samples (90%).....	84
Figure 6.30 Comparison of loss factors in SAP samples (95%).....	85
Figure 6.31 Comparison of experimental permittivity (EPR) and permeability (MUR)..	86
Figure 6.32 Comparison of permittivity in SAP with different water content (12 mm) ..	88
Figure 6.33 Comparison of permittivity in SAP with different water content (7 mm)	88
Figure 6.34 Comparison of permittivity in SAP with different water content (12 mm) ..	89
Figure 6.35 Comparison of permittivity in SAP with different water content (7 mm)	89
Figure 6.36 Correlation of relative permittivity in different sample thickness.....	90
Figure 6.37 Permittivity vs. water concentration at 2.45GHz in different sample thickness	91
Figure 6.38 Standard deviation of relative permittivity in different sample thickness.....	92
Figure 6.39 Estimated permittivity of 100% water.....	92
Figure 6.40 Comparison of loss factor in SAP with different water content (12 mm).....	94

Figure 6.41 Comparison of loss factor in SAP with different water content (7 mm).....	94
Figure 6.42 Loss factor of different samples	95
Figure 6.43 Standard deviation of loss factor in different thickness	95
Figure 6.44 Loss tangent in 12 mm SAP samples	96
Figure 6.45 Loss tangent in 7 mm SAP samples	97
Figure 6.46 Comparison of loss tangent at 2.45 GHz in 7 mm samples.....	97
Figure 6.47 Comparison of average loss tangent in SAP samples	98
Figure 6.48 Comparison of loss tangent of SAP Mixtures (65%).....	99
Figure 6.49 Antenna received power between reader antenna and tag.....	100
Figure 6.50 Power decaying in open-air with circular antenna	101
Figure 6.51 Power decaying in open-air with linear antenna	101
Figure 6.52 Tag orientation loss in different antennas	102
Figure 6.53 Power with Shielding	103
Figure 6.54 Power attenuation of circular antenna (H).....	104
Figure 6.55 Power attenuation of circular antenna (V).....	104
Figure 6.56 Power loss in 50% and 75% SAP	105
Figure 6.57 Influence of water content on power loss.....	105
Figure 6.58 Average power loss in 70% SAP specimen	106
Figure 6.59 Comparison of power attenuation with saturated SAP samples.....	106
Figure 6.60 Comparison of power attenuation with saturated SAP samples.....	107

Fi

Figure 6.61 Comparison of power attenuation with 50% and 75% water content	107
Figure 6.62 Comparison of received power with circular and linear antenna	108
Figure 6.63 Readability decaying in free space	110
Figure 6.64 Comparison of readability: tag orientation.....	111
Figure 6.65 Readability fading	112
Figure 6.66 Comparison of readability (I)	112
Figure 6.67 Comparison of readability(II).....	113
Figure 6.68 Comparison of readability(III)	113
Figure 6.69 Comparison of readability(IV)	114
Figure 6.70 Comparison of readability(V).....	114
Figure 6.71 Comparison of readability(VI)	115

L

E

F

FL

FI

KEY TO ABBREVIATIONS

AIDC	Automatic Identification and Data Capture
ANI	Automatic Number Identification
ASK	Amplitude Shift Keying
BW	Bandwidth
CPG	Consumer Packaged Goods
CW	Continuous Wave
dB	Decibel
dBm	Decibels referenced to 1 milliwatt
DBi	Decibels referenced to isotropic
DOD	Department of Defense
EAS	Electronic Article Surveillance
EIRP	Effective Isotropically Radiated Power
EMI	Electromagnetic Interference
EPC	Electronic Product Code
ERP	Effective Radiated Power
FCC	Federal Communications Commission
FDA	Federal Drug Administration
FIFO	First In First Out

FSK	Frequency Shift Keying
GHz	Gigahertz
IFF	Identification of Friends of Foe
IFRB	International Frequency Registration Board
ISM	Industrial Scientific Medical
ITU	International Telecommunication Union
JIT	Just in Time
MHz	Megahertz
MUT	Material under Test
mW	Milliwatt
NIST	National Institute of Standard & Technology
NRW	Nicholson-Ross-Weir technique
OATS	Open Area Test Site
OCR	Optical Character Recognition
PSK	Phase Shift Keying
Reader	Interrogator
RF	Radio Frequency
RFID	Radio Frequency Identification
RMS	Root Mean Square

RO	Read only
Rx	Receiver
SAP	Superabsorbent Polymer
SHF	Super High Frequency
SRD	Short Range Device
Tag	Transponder
TRL	THRU-REFLECT-LINE Calibration
Tx	Transmitter
UHF	Ultra High Frequency
UPC	Universal Product Code
VHF	Very High Frequency
VNA	Vector Network Analyzer
WR	Waveguide Rectangular

LIST OF PRINCIPAL LETTER SYMBOLS

Symbol	Definition
d, r	Distance from transmitter to receiver
E	Electric field strength, in V/m
H	Magnetic field strength, in A/m
P	Power, in W
f	Frequency, in Hz
i, j	$= \sqrt{-1}$, imaginary part of complex number
δ	Skin depth
$\epsilon, \epsilon_r, \epsilon_0$	Permittivity, relative permittivity, permittivity in free space
η	Radiation power conversion efficiency, in percent
λ	Wavelength
p	Loss tangent ($p = \tan \theta$)
ω	Angular frequency ($\omega = 2\pi f$), in rad/s

a
[
b
w
co

Chapter 1

INTRODUCTION

1.1 Overview

In recent years, the very exciting revolution throughout the supply chain is the adoption of radio frequency identification (RFID) technology. Real time tracking and tracing of goods and assets in the manufacturing and distribution processes along with other technologies have been considered as a potential management tool to enhance efficiency of corporate operations and to eliminate counterfeiting. Large retailer chains, government agencies, manufacturers and research institutes are the main stakeholders in the arena. Wal-mart, the largest retailer in the world, mandated its biggest 100 suppliers to adhere RFID tags to cases and pallets delivered to certain distribution centers after January 2005 [1]. Urged by the extremely time-sensitive necessity from retailers and agencies, large consumer packaged goods (CPG) companies launched into many efforts to implement RFID system in the supply chain and had their products tagged before the door closed. Why RFID? Because an RFID system can give real time, end-to-end visibility and control of inventory throughout the supply chain. RFID technology as a inventory management tool integrates a tangible, physical item actually kept within the facility with an intangible item existing within the company's record into together without any delay [2, 3]. In comparison with other Automatic Identification (Auto-ID) technologies like the bar code, RFID is a wireless technology that acquires remote object information often without line-of-light, which enables efficiency, visibility and security of automating data collection process for both manufacturers and retailers. Products and assets with RFID

technology can be monitored at any time as long as items with tags pass through the RFID portal systems. Simultaneously, a central database updates the latest status throughout the company via their computer network.

Anti-counterfeiting is another concern for RFID application. According to an FDA report, there were 30 counterfeit drug cases initiated in 2003 and this jumped to 58 counterfeit drug cases initiated in 2004. More counterfeiting drug cases were initiated in 2005. Therefore, the FDA launched an anti-counterfeiting project advocating item level tracking to retail packaging of drugs with RFID technology in the US [4]. Philips Semiconductors and Texas Instruments (TI) Inc. reported in 2004 that up to 7% of all drugs in the international supply chain may be counterfeit [5]. Hence more manufacturers have started to enable RFID tags in pallets and box packaging to comply with mandates from retailers and agencies.

1.2 RFID Puzzles

RFID embraces significant potential for the supply chain. However, the implementation of an RFID system involves many aspects such as infrastructure, interoperability, frequency, industrial standards and security issue, etc. Many companies impetuously launched RFID projects and pilot tests to overtake the deadline, even though not quite comprehending what RFID technology may bring to them. There were numerous reports and papers regarding RFID application, solution and analysis on various disciplines and business aspects, for instance, business strategy, the application environment, security and privacy, etc [6, 7]. Nonetheless, the potential negative effect of packaging and product contents to RFID performance and stability was addressed as it should be. Even

it was mentioned, optimistic opinions overwhelmed the unsubstantial noise [1, 8, 9]. No peer-reviewed research was found directly concerned on the effect on RFID performance and stability from water content and material dielectric properties. Some RFID system providers had done a few studies on these issues; however, the research results have not been based on Design of Experiments (DoE) and peer-reviewed. It is often hard to avoid bias and misleading statements [10]. From a long term standpoint, low performance and stability of deployed RFID systems certainly restrict its fast pace. Impressive research on the effect of package content, pallet configurations and temperature to RFID performance and stability have been performed in the School of Packaging, MSU [10-14]. Based on the previous MSU research, further studies on dielectric properties and power fluctuation would enhance recognition of intrinsic relations [10].

1.3 Research Aspects

Though robust RFID systems work very well in various environments and conditions, the low power and short range RFID signal are easily interfered with, absorbed, and/or reflected by surrounding electronic devices, dielectric materials, large amount of metallic content and even the human body. Thereafter, system performance and stability may be impacted. In a real environment, the RFID interrogator (reader) through an antenna transmits RFID signals that penetrate multiple media, such as wood (pallet), paperboard (box), and various kinds of packaging material and product content. Further, the RFID transponder (tag) backscatters the modulated RF signal to the interrogator along the same path.

With water content from 0% to 100% and water ingredients such as salt, the different materials show variable dielectric properties when electromagnetic fields are applied. To differentiate the influence of the amount of water content in any product, a special water absorbable polymer was used to simulate a wide range of water concentrations. By measuring the RFID power dissipation and dispersion in the path of the RF signal along with the water concentration, the influence of water in the product with respect to RFID performance and stability may be learned. Through measurement of the dielectric properties of the same samples, the influence of dielectric properties to RFID performance and stability may be also profiled.

1.4 Research Goals

The preliminary goal of this research is to determine the influence of water content in a sample upon RFID signals through measurement of the scattering parameters of the samples, power loss through the sample and the diversification of RFID tag readability with samples associated with the factor analysis method. A correlation and regression model interpreted the intrinsic relationship of the RFID system, product content and packaging operations. With the restricted statistical analysis, the model of readability and the results of this research allow industry to predict the feasibility of an RFID system and optimize the implementation of RFID solutions using specific products. Recognition of the influence of water content in products to RFID performance and stability can help industry recognize multiple factors associated with successful RFID implementation and eliminate the negative factors for real RFID implementation.

1.5 Thesis Summary

Chapter 2, Literature Review, presents the RFID primer, electromagnetic principles and material characterization relative to this research. In addition, the relationship among water content, superabsorbent and real food products is specified. Moreover, previous research relative to this research is reviewed as well. Chapter 3, Methodology, provides the basic methodology of this research and experimental procedures. Chapter 4, Material Characterization, particularly describes the experimental method and the computational process applied to determine the dielectric properties in term of permittivity (ϵ) of hydrated superabsorbent polymer (SAP) specimens by a vector network analyzer (VNA) and waveguide at UHF frequencies range from 2.2GHz to 3.0 GHz. Multiple hydrated SAP samples were measured with water concentration between 45% to 95%, which simulated various products with nearly similar dielectric properties and influence of tag responses.

Chapter 5, Power Measurement and Readability Survey, shows the experimental procedure of power measurement and a readability survey in the laboratory. Chapter 6, Results and Discussion, presents the correlation and the influence among dielectric properties, RFID performance and the fluctuation of water content in the SAP samples according to experiments. Furthermore, the relationship between RF power, attenuation, tag orientation, antennas style and tag readability are depicted. Chapter 7, Conclusions, summarizes the new learned results and potential application and proposes future research and the limitation of this work.

Chapter 2

LITERATURE REVIEW

2.1 Automatic Identification Technologies

Auto Identification and Data Capture (AIDC) refers to the automatic recognition of data technologies by barcode scanning, optical character recognition, biometric identification (such as voice, fingerprint and retina), smart card (magnetic stripe and microchip), RFID etc. AIDC can accelerate the throughput process and eliminate human errors, consequently. AIDC technologies have been prevalent identification solutions in requiring access control and security applications. Furthermore, AIDC technologies will make automated inventory control and integrated supply chain management possible [15].

2.2 Briefly History of RFID

Vast and expeditious entity movements in the business world make convenient object identification a necessity. Since the barcode fulfilled the identification requirement of the grocery industry in 1970's, squeezing profits from the supply chain became the common goal. Wireless object identification as a potential replacement of barcodes provides a faster and more accurate identification, without line-of-sight.

RFID, which stands for Radio Frequency Identification, is a continuously developing object identification technology that began a significant growth in the 1980's. The first application of RFID can be identified as "Identification of Friends of Foe" (IFF) for aircraft to prevent "friendly fire" accidents from dogfights in 1940's [8]. Harry Stockman

first introduced the concept of a passive transmitter in his paper "Communication by Means of Reflected Power" [16]. Modern electromagnetic theory related to RFID application was developed by R. F. Harrington. Subsequently, Kriofsky and Kaplan filed a patent on primordial RFID, "inductively coupled transmitter-responder arrangement" in 1972 [8]. In 1985, RFID technology was declassified and came into more common industry use. In 2003, EPCglobal, a nonprofit organization for RFID technology, released a recommended RFID standard [9]. In the latest RFID milestone, Wal-mart and the Department of Defense (DOD) mandated their suppliers rollout RFID technology in early 2005, thereby indicating that RFID was coming into use.

2.3 RFID System Components

A typical backscatter RFID system consists of three main components: transponder, interrogator and supported software with computer network [17, 18].

2.3.1 Transponder

A microchip based transponder (RFID tag, see Figure 2.1 left) which generally is a thin, flexible adhesive label with RFID inlay that can be attached to packaging. An RFID transponder linked to a conductive coil (tag antenna) receives radiated RF power from the RFID interrogator (reader) antenna and simultaneously reflects the modulated wireless RF signal to the interrogator.

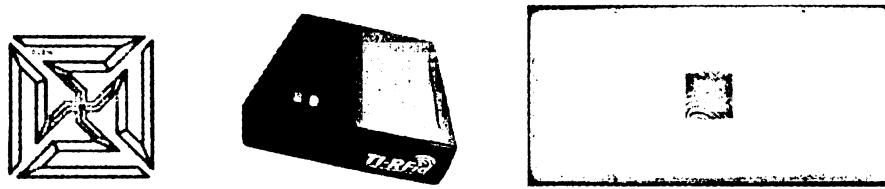


Figure 2.1 UHF 915 MHz RFID transponder, reader, and antenna

There are two kinds of transponders, passive transponder without battery and active transponder with battery. The passive RFID tag is powered by the incident RF signal exclusively that limits the distance of tag response. Because of this, the price of passive transponders is much cheaper than that of an active transponder. The price range of passive RFID transponder is about from \$0.15 to \$1.00 per item according to manufacturers and business reviews in the internet. The price remains fairly expensive while the read range is shorter than active system. For cost reasons, the passive RFID solution dominates supply chain applications. Price may continue to decline with the global RFID market expanding. If the price would reach a couple of cents per item, RFID would be more preferable for corporate use. Besides the price, another limit to RFID application is that there is no universal industrial frequency or standard.

Depending on the RFID application, information can be written and erased on the microchips more than one time. Read only (RO) tags have been written so that they have a unique identifier placed on them in the manufacturing process. The identifier in the transponder cannot be erased and rewritten at any time which provides unique identification, tamper-evidence and high-level security. Table 2.1 shows the tag classes classified by Auto-ID Center, MIT [19].

Classes	Features	Tags Characteristics
Class 0	Article surveillance	Passive tags, "Read-only"
Class I	Identification only	Passive tags, write once
Class II	Data logging	Passive, high security and memory
Class III	Environments sensors	Semi-passive RFID tags
Class IV	Ad hoc networking	Active tags
Class V	Reader	Power class I, II, III tags

Table 2.1 EPC tags classes (Source: Auto-ID Center, MIT) [19]

2.3.2 Interrogator

A RFID interrogator (reader) transmits a radio frequency signal, providing RF energy to passive transponders and communicates with each other. The interrogator, through the antenna, transmits modulated radio frequency waves to the transponders in a specific bandwidth [17]. The powered transponders backscatter the demodulated RF signal to the reader antenna (See Figure 2.2). A computer collects and processes the data via the network from the reader. A RFID reader can hook-up to multiple antennas to optimize and maximum coverage [20].

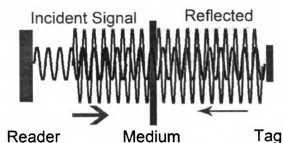


Figure 2.2 RFID signal propagation and backscattering

2.3.3 Computer and Backbone Software

The computer software system runs on a computer and/or network, which collects, processes and stores information in real time. The application software and network are considered as a part of ERP system in a supply chain [7].

2.4 Basic Principles

2.4.1 Frequency Allocation

RFID systems generally operate in several frequency ranges from LF (125 kHz) to SHF (5.8 GHz). Different frequencies have various advantages and disadvantages for RFID operation. High frequencies have longer read range while low frequencies have less interference from water content and the human body, shorter read ranges and slower data transfer rates. The radio frequency resources are regulated by the government of a given country and managed by some international organizations, such as Federal Communications Commission (FCC) and International Frequency Registration Board of International Telecommunication Union (IFRB/ITU), respectively. The specific frequency within a range such as UHF may run at different frequencies for different regions due to frequency availability and regulation. RFID systems operating in UHF (860~960 MHz) are more popular and preferable due to the read range they exhibit (see Table 2.2). The general RFID frequency allocation within each field is as follow:

- LF 125~134kHz
- HF 13.56MHz
- UHF 400~960 MHz
- UHF 2.45 GHz (S band)

- SHF 5.8 GHz (C band)

2.4.2 Near Field and Far Field

In LF and HF, the RFID system is mainly based on mutual inductance coupling in which the magnetic field produced by the loop antenna coils rapidly drops off with distance ($1/r^3$) in free space (see Figure 2.3). R is the distance for the path of the signal. The attenuation of a magnetic field limits the read range for all passive RFID devices [21].

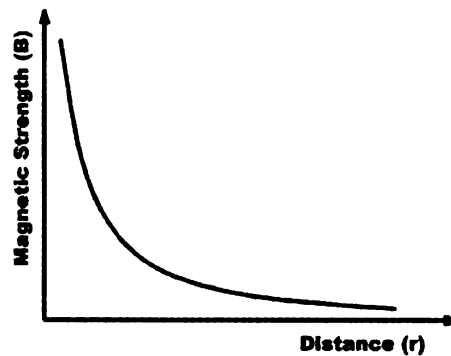


Figure 2.3 Attenuation of magnetic strength vs. distance in near field region

At UHF, the RFID transponder and interrogator communicate in both the near field and far field, which allows broader read ranges and a faster data transfer rate (see Table 2.3) [17]. Near field refers to a region generally in close proximity to the radiation source where the electric and magnetic fields do not indicate a completely plane wave characteristic, but alternates considerably from point to point [22]. The near field is further split into the reactive near field region which is the nearest to the radiation source and accommodates most or nearly all of the stored energy, and the radiating near field region where the radiation predominates over the reactive field but lacks substantial plane-wave character [22]. In the near field, both the electric field (E) and the magnetic

field (H) are relatively static, without propagation. Maxwell had proved that beyond the quasi-static near field, both the electric field and the magnetic field, at a certain distance, detached themselves from the conductor and propagated into free space as a combined wave at light speed with a constant ratio of: $E / H = 120\pi = 377\Omega$ [22].

The critical point at which separation happens is called the far field. This field has a predominantly plane-wave characteristic. Electric field strength and magnetic field strength are represented in transverse planes normal relative to the path of propagation are separated distributions. In far field, the transmission power of the propagation RF signal attenuates as the inverse square of distance.

$$S = \frac{P_t}{4\pi r^2} \quad (\text{Equation 2.1})$$

where, S is signal strength at a distance r from the source and P_t is transmission power. The farther the RFID transponder is from the interrogator, the less RF power could be received from the interrogator. If the distance is less than $1/20^{\text{th}}$ of a wavelength, it is in the near field; if the distance is longer than 5 wavelengths, it is generally in the far field (see Table 2.3). Therefore, at UHF, transponders operate both the far field and transition field (between the far field and near field) [17, 23].

Name	Frequency range	Near field region	Far field region
LF	30K-300K	<120m	>12km
HF	3M-30M	<1m	>110m
UHF	300M-3G	<1.65 cm	>1.65m
SHF	3G-30G	<0.25 cm	>0.25 cm

Table 2.2 Near field and far field regions

2.4.3 Read Range and Power Assumption

Read range is the maximum distance that the RFID interrogator and transponder can communicate with each other [18]. Read range is an important specification and characteristic of an RFID system. Active RFID transponders have longer read ranges compared to that of passive RFID transponders that are completely powered by the received RF energy. The actual read range depends on the frequency, both antenna designs and the effective isotropically radiated power (EIRP) [15, 21]. Within this read range, the RFID transponders receive enough RF energy and power up the integrated circuit to backscatter the modulated signal to the reader (see Figure 2.2) [24]. LF and HF RFID systems are based on inductive coupling, such as the TI-RFID running at 13.56 MHz. The read range of this kind of RFID system is no more than a few inches. Read ranges of ultra high frequency RFID systems, for instance 915MHz, are more than several feet, which is based on electromagnetic backscatter coupling. This system is also called a long range system vs. the forward short range system [17].

There are two ways to increase the read range. One is to increase the transmission power and the other is to decrease the minimal threshold operating power required by the transponder or increasing the power conversion efficiency [24]. Recently, technology has dropped down the minimal required operating power to the range of 0.5-1 mW, and even lower [25]. The power conversion efficiency η is about 20%, therefore, the minimum required power for the tag Integrated Circuit (IC) is about 0.1~0.2 mW. The antenna can radiate energy up to 4 watts EIRP in the UHF range, see US FCC Part 15-45 [26]. Theoretical read range is longer than real read range. Read range can be calculated using the Friis free-space formula, notice it is assumed that the read range is in free space.

$$r_{\max} = \frac{\lambda}{4\pi} \sqrt{\frac{P_t G_t G_r (1 - |s|^2)}{P_{th}}} \quad (\text{Equation 2.2})$$

where, λ is the wavelength, P_t is the power transmitted by reader, G_t is the transmitting antenna gain, G_r is the tag antenna gain, P_{th} is the minimum threshold power to power up the tag, and $|s|^2$ is power reflection coefficient at the tag resonant frequency. $P_t G_t$ is the EIRP [27]. Power or current gain can be expressed as a decibel (dB) value. The dB value is calculated by taking the log of the ratio of the measured power with respect to a reference power multiplied by 10 ($dB = 10 \log_{10} \frac{P_{out}}{P_{in}}$, $dBm = 10 \log_{10} \frac{P_{out}}{1mW}$).

2.4.4 Modulation

Radio frequency communication transmits and receives data through modulating a carrier wave. There are three digital modulations: Amplitude Shift Keying (ASK), Frequency Shift Keying (FSK) and Phase Shift Keying (PSK). Each of them has different power consumption, bandwidth and reliability (see Figure 2.4). In time domain, the carrier, sinusoidal signal can be expressed as:

$$v(t) = A \cos(\omega t + \phi), \quad \omega = 2\pi f \quad (\text{Equation 2.3})$$

Each of the three variables, amplitude A , angular frequency ω , and phase ϕ can be applied to different modulation techniques [28].

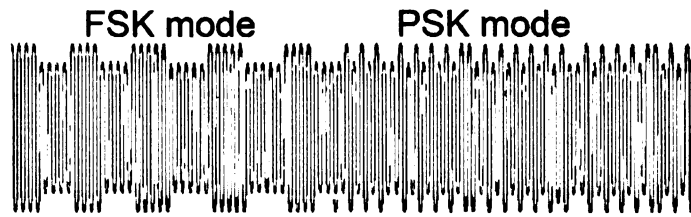


Figure 2.4 FSK and PSK digital signal modulation

In passive RFID systems, power reflected from the tags is neglectable in comparison with the power radiated from the reader. Consequently, the reader might not be able to pick up the coupled response from the tags. A low frequency subcarrier modulated within the RFID system can avoid this from occurring. For an RFID system with a carrier frequency of 13.56 MHz, the subcarrier frequency could adopt 847 KHz (1/16), 424 KHz (1/32) or 212 KHz (1/64). This depends on the data transfer rate required in the application, and standards for the system. [17]

2.5 Electromagnetic Properties

2.5.1 Dipole Moment and Molecular Polarity

According to molecular polarity, molecules can be classified as polar and nonpolar. The polar molecules possess an electric dipole moment in lowest energy-level in comparison with nonpolar molecules [29]. Chemical bonds, van der Waals attraction, and repulsion forces are considered distinguished interaction forces over short ranges, while dipolar interaction forces have a very long range. Polar molecules examples are HCl and CO and whereas non-polar molecules examples are H₂ and O₂. The easy way to recognize each type is whether the molecules have a point of symmetry. Triatomic molecules, for

instance H_2O (see Figure 2.5), are polar unless three atoms lie on a straight line with a direct line from O to the 2 H atoms [29].

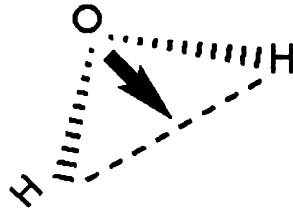


Figure 2.5 Orientation of atoms and direction of the electric dipole relative in H_2O

Molecular dipole moments in gaseous state and in liquid state are different. In a liquid state, the dipole moment is considered as consisting of a continuous medium with dielectric. In liquids, the average energy of a single dipole is the same in all direction because a liquid does not possess any preferential direction and the neighboring molecules do not form an orientation. In a solid, the average potential energy of a molecule is contributed to crystalline field acting on the dipoles normally depends on temperature. The direction of dipole relative to the crystal axes in a crystalline solid determines the average potential energy of a polar molecule. When the average energy of molecules doesn't reach a relative minimum, the molecules can't rotate freely until the average energy breaks the equilibrium [30].

2.5.2 Dielectric Permittivity

Permittivity (ϵ) of a dielectric substance describes quantitative characteristic of any electric field affected by the dielectric substance, which presents the polarized ability of the substance to an applied electric field. In comparison with electrical conductivity (σ), it relates to charge in isolation rather than current. When a voltage is applied to dielectric

substance, if there are no free charge carriers, such as electrons and ions, the substance tends to pass current; the voltage source provides the energy to move charge. The charge that displaced is restricted by the polarity of molecules in the substance. Permittivity is a complex, frequency-dependant quantity with the real part and imaginary part, expressed as,

$$\varepsilon = \varepsilon_1 \pm j\varepsilon_2 \quad (\text{Equation 2.4})$$

the real part, $\text{Re}(\varepsilon)$ presents the propagation characteristics of the energy. The imaginary part, $\text{Im}(\varepsilon)$ referred to as loss factor represents energy loss in the substance due to polarization of molecules [22]. The sign of the imaginary part is dependant on the numeric sign conversion. The dielectric permittivity of free space ε_0 is 8.85×10^{-12} F/m. Permittivity is usually given as the ratio of that of free space, known as relative permittivity or dielectric constant (ε_r) which is frequency dependent in parts of frequency range and dimensionless. Relative permittivity of free space is defined as 1, relative permittivity of air is about 1.0005 and relative permittivity of water is approximately 80. Higher permittivity of substances stores greater charges with the same applied electric field. As a result, the substance has higher capacitance. For most materials, dielectric constant depends on temperature, frequency, atomic structure, and salinity of the material [29].

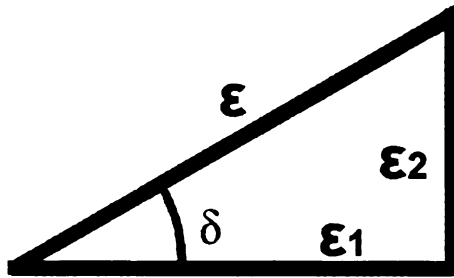


Figure 2.6 Complex permittivity and loss tangent ($\tan \delta = \varepsilon_2 / \varepsilon_1$)

2.5.3 Loss Tangent

The loss tangent (p) defined as the ratio of dielectric loss factor (ε_2) to dielectric permittivity (ε_1) ($\tan \delta = \varepsilon_2 / \varepsilon_1$) and, is roughly, wavelength independent. Loss factor is a product of the dielectric constant and loss tangent (see Figure 2.6). High or low values of loss tangent of the substance impacts the penetration of radio wave with the substance, and the radio absorption length. When a radio frequency wave penetrates into the dielectric substance, the wave field strength attenuates exponentially with depth. For example the distance where the field strength decreases to e^{-1} is the skin depth δ .

$$\delta = \sqrt{2 / \omega \mu_0 \sigma} \quad (\text{Equation 2.5})$$

2.5.4 Dielectric Absorption

Dielectric absorption indicates the conversion of electromagnetic energy into heat energy. Dielectric absorption has a few mechanisms: relaxation effects associated with permanent and induced molecular dipoles and resonance effects occurred in the rotations or vibrations of atoms, ions, or electrons [31]. Dielectric relaxation occurs in insulating

materials with negligible or small electrical conductivity. Polarization relaxation occurs in the high dielectric constant substances. Absorption of the field's energy leads to energy dissipation. The mechanism of dipoles relaxing is called dielectric relaxation and, for ideal dipoles without dampening, is described by classic Debye relaxation [31]. As mentioned in section 2.5.1, polarity of a molecular structure and ionized molecules solicit energy dissipation to change the moments of polar molecules in applied electromagnetic fields. The traits of RF absorption in dielectric substance represents the electromagnetic properties. Dielectric permittivity and loss factor generally represent the material's electromagnetic properties. Radio frequency waves propagate in a straight line in free space. They may be reflected, transmitted or absorbed by dielectric substances in the path. Products, such as foods or drugs with water content, absorb RF energy and transform it into heat. A typical example that describes this process is a microwave oven in the kitchen.

2.6 Water Content in Foods

2.6.1 Water Activity

Foodstuffs and medication materials contain water. As a polar molecule, water can be partly aligned by an applied electric field; however, there are forces in water preventing its molecules from moving freely. Thus, the energy counteracting this resistance is transferred to the ions and then to neighboring atoms or molecules. Food products or any material containing such charged ions are able to interact with any electric fields. Water absorbs radio frequency energy and turns it into heat [32].

Water content is a very important factor in determining food quality, shelf stability and textural properties. Natural moisture content in produce offers freshness and quality. The crisp, fragile biscuit or one in a limp state are determined by the water content and its distribution within the biscuit. To maintain the special textures and flavors in a food product, the food ingredients strictly limit the water content and distribution within the food product. Controlling the water activity and reactivity with unbound water content in food product will really help to attain food stability. In spite of the microstructure, local viscosity and associated molecular mobility are very important to food stability. Nevertheless, moisture content is the one of key factors to determine these parameters of a food matrix [33]. To extend the shelf life, adjusting the water content is a common approach. Sublimation or evaporation is often used to remove liquid water to enhance the product stability [34].

2.6.2 Water Forms

The water molecules in foods appear in different forms depending on surrounding molecular environments, generally in forms that have different physiochemical properties as follow:

1. Free water. Water in this form that is enveloped by other water molecules only. The physicochemical properties are the same as these of pure water.
2. Capillary water or trapped water. Water in this form is enveloped by a physical barrier or retained by tiny channels. The physicochemical properties are the same as those of free water due to normal water-water bonding in this form.

3. Bound water. Water in this form is partly enclosed by other food components in molecular contact, which leads to a significant difference in physiochemical properties compared to free water.

Due to different bonding existing in foods, they are considered as heterogeneous mixtures from the standpoint of chemistry, though the macrostructure of the food material may be homogeneous [35, 36]

2.6.3 Dielectric Properties

The state of water in a food substance lies in the degree of interaction between water molecules and the glassy solid pertaining to hydrogen bonding. Lechuga-Ballesteros *et al* found that the proportion of high mobility water molecules at 1 GHz increased for hydration levels above the hydration limit [37]. Thus, more water molecules are relatively free to respond to applied electric field and showed a dipole moment near to gaseous water molecules due to hydration-induced conformational changes. The dielectric parameter increases is proportional to the increasing of water concentration in the foods [37].

The amount of water content in a material greatly affects its electromagnetic properties [38]. Water has a high dielectric constant at room temperature (see Table 2.3). Dry materials have low dielectric constants often less than 10. Therefore the percentage of water content in the substance is indicative of the dielectric properties. A high water percentage usually shows proportional increases of the loss factor of the substance and a high dielectric constant. The dielectric constant of a mixed substance commonly is based on its components and stands between the medial of its components. Dielectric loss has a

complicated transaction mechanism. For example, it may increase 20~30% with raising the water content percentage of the substance, and then decrease rapidly [38].

Substance	Dielectric constant	Loss factor	Loss tangent
Water	80	12.5	0.16
Mashed potato	65	22.1	0.34
Cooked ham	45	25.2	0.56
Peas	63	15.8	0.25
Most Plastics	2~4.5	0.002~0.09	0.001~0.02
Woods	1.2~5	0.01~0.5	0.01~0.1
Papers	3~4	0.15~0.4	0.05~0.1

Table 2.3 Dielectric properties of foodstuffs and other packaging materials at 2.45GHz and 68°F (Source: Sacharow, *et al*: Microwave Packaging [38])

2.6.4 Gel Structure and Food Biopolymers

Gel structure refers to the crosslinking of long polymer chains to shape continuous three dimensional networks that retain fluid. Many food biopolymers form gels. Such networks and structures consist of carbohydrates, protein and lipids. Retained water within the networks and structure is not permanent, and depends on environment conditions such as temperature, shear and maintained by the bonds within the structure [33]. The mechanism of retaining water in a food biopolymer and the superabsorbent polymer that will be described in later sections are similar. Hydrated superabsorbent polymers can be used to simulate the water behavior and properties as found in food biopolymers.

2.7 Superabsorbent Polymer

2.7.1 History of Superabsorbent

Superabsorbent polymers (SAPs) are hard, dry, granular powders with a white or slight yellowish color. Generally, 1 g of dry, fluffed, cellulose pulp fibers will take up to 12 g of water, whereas 1 g of SAP may retain up to 1,000 g of water (see Figure 2.7) [39]. In 1970, Weaver developed the first uncrosslinked starch graft polymer at the Northern Regional Laboratory of the US Department of Agriculture. Japan was first to commercially manufacture a superabsorbent polymer in 1978. SAP was used in infant diapers in Europe in 1980 [39].

Polyacrylic acid is the primary polymer for superabsorbent polymers today. The swollen gel holds the fluid in a solid, rubbery state and locks the fluid from leaking out of the polymer.



Figure 2.7 Hydrated superabsorbent polymer sample, with more than ten times of its weight of water absorbed by the SAP particles

2.7.2 Structure and Properties

Water-swellaible superabsorbent polymers are synthesized by free radical crosslinking polymerizations of hydrophilic acrylate monomers in suspension of the aqueous solution in a hydrocarbon [40]. The swelling capacity and gel modulus of SAP are controlled by the crosslinkers. The new gel like polymerized product is dehydrated in a continuous oven, and then milled to the desired particle sizes to form free-flowing powder or a granule polymer. SAP is widely used in absorbing and retaining water and body fluid in personal hygiene product, droughty planting and moistureproof products, such as infant diapers, agriculture mulches and biosorbents in preparative chromatography. SAP particles tend to swell quickly when they osculate with water or fluid, whereas saturation or equilibrium swelling comes much later [40]. Swelling capacity is related to the properties of the network. By increasing the crosslink density of the gel particles, fluid retention may be enhanced under shear. It is more rigid in the swollen status; however, it does not condense the equilibrium swelling capacity. The chemical structure of polyacrylic acids is shown in Figure 2.8, where there is an ionizable group on each repeat unit (-COOH). Crosslinking occurs at the -OH bonds in the polymer chains. Minor crosslinkers act in a primary role for attaining the preferable swelling property of superabsorbent polymer in addition to modifying the swelling and mechanical properties [39, 40].

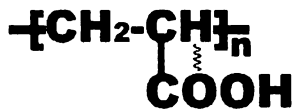


Figure 2.8 Crosslinking structure in a superabsorbent polymer

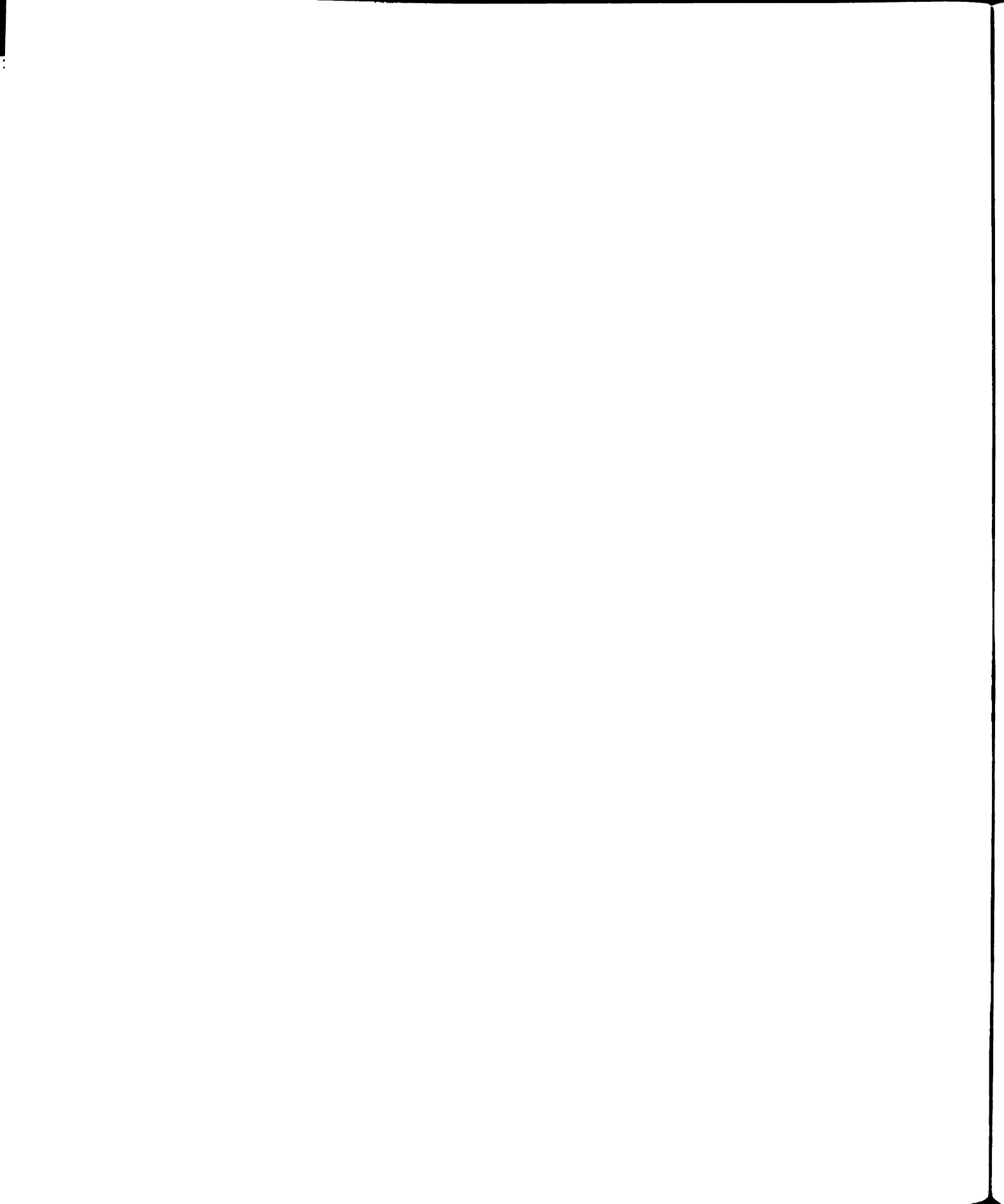
2.7.3 Mechanism of Water Absorption

Binding water in the SAP is not a chemical reaction. The hydrated superabsorbent polymer is rather a mixture instead of a new chemical. Retention of water in SAP is similar to cotton. Water diffuses on the long chain molecules that are like the long cotton fibers, while cotton fibers suck up water by convection. These flexible polymer networks carrying dissociated ionic hydrogen groups are the most efficient water absorbers. When water diffuses into the SAP particles, SAP inflates to accommodate the additional water molecules. Crosslinked networks in SAP molecules prevent it from dissolving in the absorbing fluid. The hydrated superabsorbent mixture in equilibrium is considered an isotropic, homogeneous (ideally) dielectric material. The dielectric properties and water activity may comply with the rules as mentioned in this chapter. There are a few of literature sources on superabsorbent polymers which related mechanism of swelling, swelling capacity, cross-linking in SAPs, application, and manufacture etc, please see [39-41].

2.8 Previous Research

2.8.1 RFID Application

Clarke and Tazelaar (2005) found that tag orientation and product type had a significant effect on tag readability based on his research on a pallet load having Matrics 915 MHz Class 0 RFID tags. Moreover, the tier, column and row of tagged cases also had an effect on tag readability [7, 10, 18]. Jonson (2005) presented a RFID tag failure mode with class 0 RFID transponders using ASTM vibration and impact procedures to evaluate the robustness of the RFID tags in simulated transportation status. The results showed shock



and drop impact damaged the transponders. Nonetheless, vibration did not affect the function of tags. However, tag placement was another influential issue in the failure mode. Transponders adhered perpendicular to the corrugated fluting have a significant failure level compared with those adhered parallel to the box fluting [13]. Ryan (2002) described a model for implementation of a RFID system into a warehouse environment that offers companies an unbiased method in the form of decision trees which are based on how packaging is tracked through the warehouse [12]. Onderko (2004) found that a HF RFID system running at 13.56 MHz had higher stability for data transmitted through a package of frozen beef. However, those systems operating at 915 MHz encountered a loss of data when transmitting in the same situation [11]. Clarke and Vorst (2002) found that RFID tags might affect the quality and consumer acceptance of beef products [42, 43]. Ramakrishnan (2005) provided a set of benchmarks for comparing the performance of UHF passive transponders, which revealed the current state of commercial RFID tags [44]. Ramchandran, A R (2004) described a type of plant scanner with a handheld PDA (personal digital assistant) using RFID tags for child visitors to the Michigan 4-H Children's Garden. The visitors can instantly receive the plant background knowledge from remote server where they approach a plant in the garden [45]. Weis (2003) identified several potential threats to security and privacy and proposed several efficient security mechanisms in his research [19]. Hardgrave *et al*, at the University of Arkansas suggested that RFID reduced the out of stocks through investigation of 24 Wal-mart store in a study [46].

2.8.2 Material Characterization

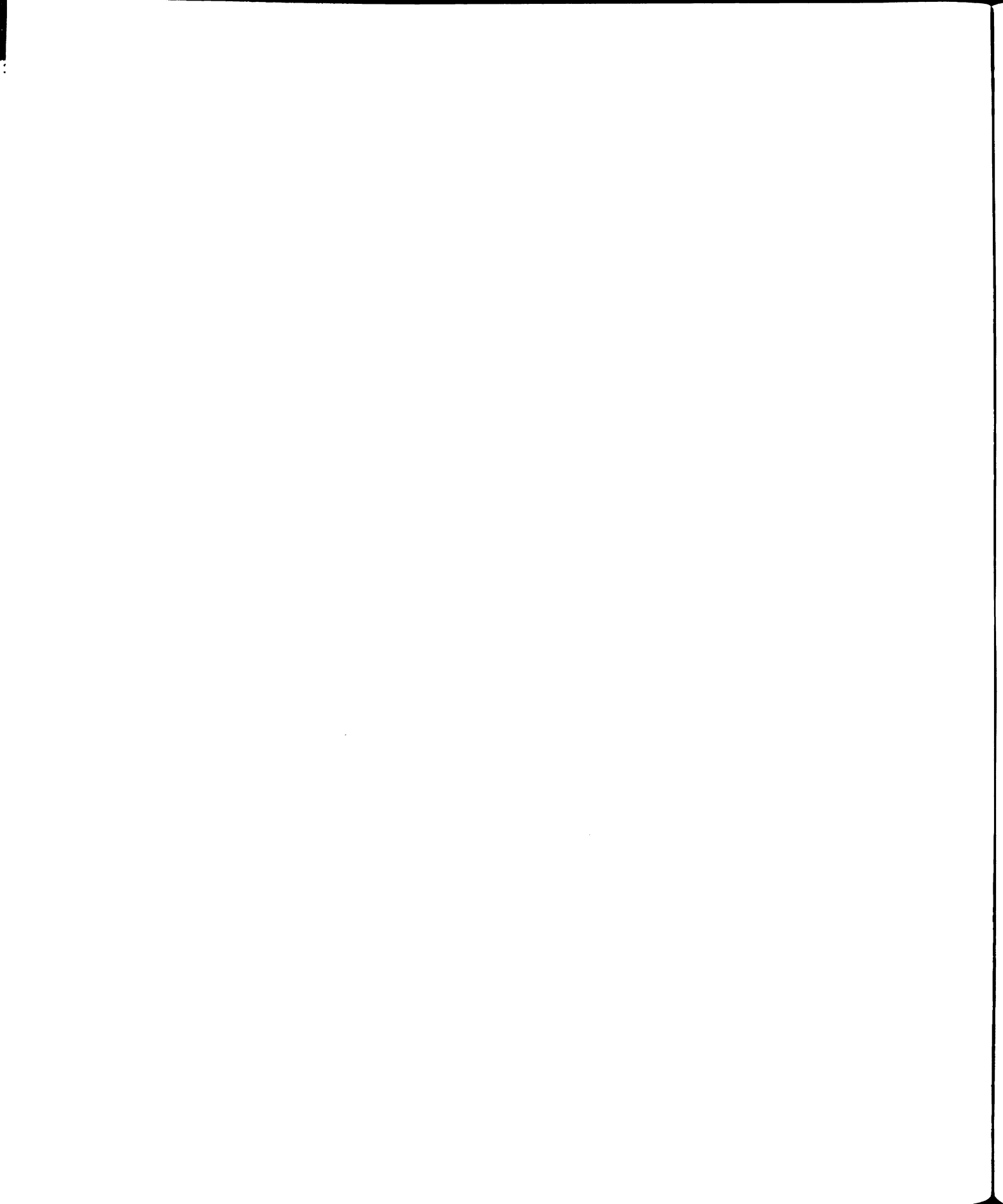
Janezic (2003) presented nondestructive relative permittivity and loss tangent measurements for several dielectric materials using a split-cylinder resonator, which were in good agreement with other methods [47]. Bogle (2004) developed a material characterization measurement technique for highly reflective or lossy material using a partially filled rectangular waveguide [48]. Meeusen (2004) discussed the identification of errors in the extraction of the electromagnetic properties of a material using an X-band waveguide system. In addition, the results showed the factors with respect to the uncertainty of the dielectric properties in terms of permittivity relies on the electromagnetic properties of the material sample [49]. Killips (2004) presented classical mixing approaches to determine effective electromagnetic properties of a two-phase mixture. The same formulations were calculated in relative permittivity with the measured data. However, there were some differences between these parameters due to the interaction between particles that was evident in magnetism [50].

2.8.3 Material

Hoepfner (2001) presented the influence of dielectric permittivity to the microstructure of material, the relative dielectric permittivity and Q factor of the material had a significant variety with different relative density [51].

2.9 Relevancy

Previous research and literature information discussed in this chapter provide valuable hints and relevant measurement procedures for the research conducted in this thesis. It succeeds to the methodology of material characterization and RFID tag readability survey



specified in this chapter. However, due to the different research goals in those research, creative procedures are specified for our purpose in this thesis which describe in Chapter 3 Methodology and other chapters.

Chapter 3

METHODOLOGY

3.1 Introduction

This chapter describes experimental and numerical techniques to extract constitutive dielectric parameters of homogeneous hydrated superabsorbent polymer (SAP) samples placed in a WR340 waveguide using HP8510C vector network analyzer. Furthermore, data acquisition technique was applied to measure power gain near the RFID transponders and RFID tag readability with distinct reader antenna styles and configurations. The hydrated SAP sample was placed in sample window with the thickness 20 mm. The RFID transponder and antenna of power sensor were placed behind the sample.

Testing and measurement procedures, experimental setup, sample preparation, calibration, extraction processing will be explained in the next chapter. The following sections presented the principles of performing the dielectric properties measurement, RFID power measurement and tags readability survey. The results and analysis for hydrated superabsorbent polymer with water content from 55% up to 95% will be reported in the chapter 5 and chapter 6.

There are typically several steps to measure the complex constitutive dielectric parameters:

1. The linear, homogenous and isotropic sample is prepared and placed in the testing equipment.

2. Vector network analyzer (VNA) measures the scattering parameter (S-parameter) with the connection to the testing devices through transmission/reflection technique [52-54].
3. The complex dielectric constitutive parameters in term of permittivity and permeability are able to be extracted from the experimental scattering parameters using an extractor with an iterative complex Newton's root-searching algorithm or the Nicholson-Ross-Weir (NRW) method [48].

In comparing with material characterization, the power measurement and readability survey were pretty straightforward. The sample was placed in a sample window between the interrogator and transponder, with data acquisition program, power sensor and Alien® RFID Gateway. The average power can be acquired from a 2-wire folded dipole antenna (see Figure 3.1) connected to a power sensor, from which was placed in the same location and orientation with RFID transponder behind the sample and saved into a data file by LABVIEW program. Meanwhile, the readability of RFID transponders placed in the same position will be recorded into data file through Alien® RFID Gateway software. Tests were repeated and recorded with different tag orientations, antenna style and distance.

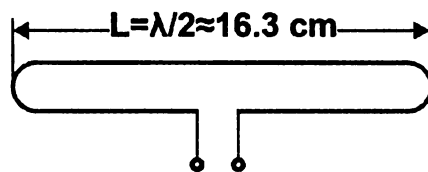


Figure 3.1 Dimension of 2-wire folded dipole antenna [17]

Experimental scattering parameters measurement using NRW technique can rigorously characterize dielectric properties in comparing with these theoretical values [48]. The result of power measurement and instantaneous RFID tag readability on same SAP sample associated with dielectric properties in term of permittivity provide coincident correlation among intrinsic dielectric properties of the substance, average antenna receiving power, RFID tag performance and stability.

3.2 Product Simulation

The dissipation and dispersion of radio frequency energy in material are affected by multiple factors, such as molecular structure, loss tangent and signal frequency. Suppose that linear, physically homogenous isotropic samples in which water concentration is the exclusively variational factor that determines the pattern of component proportion of the sample were existed, meanwhile, the other component in the sample has enough flexibility and network to lodge water content that normal water-water hydrogen bonds were dissociated to form new bonds between water and the other component. If that is the case, whatever water concentration were diversified, the water is free water. Thereby physicochemical properties and electromagnetic absorption spectra of water in the samples are similar to these of free water. That differentiation of dielectric properties in these samples is depending on the water concentration. Obviously, with controlling the hydration process of samples, we would be able to perform measurements of material characterization and differentiate impact by the water content exclusively besides the potential minor effect factors, such as density, hydration time etc. Water in hydrated superabsorbent polymer (SAP) presented these characteristics.

Thereafter, a wide range of products with one independent variable – water content using unique SAP particles can be simulated. The dielectric properties of the new SAP-water mixtures would be similar or near to the food products with which have the same water concentration.

3.3 Measurement Description

The experimental specimens in this thesis were hydrated SAP mixtures. The SAP exhibits large capacity of water absorbency. Due to its crosslinked network structure, SAP is easily mixed with aqueous fluid to puff up long chain structures to lodge the water molecules. Water absorbed by this polymer keeps its physiochemical properties and electromagnetic absorption spectra [40]. Based on these properties, the superabsorbent polymer is low cost and practical material to simulate real products with certain amount of water content.



Figure 3.2 Hydrated SAP mixtures in the sample window

The SAP mixtures with holding 45% to 95% by weight water content were measured, four different trials were performed. The dielectric properties of the mixtures with 55%, 60%, 65%, 70%, 75%, 80%, 85%, 90%, 95% water content respectively were reported in

this thesis. The thicknesses of the samples filled in the waveguide were 12mm and 7mm respectively. (See Figure 4.5) The sample thickness in power measurement was 20mm. the width and length of sample window in power measurement is 170mm*170mm. Figure 3.2 showed the measurement window and sample in the measurement.

Since the dry SAP has a low dielectric constant, very little loss and no magnetic properties. Water is a high dielectric constant material, it was expected while water concentration increasing, the measured permittivity would increase as well. The result is listed in Chapter 6.

3.4 Superabsorbent Specifications

Corn starch/Acrylamide/ Sodium Acrylate Copolymer are classified as starch graft polymer (2-propenamido-co-2-propenoic acid, sodium salt). The commercial name is Water Lock A-100, was packaged in 20 kg multiwall paper bag with polyethylene liner stored in a low humidity conditioning room. Water lock A-100 superabsorbent polymers are tan, free flowing powders can absorb and/or immobilize large quantities of aqueous fluid, at neutral or alkaline pH. More than 98% particle size of the polymer is less than 20 meshes. 1 g of the polymer can lock as much as 175 ml distilled water and 60 ml 1% NaCl solution. The polymer absorbs water and becomes very slippery when wet. The manufacturer is Grain Processing Corporation, Muscatine, Iowa 52761 [55].

3.5 Specimen Preparation

Isotropic and homogenous properties are the basic requirement for the measurement to determine the electromagnetic characteristics. The hydration of SAP particles is the

critical process to form consilient samples. SAP particles tend to puff up rapidly when the surrounding environment is aquatic whereas saturation swelling comes much later [40]. On the other hand, big capacity of water absorption and deficiency of water is a pair of contradictions in making samples in low water concentration. Well-blended sample, uniform density and glabrous surfaces of samples are the major treatment to eliminate the potential sources of error and measurement deviation in the measurement procedures. Particle blender and well-proportioned water supply can make the uniform water and particles distribution. When SAP samples are stored in containers, it is common practice to wrap up the samples and containers to prevent the evaporation of water. Calculation of water concentration in the sample is discussed in the next section.

3.6 Determination of Water Content

When determining the water content in the sample it is important to prevent any loss or gain of water or particles in blending. For this purpose, excessive water supply fluctuations should be avoided. The water content of superabsorbent polymer is determined by the following equation:

$$Wt\% = \frac{m_w}{m_{total}} \times 100 \quad (\text{Equation 3.1})$$

$$Wt\% = \frac{m_{total} - m_{initial}}{m_{total}} \times 100 \quad (\text{Equation 3.2})$$

Where, m_w is the mass of the water, m_{total} is the mass of hydrated superabsorbent polymer mixture. The water content of superabsorbent polymer can be determined

accurately by measuring mass of water molecules present in a known mass of sample. According to the above equations, practically, by measuring the total weight of SAP sample after absorption equilibrium and measuring the total weight of water absorbed, the weight percentage can be calculated, versus versa, the weight percentage can be calculated by measuring the total weight of SAP sample after absorption equilibrium and measuring the initial weight of SAP particles. It assumed that no new bonds formed between water molecules and SAP molecules while water infused in SAP and water is free water in the mixture.

3.7 S-Parameter Measurement

A vector network analyzer (VNA) model HP 8710C operating in the transmission/reflection mode connecting with a WR340 waveguide was used for the measurement of scattering parameters, S_{11} , S_{22} and S_{12} , S_{21} over frequency range from 2.2 GHz to 3.0 GHz with resolution of 4 MHz which covered the frequency allocation of 2.45GHz (S-band) RFID application. A total 201 points were swept over the frequency range. The data were saved in a floppy disk and then transfer to PC. Figure 4.1 to Figure 4.8 showed the VNA, waveguide, calibration set, sample holder, sample filled in holder and signal transmission and reflection diagrams. The experimental results showed the frequency responses vs. S_{11} , S_{22} and S_{12} , S_{21} respectively in Chapter 5. These figures presented that water concentration is a suitable parameter for SAP dielectric characterization in term of permittivity, since the responses are well defined and visibly apart for SAP samples with 55%, 60%, 65%, 70%, 75%, 80%, 85%, 90% and 95% of water content from 2.2GHz to 3 GHz in the measurement.

3.8 Power Measurement

The objective of power measurement was to determine the effect of highly lossy water on the RFID readability. A 2-wire dipole antenna connected to a power sensor and placed on the backside of the sample window captures the RF signal radiated from the RFID reader that was placed on the other side of the sample window. Besides the sample window, the two sides were separated by the Aluminum shield template. Presumably, the only path for RFID signal radiating was the sample window. The power level comparison of the shielded area and unshielded area is listed in chapter 6.

Alien® circular and linear reader antennas were in measurement. Fourteen locations were measured at the distance of 1cm, 5cm, 10cm, 15cm, 20cm, 25cm, 30cm, 35cm, 40cm, 45cm, 50cm, 55cm, 60cm and 65cm respectively. Two kind of tag orientation, horizontal to reader antenna and vertical to reader antenna were measured. The results are listed in chapter 6.

3.9 Readability Survey

The Alien squiggle UHF RFID tags were placed in the same location with the antenna of power sensor. Theoretical, the transponder in that location and the receiving antenna of the power meter were radiated the same level of RF power from the reader antenna that located in the other side of the sample window. Two antennas have different radiation power conversion efficiency η [17]. However, normalized power reads from power sensor were equivalent to the received power of the transponder antenna at the same location, incurred in the same time and with the same orientation. Under the circumstance, the readability of the RFID tag with corresponding configuration and the power reads

showed some correlation and intrinsic relationship. Therefore, a consistency model could be profiled by linking these measurements.

Chapter 4

MATERIAL CHARACTERIZATION

4.1 Material Characterization

Network analysis technique involves the measurement of incident, reflected and transmitted electromagnetic waves that pass through the transmission medium. For fully characterization of a linear network, it is necessary to measure both magnitude and phase of components.

Vector network analyzer (VNA) system measures the magnitude and phase characteristic of network and of components. VNA and a closed waveguide, which measure S-parameter are commonly used instruments for the measurement of dielectric properties and material characterization [56]. The S-parameters are measured with constitutive parameters may be determined using the NRW experimental technique. According to Nicholson-Ross-Weir (NRW) technique, the sample under the measurement should be linear, isotropic homogenous samples with parallel front and back surfaces [48]. In this thesis, the SAP specimens infused with variable water content measured in the frequency range of 2.2GHz~3.0GHz using a WR340 waveguide were subject to the restriction. In the measurement, scrupulous preparation process and stringent physical treatment method were taken to improve the accuracy of measurement.

4.2 Measurement Equipment

4.2.1 Vector Network Analyzer

Network analyzer measures the magnitude and phase characteristic of material under testing (MUT). The basic principle of network analyzer is simple. Signal source controlled by the network analyzer generates an incident signal and applies to the test network and component. The network analyzer contrasts the reflected signal from the MUT or the transmitted signal through the MUT.

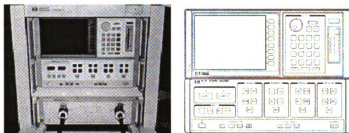


Figure 4.1 HP-8510C Network Analyzer and panel block (Courtesy of Agilent Corp.)

4.2.2 Waveguide

The WR340 waveguide (where WR stands for “waveguide rectangular” and 340 refer to the inner waveguide dimension 3.4 inches) has low attenuation, good operational bandwidth for single-mode propagation and good mode stability [57]. Below the designated frequency range and cutoff frequency, attenuation of waveguide augments quickly tending to infinity. Waveguide material is aluminum or brass (copper alloy). The detail specification is listed in Table 4.1.

The cutoff frequency of the waveguide is given by:

$$\text{Lower: } f_{\text{cutoff}} = \frac{c}{2a} = \frac{2.9979 \times 10^{10} \text{ cm/s}}{2 \times 2.54 \times 3.4 \text{ cm}} \approx 1.736 \text{ GHz}, \text{ Upper: } 2 \times f_{\text{cutoff}} \approx 3.47 \text{ GHz}$$

where, a is the length of cross section (see Figure 4.2 right) and c is the light speed.

Designation	Freq. Range	Cutoff Freq.	Guide Wavelength	Inside Dimension	Wall Thickness
WR340	2.2-3.3 GHz	1.736 GHz	6.83 in	3.40*1.70 in	0.08 in

Table 4.1 WR340 waveguide characteristics [23]

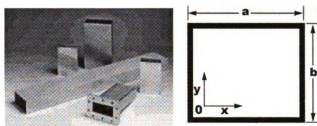


Figure 4.2 WR340 waveguide components and cross section (Courtesy of Penn Engineering Components)

4.3 Experimental Setup

The instruments and experimental setup of electromagnetic characterization of the hydrated SAP sample were shown in Figure 4.1–Figure 4.4. A WR340 waveguide was connected to an HP 8510C Vector Network Analyzer via coaxial cables (See Figure 4.3). The brass waveguide sample holder used to measure the S-parameters is shown in Figure 4.4. The thickness of sample holder is 1.0 inch. The sample holder is connected to the waveguide WR340 with eight precision alignment screws to minimize the discontinuities across the interfaces and reduce the uncertainty measurement errors. The brick base should be in the same ground plane to ensure two waveguide sections to be placed in the

same horizontal plane. The coaxial cables must be spatially stabilized without any movement while calibrating and measuring samples (See Figure 4.3).

Before measuring any test sample, a standard baseline was checked to further validate the experimental setup. After performing the calibration, the two waveguide sections were placed together and the magnitude and phase of the S-parameters was checked to ensure that $s_{21,12}^{\text{exp}} \approx 1 - j0$ and $s_{11,22}^{\text{exp}} \approx 0 - j0$. Meanwhile, an extraction was performed on the S-parameter measured from the empty sample holder to ensure a free space baseline for the system.

4.4 Calibration Processing

Imperfection of test equipment and test procedures leads to systematic errors. In radio frequency network measurement, systematic error is the most significant factor of measurement uncertainty [49]. Systematic error is unable to be removed from measurement. We can characterize and eliminate the systematic errors through calibration procedures and mathematical model optimum during the measurement process. Repeatable systematic errors will be greatly reduced and the accuracy of calibration standard will be able to transfer to the measurement of the device through standard calibration procedure [58].

The process of eliminating uncertainty at S-parameter measurement within the network analyzer and waveguide system was named as measurement calibration. Some special procedures and scrupulous considerations for calibration and measurement must be performed using network analyzer to acquire accurate data. The required and common calibration and measurement techniques used in a HP8510C vector network analyzer

were discussed in this chapter. The frequency range of WR340 waveguide system is 2.2GHz to 3.3 GHz, sweeping frequency range in the measurement was 2.2 GHz to 3.0 GHz; hence, the frequency span was 0.8GHz.

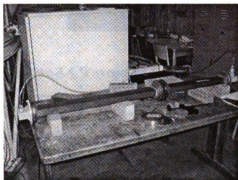


Figure 4.3 VNA and WR340 waveguide set-up

4.5 Measurement Calibration

Transmission and reflection measurement general utilize vector accuracy enhancement technique to cut down the systematic errors and remove error contributions. The basic steps of the calibration techniques:

1. Measuring the magnitude and phase response of standard device.
2. Estimating model coefficients in the measurement system with measured data from step 1.
3. Measuring a test device.
4. Computing the actual test device response with vector mathematics. [56]



Figure 4.4 Waveguide sample holder

4.6 Calibration of Network Analyzer

There are different calibration types available for transmission measurements: response calibration, response and isolation calibration, one-path 2-port calibration, 2-port calibration. These types differ in accuracy or in the type of errors they remove as well as what type of measurement is required [56]. The measurement calibration process for HP8510C VNA must be one of seven types: Response, Response & Isolation, S11 1-port, S22 1-port, One Path 2-Port, Full 2-Port, TRL 2-Port. Which process should be selected depends on the accuracy desired and the device to be measured [56].

4.6.1 One-path 2-Port Calibration

This model provides fully corrected transmission and reflection measurements for a reflection/transmission test set. It uses a thru, a shielded open circuit, a short circuit, and loads to calibrate at Port 1. The operator follows instructions displayed on the CRT to manually reverse the test device for measurement of the reverse parameter.

4.6.2 Full 2-port and TRL Calibrations

This model provides fully corrected transmission and reflection measurements with an S-parameter test set. The Full 2-port typically used a thru, a shielded open circuit, a short circuit, and loads to calibrate at Port 1 and Port 2. The TRL 2-port technique uses a thru, short, isolation loads, and a precision transmission line. Multiple 2-port calibration is used in the procedure for measurement of noninsertable devices.

4.6.3 Full 2-Port Calibration

Applying the standard from the calibration kit to both ports in the procedure, the response of each standard is defined and then adjusted into standard classed that correspond to the error model in the device, in our case, used by HP8510C VNA, three known impedance reference and a single transmission standard are required. The accuracy depends on the accuracy of the equipment, how well the standard are modeled and the exactness of the error correction [58].

4.6.4 TRL Calibration

TRL calibration refers to the three steps in the calibration procedure:

- 1) THRU: direct connection of both ports or with a short piece of transmission line.
- 2) REFLECT: connect identical one-port high reflection coefficient devices to each port.
- 3) LINE: insert a short length of transmission line within both ports.

In TRL calibration, a zero length thru used as THRU, a zero offset short, a piece of WR340 waveguide blanking plates used as REFLECT and an existing WR340 waveguide standard section used as LINE.

4.6.5 TRL Calibration Procedure

- 1) THRU: set center frequency (2.2~3.0 GHz), frequency span (0.8 GHz), number of points (201) and averaging if necessary in HP8510C VNA front panel (see Figure 4.1). Press (a) Cal. (b) WR340 – TRL. (c) TRL 2-port. (d) THRU, TRL, THRU.
- 2) REFLECT: Disconnect junction of WR340 waveguide straight pieces and connect a WR340 blanking plate to each waveguide piece (See Figure 4.5). In front panel, Press: (a) S11 Reflect, TRL Short. (b) S22 Reflect, TRL Short. (c) Isolation. (d) Omit Isolation. (e) Isolation Done.
- 3) LINE: Disconnect both WR340 waveguide blanking plates and connect the standard section between both waveguide straight pieces. In front panel, Press: (a) line/match, LINE 14.9. (b) Save, TRL 2-Port. (c) Select **cal** set.

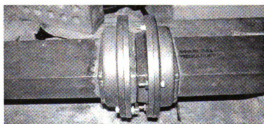


Figure 4.5 WR340 standard calibration line section

- 4) Procedure done. Now, the system has been calibrated and ready to use.

- 5) Calibration procedure should be done before the measurement starts. In both calibration and measurement processes, minimizing the cable and device movement as much as you could until all the calibration and measurement has been completed.

4.7 S-Parameters Measurement Procedure

Samples were measured using a rectangular waveguide operating in the principal TE_{10} mode. Summarized measurement procedure provided to show how to measure the S-parameter and save to a data file on the HP8510C VNA.

- 1) Power on the HP8510C and perform calibration process as we described in the measurement calibration.
- 2) Prepare the hydrated SAP specimen and place the desired specimen into the sample holder section of WR340 waveguide (see Figure 4.4). The sample must be homogenous and glassy on the both surfaces. Sample thickness should be less than 12 mm due to restriction imposed by the inversion process. Scrupulous filling the SAP sample into the sample holder and make sure 100% fulfilled in the cross section.



Figure 4.6 SAP specimens in the wrap

- 3) From the VNA front panel (see Figure 4.1), Press the **menu** button from the stimulus menu section. Press **more** from the display menu list. Select **single** at the display menu list. This procedure measures four S-parameters simultaneously.
- 4) Press the **disc** button on the front panel of HP8510C and insert a disk into the HP8510C, now the data file saves to a disk and is able to transfer to a computer in which the FORTRAN Extractor installed.
- 5) Pick **store** from the display menu list, select **memory** from the display menu list.
- 6) Use the control wheel and the select letter key, input the file name.
- 7) Select the **store file** from the display menu.
- 8) Pull out the sample from sample holder and reload a new sample and repeat the complete procedure until all the specimens have been measured.

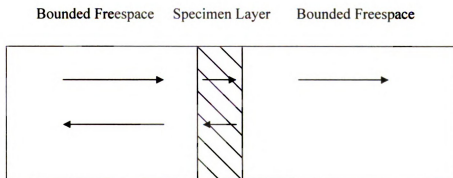


Figure 4.7 Transmission and reflection of signals: side view of waveguide with specimen layer

4.8 Validation of Measurements

Calibration process minimizes the systematic errors; however, measurement results have deviation due to the imperfection of samples and other factors, such as temperature,

- b. Initial value input
- c. Acquire saved data file
- d. Computation
- e. Output extracted data file.

Initial values and steps include:

1. Fraction D/A: 0.999
2. Number of modes: 1
3. Number of frequency points: 201
4. Estimated initial values: $\text{Re}(\mu)$, $\text{Im}(\mu)$ and $\text{Re}(\varepsilon)$, $\text{Im}(\varepsilon)$
5. Enter input filename and path
6. Enter output filename and path.
7. Run.

That transmission/reflection method with Newton's iterative algorithm extracts the complex permittivity avoids the frequency instability usually found in the process of solving the complex constitutive parameters. The extraction process requires the estimation of initial values for the real and imaginary parts. In many cases when the estimated initial value does not approach the corresponding calculated values of ε and μ , the extraction computation would be suspended since convergence is not guaranteed. If that is in case, iterative augment or reducing the initial values is appropriate. In the extraction, the foregoing successful extracted values were good hints to estimate the next initial values because the regular dielectric properties of hydrated SAP specimens presented considerable effect of water content. It reveals that in frequency range from 2.2GHz to 3.0GHz, it is possible to have clearly estimation according to water

concentration in different SAP samples. The extracted constitutive parameters were shown in Chapter 6.

Chapter 5

POWER MEASUREMENT AND READABILITY SURVEY

5.1 Introduction

Power is energy per unit time or energy transfer rate. For radio frequency applications, the unit time is averaged over many periods. Average power measurement on pulsed RF modulation signals can be measured with power sensor [60]. The received power level of the tag is the exclusive energy to activate the tag IC and reflect digital signal to the reader. Acquiring the power level on the transponder is the key for understanding the effect of RF power attenuation by the SAP specimens beyond the regular path loss.

The goal of power measurement was to determine the effective power from the RFID reader antenna after path loss and receiving power by the RFID antennas in a certain location. The basic strategy for power measurement was to place a dipole antenna connected to power sensor at the same location as that of the tag. Due to difference of the impedance, area and power conversion efficient, the tag antenna and dipole antenna of power sensor receive different power levels; however, the ratio of both power reads is a constant. Therefore, the normalized power reads of power sensor can be considered as the power of tag received.

5.2 Experimental Equipment

5.2.1 Power Sensor

The R&S® NRP-Z22 power sensor is a smart standalone device that communicate with the basic unit or a PC via a USB port. The power sensor with nominal powers of 2 W in the frequency range from 10MHz to 18GHz, include 90 dB dynamic range are suitable for RFID RF signals measurement. Sensor type is 3-path diode sensor with preceding power attenuator in stationary and periodically modulated signals. There are four measurement functions: continuous average, burst average, timeslot, and scope for recurring waveforms. (See Table 5.1) In non-recurring waveforms, there is one measurement function: scope. Default sampling frequency is 133.358 kHz. For lower frequency at 100 kHz to 1M Hz, sampling frequency reduces to 119.467 kHz to prevent aliasing.



Figure 5.1 Default data acquisition interface for power sensor

Figure 5.1 showed the default power meter interface. Power units can be shown as W, mW, nW, dB. Measurement Resolution is 1dB, 0.1 dB, 0.01dB, 0.001dB, depends on the

requirements of the measurement. Power reads acquired can be logged as a data file in PC for further processing. The default interface for power sensor is simple and easy to use.

Measurement Mode	Range
Continuous Average	200 pW~200mW (-67dBm ~+23dBm)
Burst Average	200nW ~200mW (-37dBm~+23dBm)
Time Slot	650pW ~200mW (-62dBm~+23dBm)
Scope	10nW to +23mW (-50dBm~+23dBm)

Table 5.1 Power measurement range

5.2.2 Calibration

Uncertainty

The uncertainty comes from level, temperature and frequency influences that are impossible to eliminate in a power sensor. The specifications of uncertainty in R&S® NRP-Z22 power sensor are based on the assumption that the measurement follows each other so fast that the temperature of the pad does not change significantly. S-parameter correction and frequency response correction are the basic calibration processes to eliminate the systematic errors.

S-parameter correction

Standard number of frequencies parameters is from 1 to 1000, for S_{11} , S_{21} , S_{12} , S_{22} calibration data was saved in an s2p format. When performing the calibration procedure, the standard file should be imported into the program.

Frequency response correction

Carrier frequency is the center frequency (915MHz), the calibration factor is relevant for the test frequency, $0.05 * f$ (below 1 GHz) for specified measurement uncertainty, therefore, permissible deviation from actual value 46MHz ($0.05 * 915\text{MHz}$) [61].

Average Power and Measurement time

The average power is equal to RMS value of power in the certain time slot. At the continuous average mode, is $N * (\text{duration of measurement widow} + 0.2 \text{ ms}) + t_z$. At buffered without averaging mode, is $\text{buffer size} * (\text{duration of measurement window} - 0.5 \text{ ms}) + t_z$. At burst average mode, $(2 \text{ to } 4) * N * \text{burst period} + t_z$. At timeslot and Scope mode, is $(2 \text{ to } 4) * N * \text{trigger period} + t_z$. $T_z : < 1.6 \text{ ms}$ (0.9 ms on average), if averaging is activated, the average factor determines the number of measurement windows to be averaged [61].

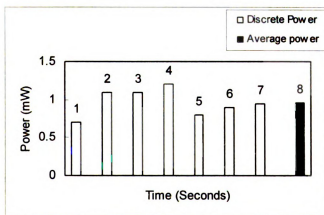


Figure 5.2 Average power measurement

5.2.3 2-Wire Folded Dipole Antenna

To detect the RF signal and measure the radiated power from a reader antenna at the tag location, 2-wire folded dipole antenna which was parallel connected two half wave long ($l = \frac{1}{2}\lambda$) lines at a very small apart had been made in the laboratory (see Figure 3.1).

The length of the 2-wire folded dipole antenna was about 16.4cm equal to half of the wavelength (915MHz), $l = 1/2\lambda = c/f = 1/2 * 3e8/915e6 = 16.4\text{cm}$. The antenna Gain of 2-wire folded dipole is 1.64 or 2.15dBi. Actual gain could be a little less due to resistive losses.



Figure 5.3 Two-wire folded half-wavelength dipole antenna of power sensor

5.2.4 RFID Equipment

The RFID testing equipment used for this thesis was from Alien Technology. The passive RFID system was operating in 902-928MHz UHF ISM band. The transponders used in the test were Alien Squiggle Class 1 Gen 2 tags (See Figure 5.4). The antennas were circular or linear polarization, antenna gain is 6dBi. The antenna served as both sender and receiver. Alien RFID Gateway v.2.12 was used in the readability survey. Two host PCs were used in the test. One hooked-up RFID system with Intel Pentium II 300 and Windows XP sp1. The other HP Laptop hooked-up Power sensor with Window XP SP2.

RFID system was connected by serial port. Reader antennas were connected with coaxial cables.

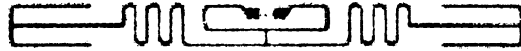


Figure 5.4 Alien Squiggle ALL-9338 RFID tag (Courtesy of Alien Technology)

5.2.5 Virtual Power Meter Configuration

There are a number of ways to measure the RF power, including the use of power meter [60]. In our approach, an R&S NRP-Z22 standalone smart power sensor directly connected with PC via USB port was used to measure power near the transponders radiated from the RFID reader. The 2-wire folded dipole antenna places on the same location with transponders. The power reads of power sensor from the antenna were considered as normalized power of the transponders at that location. Distance, tag orientation and reader antenna styles associated with water content were alternated to measure and differentiate the influence of these combined conditions to power decaying and readability within RFID system. These measured results were compared to each of the measurement setup; the results presented in chapter 6. A virtual control program based on LabVIEW for the R&S NRP-Z22 was developed. (See Figure 5.5)

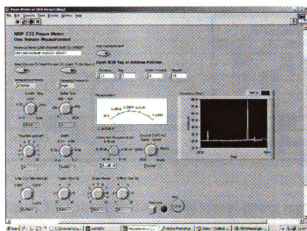


Figure 5.5 Program interface of virtual power meter for R&S® NRP-Z22 power sensor

5.2.6 LabVIEW Programming

LabVIEW, graphic development platform for virtual instrument by National Instrument, TX, USA, is the leading graphic development environment (GDE) for testing and measurement with built-in functionality for data acquisition, instrumental control, measurement analysis etc advanced features [62]. With the help of R&S LabVIEW development library, many new control features and automation functions can be developed in LabVIEW platform, which enhanced the application and convenience of power sensor. Figure 5.6 showed the LabVIEW diagram for R&S NRP-Z22 power sensor. In comparing with the default virtual power meter program, the customized virtual power meter provides automatic data saving, data conversion and instantaneous indication and graphing. More measurement modes could be easily switched as the measurement needed.

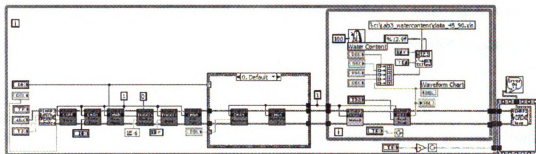


Figure 5.6 LabVIEW diagram of virtual power meter

5.3 Receiving Antenna Placement

In a RFID System, conductive antenna coil of a transponder is a key component to receive the RF signal and power on the passive RFID tag. Meanwhile, it can reflect RF signal from the transponders to the reader antenna [21]. The RF energy path loss, absorption and obstructions by media between RFID reader and tags lead to reduced tag readability. Some research suggest, using multiple antennas in a portal system enhances the coverage and improves the readability [10]. All the steps facilitate the transponders receiving the enough energy; however, how much energy may the tag can be received and how much was lost in the path? The dipole antenna to power sensor measured this parameter.

In the measurement, the 2-wire folded dipole antenna was pasted on one side of the hydrated SAP specimen and a reader antenna was placed on the other side. The reader antenna was moveable. The distance between reader antenna and tag antenna was 1cm, 5cm, 10cm, 15cm, 20cm, 25cm, 30cm, 35cm, 40cm, 45cm, 50cm, 55cm, 60cm, and

65cm respectively. According to the tag orientation, rotating the receiving antenna of power sensor was repeated and the power level was measured and recorded in data files.

5.4 Aluminum Shielding

Radio frequency signals are susceptible to shield by aluminum or other metal obstructions. A large aluminum template obstruction ($200\text{cm} \times 200\text{cm}$) with a rectangular open window ($17\text{cm} \times 17\text{cm}$) to admit the RF signal transmission was placed between the RFID reader antenna and receiving antenna. In free space, theoretically, signal strength and distance indicate an inverse square relation in the far-zone, which was referred in Chapter 2.

The following graph (Figure 5.7) indicates a diagram of the components involved with experimental setup of power and readability measurement. The Alien RFID reader antenna (Circular and Linear) and tag antenna shown in graph were movable components according to measurement procedures.

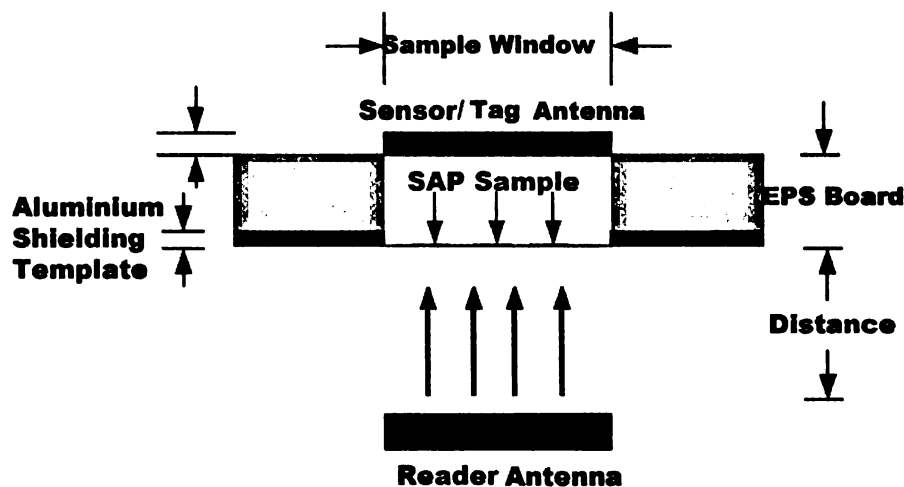


Figure 5.7 Experimental setup of power measurement and readability survey

5.5 Measurement Deviation

Calibration is necessary to achieve the accuracy of power meter, even if the power sensor was factory calibrated. Before each measurement, a standard calibration procedure should be performed due to the uncertainty attributed to different sources. In general, the power meter is very sensitive and accuracy after performing standard procedure; however, the radiated power level of reader is not stable. Graphs in Figure 5.8 to Figure 5.12 illustrated the standard deviation of power was variance in the measurement. Measurement experience presented reader antenna powered up time, antenna position displacement, cables mobility, even the experimental personnel's body in the measurement might affect the measurement results. Figure 5.8 showed the measurement result at a typical setup. The first 800 reads have a relative low undulation. After that, the power reading tended to larger deviation instead of tranquilization. Standard deviation of first 800 reading is 0.00000019 and the standard deviation of next 400 reading is 0.00000020.

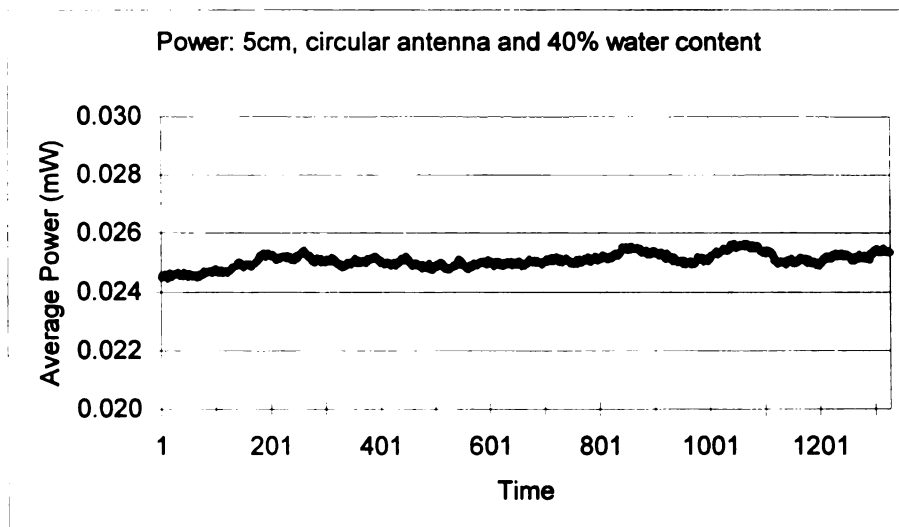


Figure 5.8 Periodical fluctuation of discrete average power reading

Figure 5.9 to Figure 5.11 showed three kinds of different deviation situation in power measurement with a vertically polarized antenna. Table 5.2 showed the mean, standard deviation of each data group. Situation b showed a continuous decline result, the standard deviation in that category was larger than other two situations. Thereby, in the real measurement, though the standard calibration procedure had been performed, the measurement was not as accurate as it should be. The strategy is to avoid the situation b, sometimes measure the power again whenever the situation b occurs.

	N	Minimum (dB)	Maximum (dB)	Mean (dB)	Std. Deviation
a	10	-32.33	-32.22	-32.2690	0.03635
b	10	-15.28	-14.87	-15.0660	0.13922
c	10	-26.53	-26.23	-26.3950	0.09733

Table 5.2 Descriptive statistics of measurement deviation

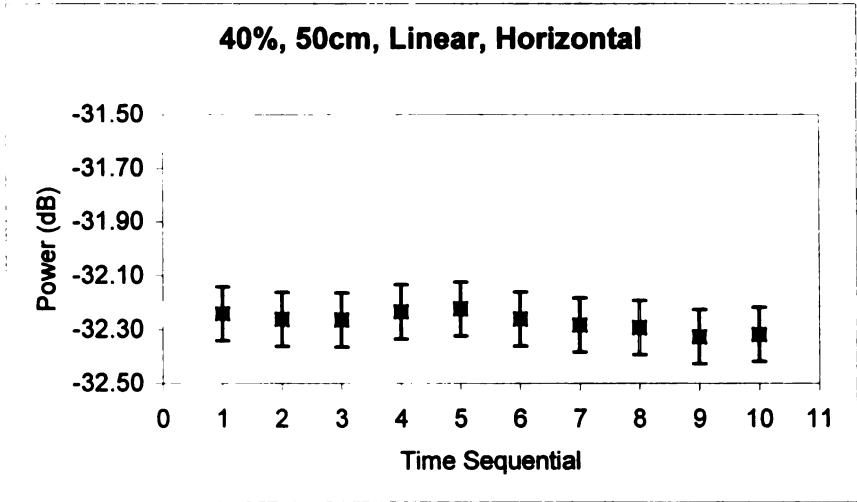


Figure 5.9 Stable average power in measurement

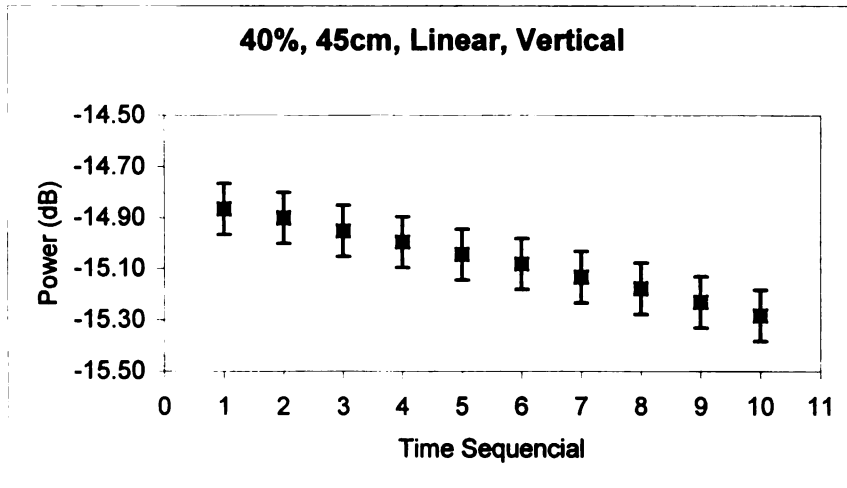


Figure 5.10 Continuous decline or incline deviation in power measurement

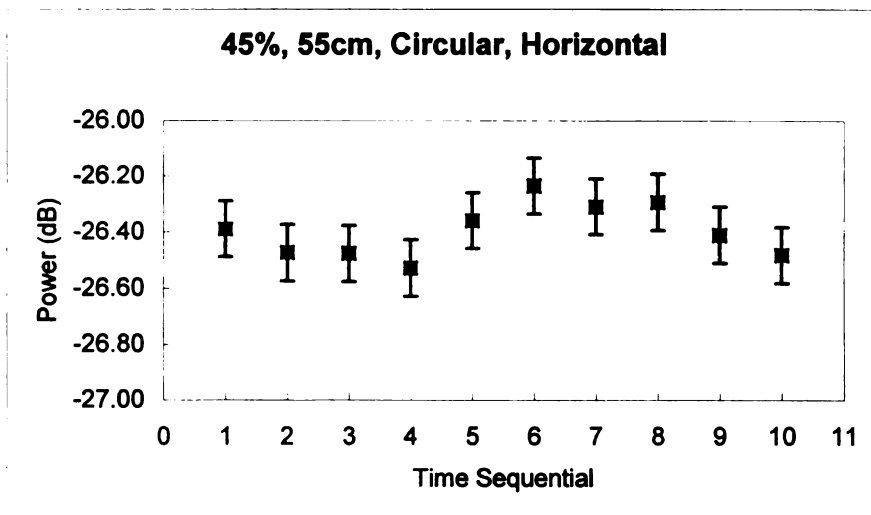


Figure 5.11 Undulation in power measurement

In each of situation, a visible deviation was presented in the Figures 5.9-5.11. However, comparison of these three situations in one graph, the line in each of situation showed a pretty consistency measurement (see Figure 5.12). Obvious, the accuracy is really depending on what accuracy you need in the measurement.

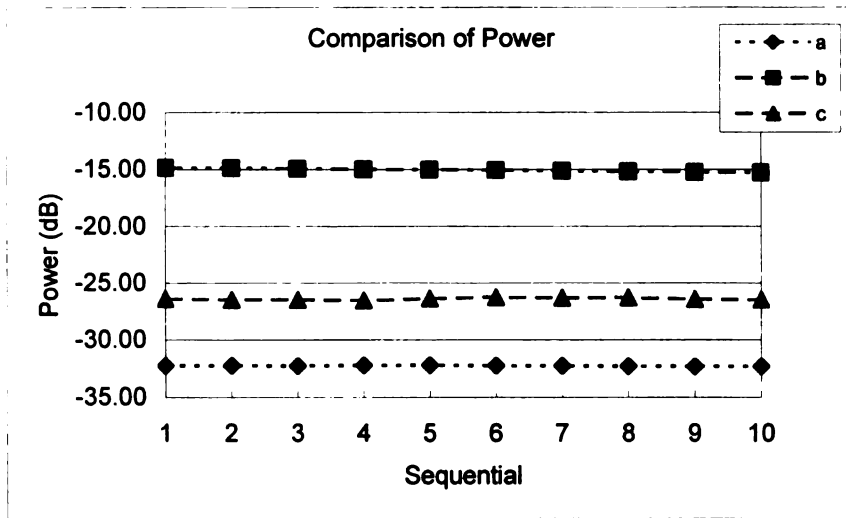


Figure 5.12 Comparison of measurement accuracy

5.6 Power Measurement Procedure

- 1) 100% fill the desired hydrated SAP specimen into sample window. Other requirements are the same as in the waveguide measurement (see Chapter 4).
- 2) Place the 2-wire folded dipole antenna at the same location as the transponders pasted.
- 3) Move the reader antenna to desired distance. Change the antenna style according to measurement (circular and linear).
- 4) Make sure the sample window, both reader and dipole antenna are parallel and the center of the components located in one straight line.
- 5) Open power meter program in LabVIEW.
- 6) Input the initial values of the measurement in power meter, such as distance, antenna style, water content, tag orientation etc.

- 7) Run the power meter and watch the discrete power reading graph when the curve is stable, then start to log the measurement into a data file.
- 8) Change the measurement configuration and repeat the measurement.

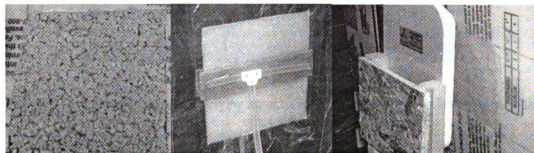


Figure 5.13 Hydrated SAP specimen, dipole antenna connected with power meter and reader antenna in the other side of sample window

5.7 Readability Survey

After the power measurement procedure, removing the power meter antenna and replacing Alien squiggle RFID tags in the same location for 100 reads using Alien RFID Gateway (See Figure 5.13 and Figure 5.15). Recording the total successful reads in a spreadsheet. Moving the RFID Reader back and forth what is the same procedure as the power meter measurement. The distance between RFID tag and Reader is from 2 cm to 67 cm in step of 5 cm respectively. Keep moving the reader antenna outward as far as the RFID reader does not response to the tags. The results of readability were reported in chapter 6.



Figure 5.14 Power sensor and receiving antenna in one side, mobile reader antenna in the other side



Figure 5.15 Alien RFID Gateway for readability survey

5.8 Antenna Orientation

A significantly different performance can be attained by optimizing tag orientation in accord with the polarization of the readers and combining dual polarized reader antennas as a circular antenna in practical RFID implementation. The 2-wire folded dipole antenna is a linear polarized antenna that RF energy transmits from one linear antenna to another linear antenna is more preferable while both of antennas are co-polarized direction. However, if the pair of linear antennas are vertical polarized to each other (90° or 270°),

approximate 20dB extra damping would be lost due to polarization losses. In the real measurement, about 15dB loss was observed due to tag orientation (vertical and horizontal), see Figure 5.16. According to Rothammel's research, only 1/100 of the normal power could be received from the radiated electromagnetic field [17]. However, combining two linear polarization antennas in form of a circular antenna which reduces the polarization losses to 3 dB [17]. Measurement was performed in multiple configurations among linear and circular reader antennas, tag and receiving antenna orientations (vertical/horizontal). The results are reported in Chapter 6.

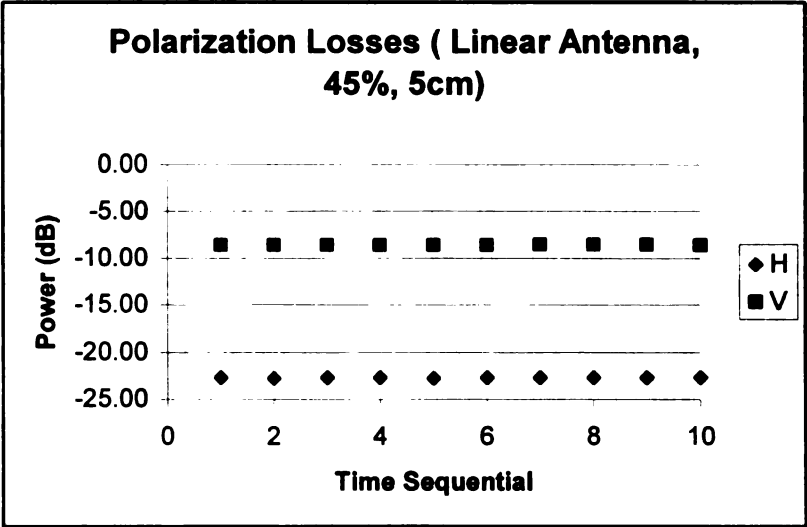


Figure 5.16 Polarization losses in a linear reader antenna

Chapter 6

RESULTS AND DISCUSSION

The purpose of this chapter primarily deal with the experimental S-parameters, derived permittivity from experimental result and radiated power received by power sensor near the RFID transponders, along with tag readability using different configurations. All the experiments in this thesis were performed on the equipment described in the proceeding chapters. Experimental dielectric properties of saturated SAP mixtures imply that permittivity is the critical parameter to differentiate the influence of water content in SAP samples on RFID performance and stability. Meanwhile, effective radiated power measured by power sensor near RFID tags presented a straightforward influence factor and indicated logarithm correlation on distance. Consequently, identified correlations between water content and tag readability were created based on the affiliation of permittivity, power, water content and readability using precise measurement methods and data acquisition technique.

6.1 S-Parameters

According to transmission/reflection method and computation technique based on iterative Newton's root searching arithmetic [48], 11 saturated superabsorbent polymer (SAP) mixtures with different water content, 45%, 50%, 55%, 60%, 65%, 70%, 75%, 80%, 85%, 90% and 95% respectively were measured over the frequency range of 2.2 GHz to 3.0 GHz at room temperature (68°F). The calibration and measurement procedure were presented in the Chapter 4.

Figure 6.1 shows incident waves (a_1 , a_2), reflected waves (b_1 , b_2) and S-parameters in a typical two-port network. The below linear equations describes definition of S-parameters,

$$b_1 = S_{11}a_1 + S_{12}a_2 \quad (\text{Equation 6.1})$$

$$b_2 = S_{21}a_1 + S_{22}a_2 \quad (\text{Equation 6.2})$$

Input reflection coefficient $S_{11} = \left. \frac{b_1}{a_1} \right|_{a_2=0}$, Output reflection coefficient $S_{22} = \left. \frac{b_2}{a_2} \right|_{a_1=0}$

Forward transmission gain $S_{21} = \left. \frac{b_2}{a_1} \right|_{a_2=0}$, Reverse transmission gain $S_{12} = \left. \frac{b_1}{a_2} \right|_{a_1=0}$ [63].

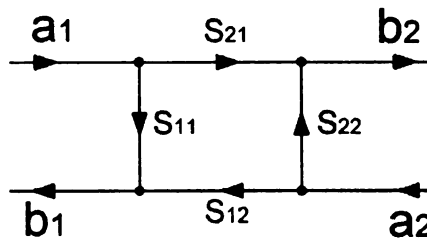


Figure 6.1 The diagram of incident waves (a_1 , a_2), reflected waves (b_1 , b_2) and S-parameters in a typical two-port network [63]

The following graphs (figures 6.2 to Figure 6.22) were created based on the experimental result of S-parameters measurement acquired from HP8510C VNA. The thicknesses of hydrated SAP specimens (see Figure 4.4) were 12mm and 7mm in two independent trials. In most graphs, S-parameters showed a small fluctuation with frequency increasing. water content in high frequency has larger influence to S-parameters.

1. Input reflection Coefficient:

The real part of S11 increases with the frequency increasing, on the contrary, the imaginary part of S11 decreases. Higher water concentration in thinner samples (7mm) shows faster increasing in real part of S11,

2. Output reflection coefficient

Both real part and imaginary part increase with frequency increasing, water content is a major influence, higher water concentration, faster increasing.

For ideally lossless dielectric substance, the magnitude of S11 ($= \frac{b_1}{a_1} \Big|_{a_2=0}$) and

S22 ($= \frac{b_2}{a_2} \Big|_{a_1=0}$) are equal [63]. However, they can deviate from one another whenever

loss is presented.

Figure 6.2 showed that input reflection coefficient (S11) in hydrated SAP mixture with 70% water content has a linear relationship with frequency. However, in homogenous samples, the thickness is another major influence to S11. The slope of 7mm sample was larger than that of 12mm sample. Consequently, the deviation may be occurred in different trials due to sample thickness, density etc. Figure 6.3 showed that output reflection coefficient (S22) at SAP mixtures with 55% water content has a linear relationship with frequency. However, the same reason as we mentioned, in homogenous samples, sample preparation as such thickness is major influence to S22. The slope at 7 mm SAP sample was larger than that of 12mm sample. In the ideally substance, S11=S22. However, the hydrated SAP mixtures in the experiments presented a lossy characteristics. S11 showed the linear relation over the frequency range, in different trials

with same water content, 7mm sample had a larger slope and 12 mm sample had a larger slope in the graph. S22 showed the same property as S11.

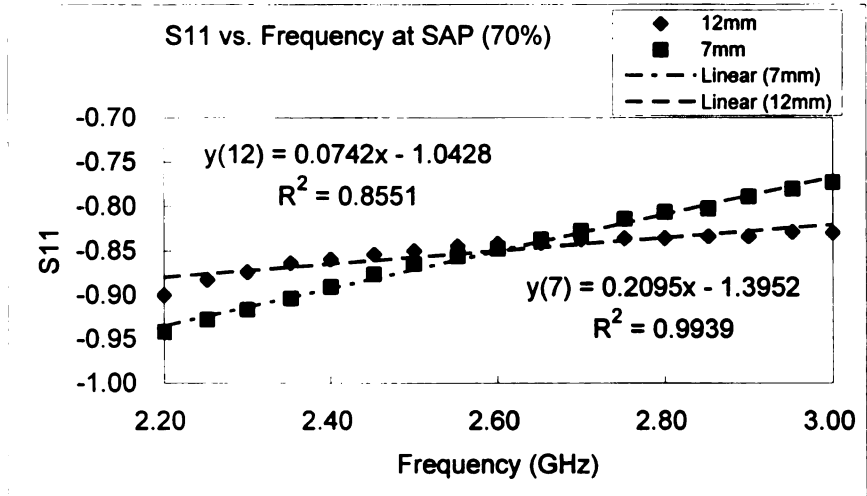


Figure 6.2 Comparison of S11 in SAP specimen with 70% water content

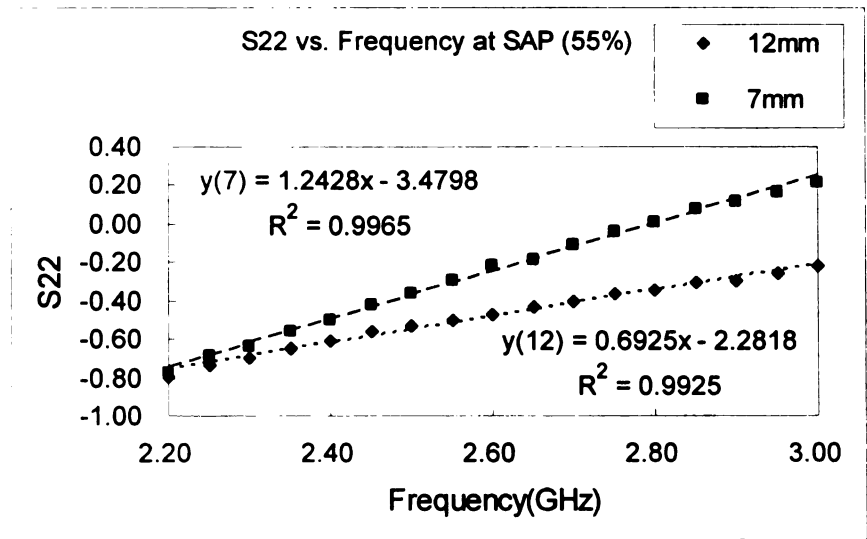


Figure 6.3 Comparison of S22 in SAP specimen with 55% water content

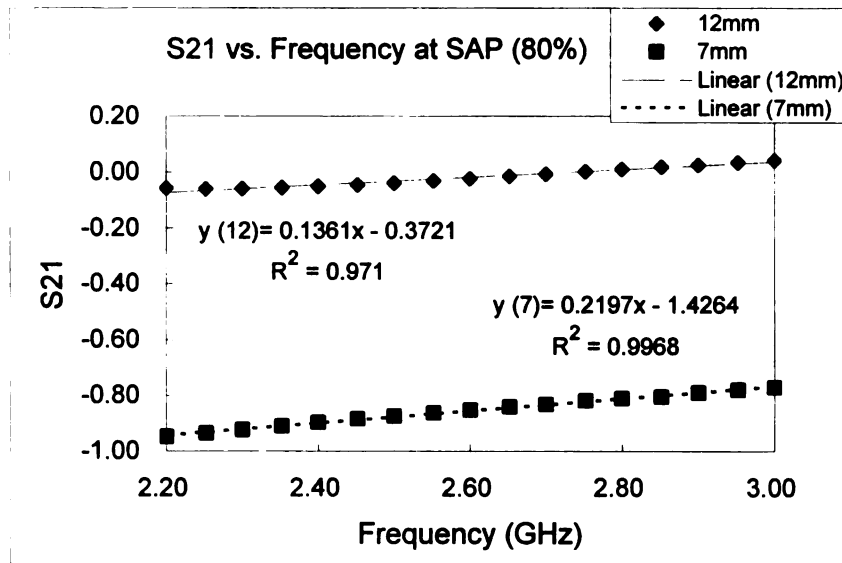


Figure 6.4 Comparison of S21 in SAP specimen with 80% water content

Figure 6.4 showed that forward transmission gain S21 over frequency in two trials with same water content and different thickness. The thicker sample had small slope that indicated it was more sensitive to frequency in thinner sample with the high water content. In Figure 6.5, reverse transmission gain, S12 showed relative complex relationship over frequency. S12 at 12mm sample slowly increases with frequency increasing, however, S12 at 12mm sample gained a quickly decline over frequency.

Because permittivity and permeability were extracted from the experimental S-parameters, we discussed the S-parameters only limited on the data integrity and validation purpose. Figure 6.6 to Figure 6.21 showed the comparison of S-parameters in all measured SAP samples with different water content.

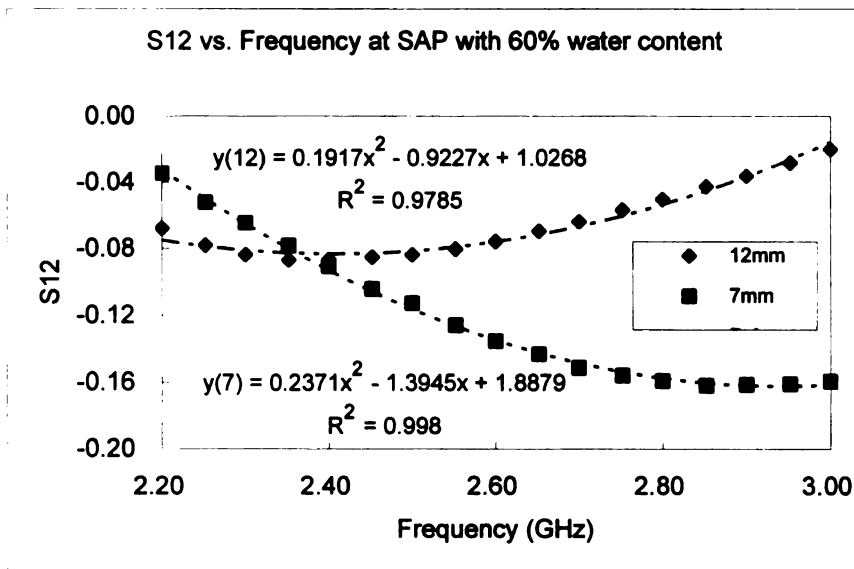


Figure 6.5 Comparison of S12 in SAP specimen with 60% water content

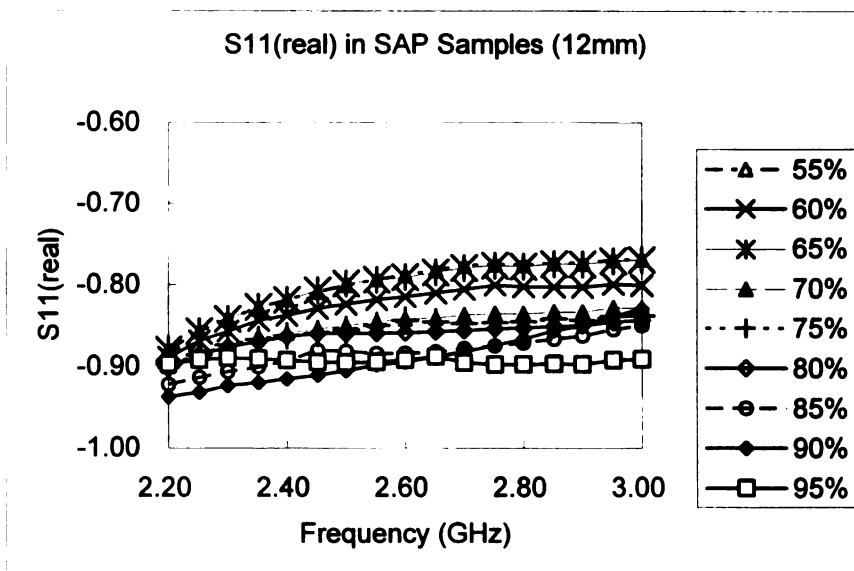


Figure 6.6 Comparison of experimental S11 (real) in SAP mixtures (12 mm)

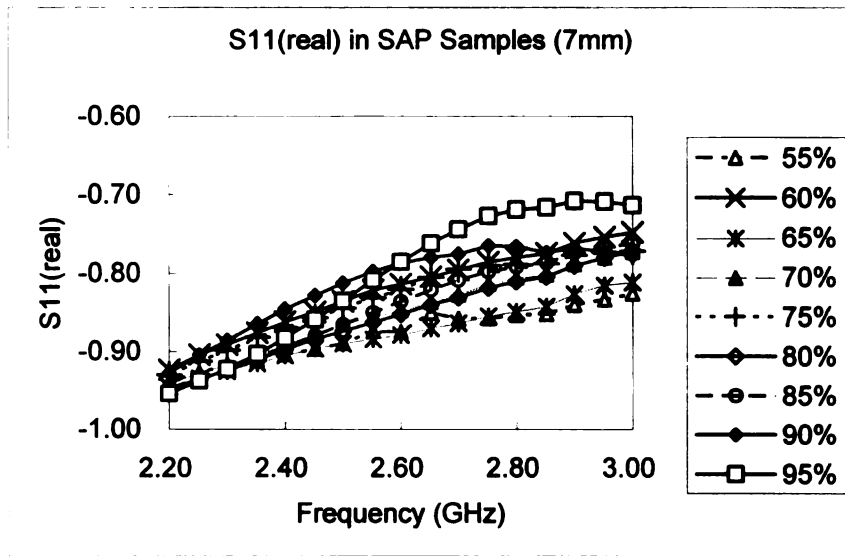


Figure 6.7 Comparison of experimental S11 (real) in SAP mixtures (7 mm)

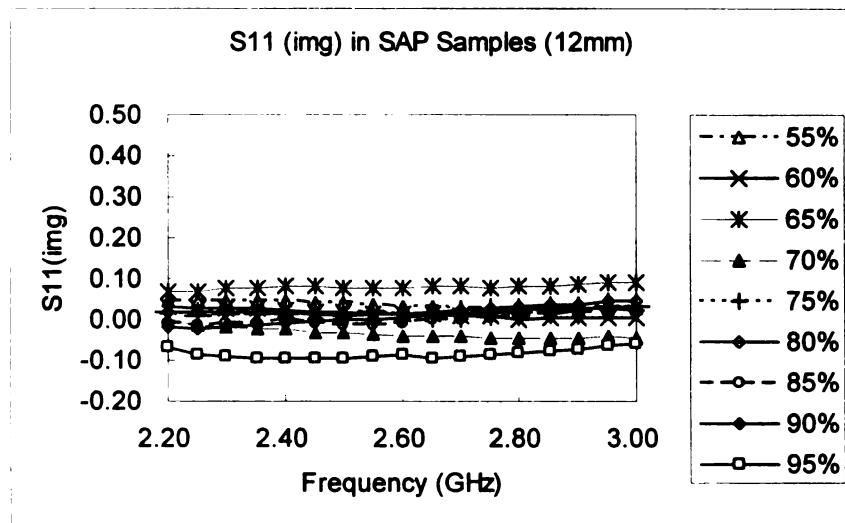


Figure 6.8 Comparison of experimental S11 (img) in SAP mixtures (12 mm)

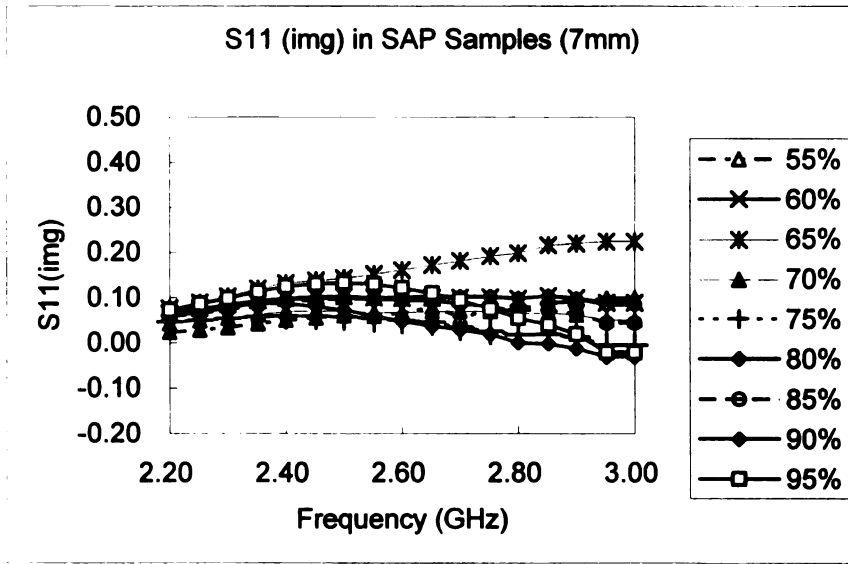


Figure 6.9 Comparison of experimental S11 (img) in SAP mixtures (7 mm)

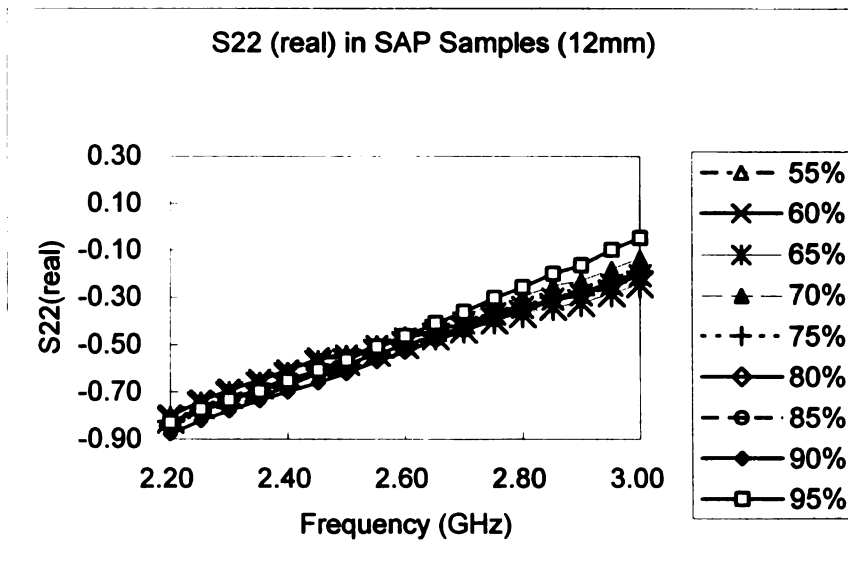


Figure 6.10 Comparison of experimental S22 (real) in SAP mixtures (12 mm)

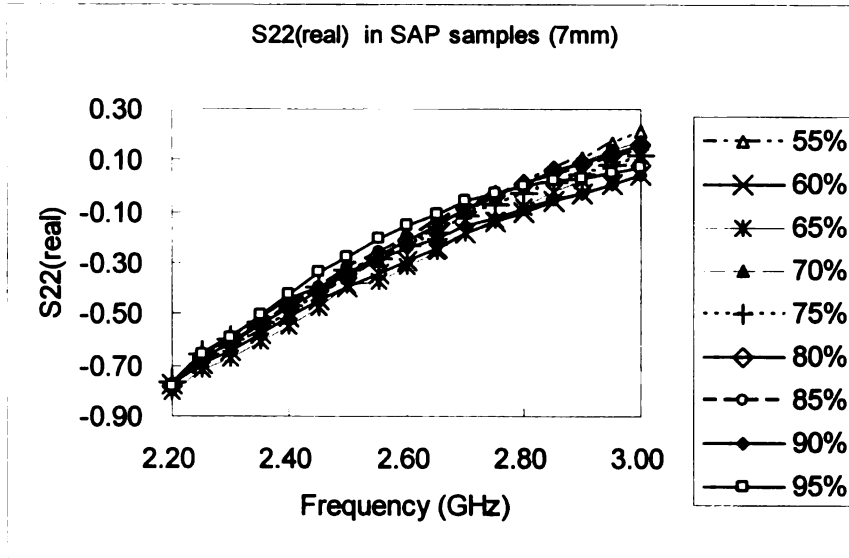


Figure 6.11 Comparison of experimental S22 (real) in SAP mixtures (7 mm)

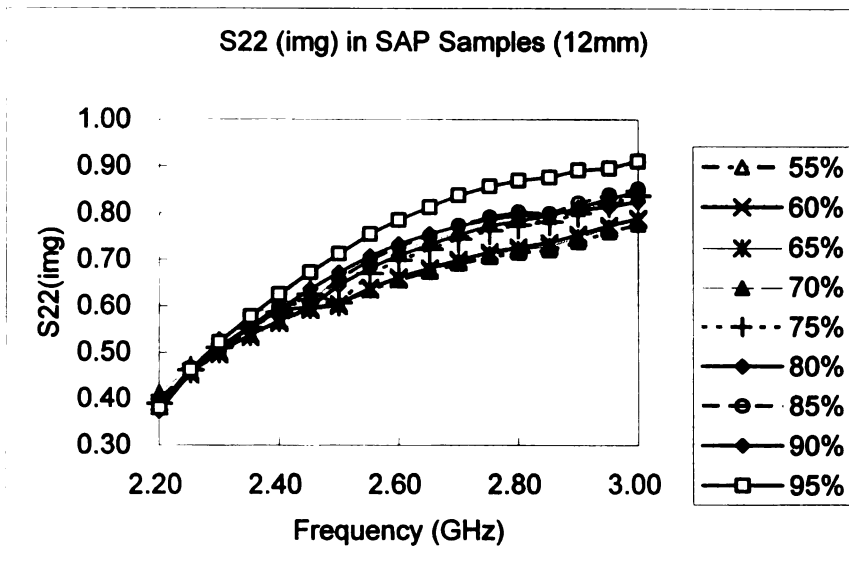


Figure 6.12 Comparison of experimental S22 (img) in SAP mixtures (12 mm)

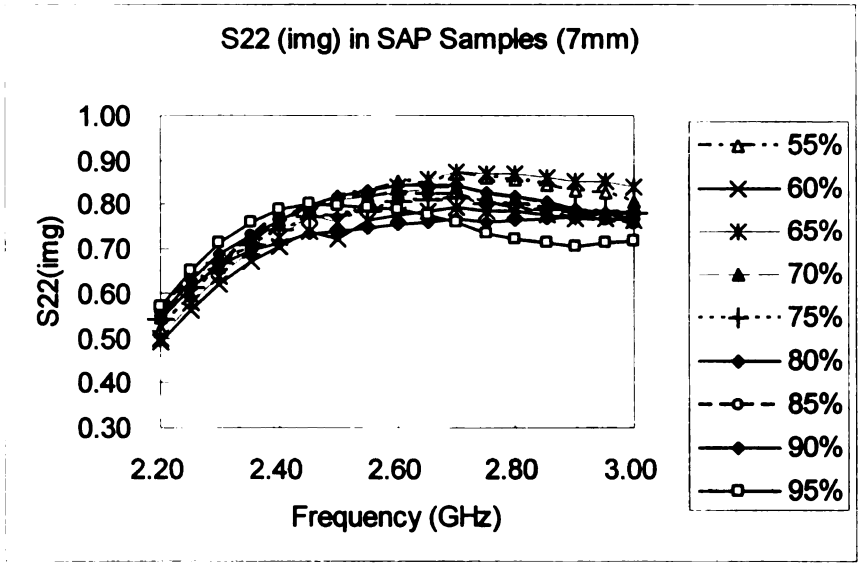


Figure 6.13 Comparison of experimental S22 (img) in SAP mixtures (7 mm)

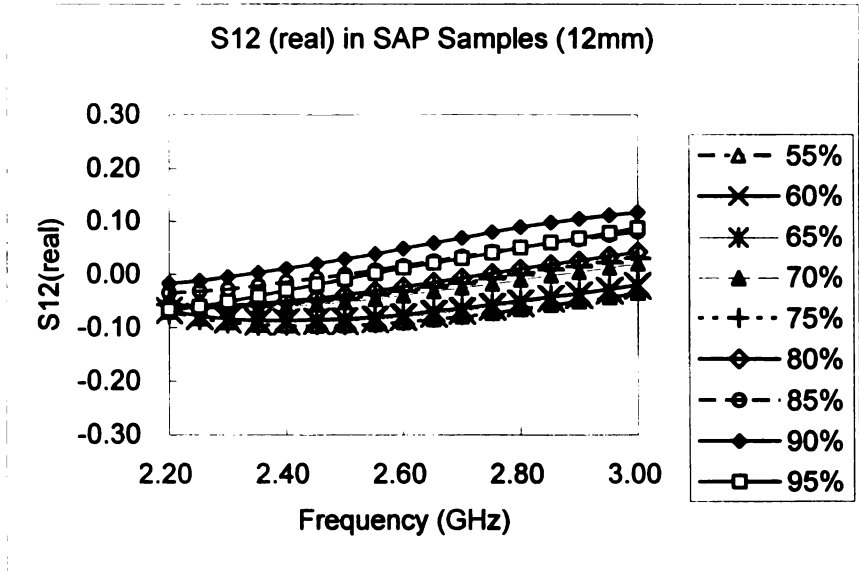


Figure 6.14 Comparison of experimental S12 (real) in SAP mixtures (12 mm)

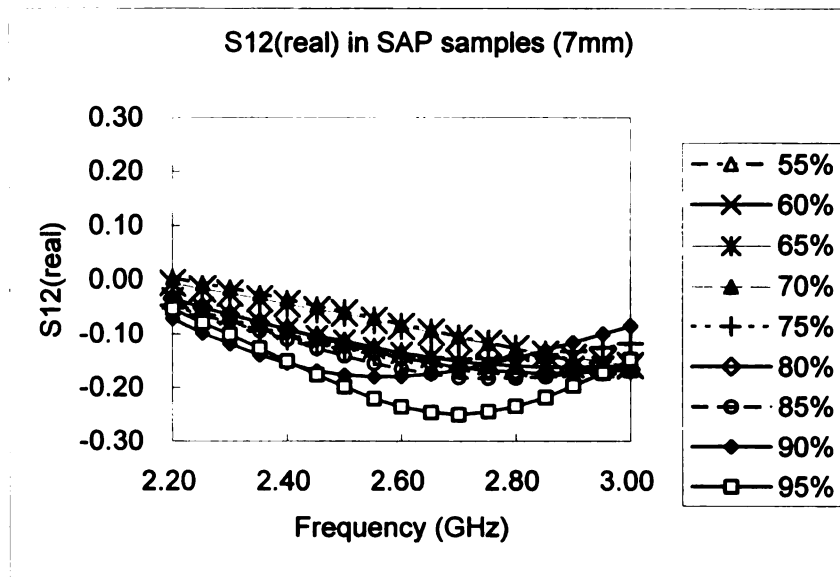


Figure 6.15 Comparison of experimental S12 (real) in SAP mixtures (7 mm)

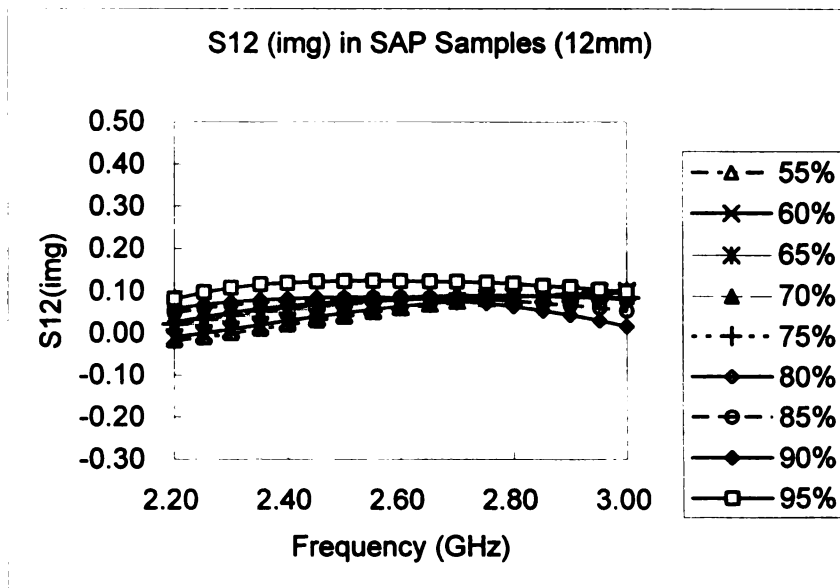


Figure 6.16 Comparison of experimental S12 (img) in SAP mixtures (12 mm)

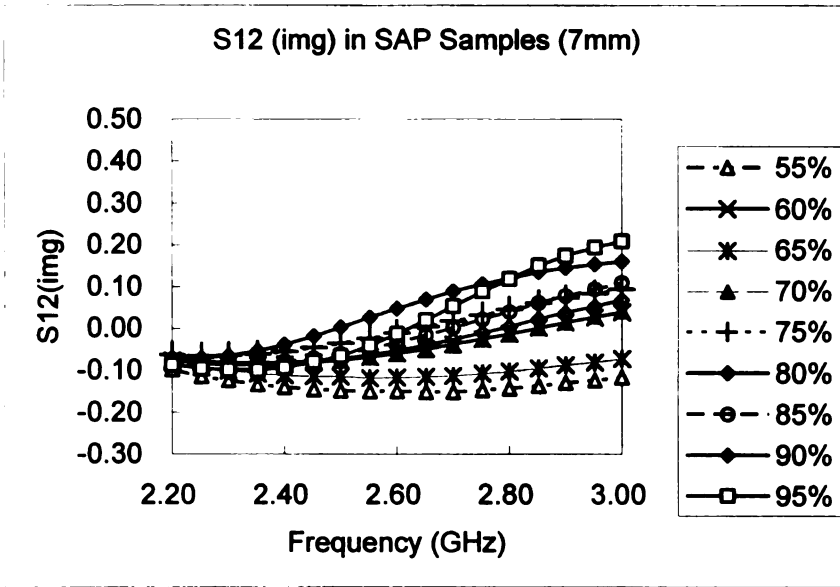


Figure 6.17 Comparison of experimental S12 (img) in SAP mixtures (7 mm)

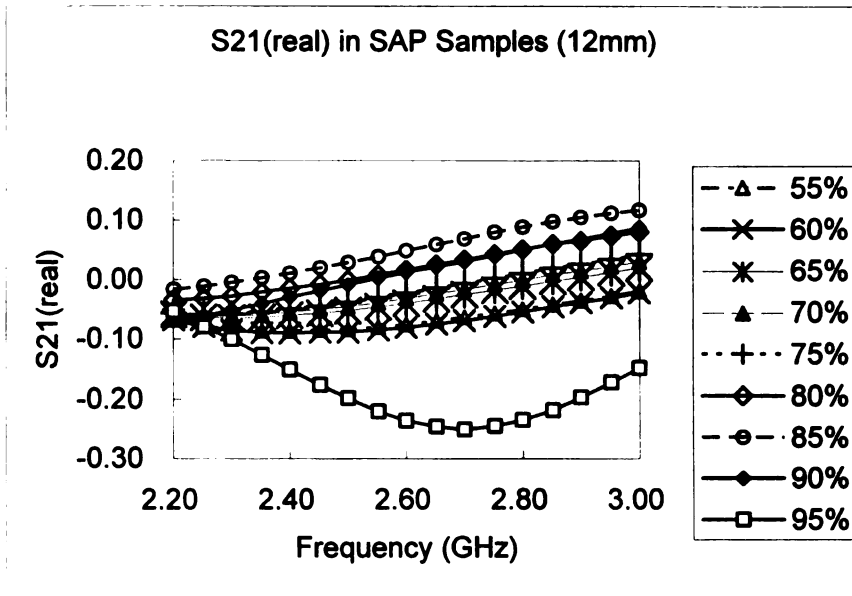


Figure 6.18 Comparison of experimental S21 (real) in SAP mixtures (12 mm)

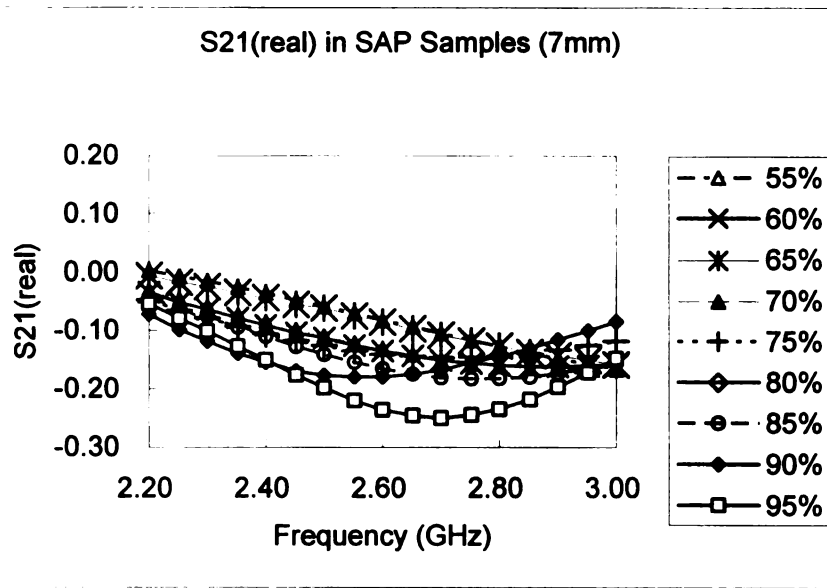


Figure 6.19 Comparison of experimental S21 (real) in SAP mixtures (7 mm)

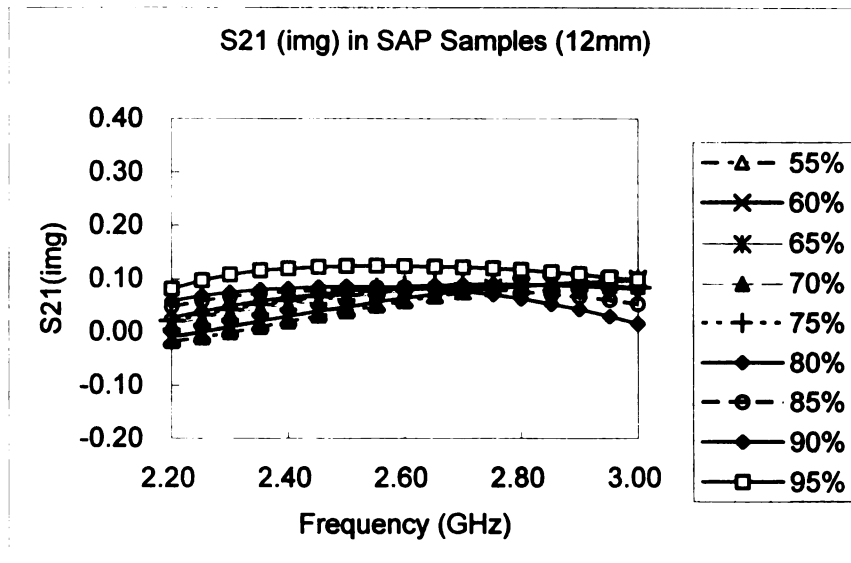


Figure 6.20 Comparison of experimental S21 (img) in SAP mixtures (12 mm)

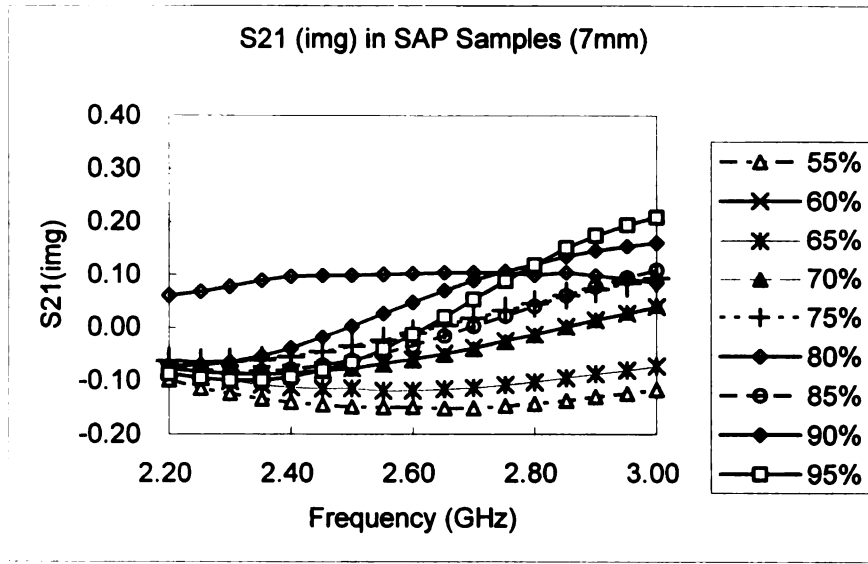


Figure 6.21 Comparison of experimental S21 (img) in SAP mixtures (7 mm)

6.2 Validation

Calibration procedure eliminates the systematic errors. However, ideally homogenous status is far to reached, the imperfect samples causes deviations in measurement. Validating measurement ensures data integrity. In the material characterization measurement, two independent experiments were performed to validate the consistency of measurements. In two independent trials, the sample thickness was 12 mm, 7 mm respectively. Loss factor is a constant that reveals the power damping in a network. However, loss factor calculations shown the measurement quality are able to validate passive S-parameter measurements [59]. The forward loss factor (FLF) and reverse loss factor are determined by S-parameters as follow equations:

$$\text{Forward Loss Factor: } FLF = 1 - |S_{11}|^2 - |S_{21}|^2 \quad (\text{Equation 6.3})$$

$$\text{Reverse Loss Factor: } RLF = 1 - |S_{22}|^2 - |S_{12}|^2 \quad (\text{Equation 6.4})$$

Figure 6.22 to Figure 6.30 was based on the calculations and presented the validation results with loss factor calculations. It showed data inconsistency in FLF with 80% water content, nonetheless, in all other graphs, it showed pretty good data consistency. We discarded the deviated parameters of SAP with 80% water content in later discuss.

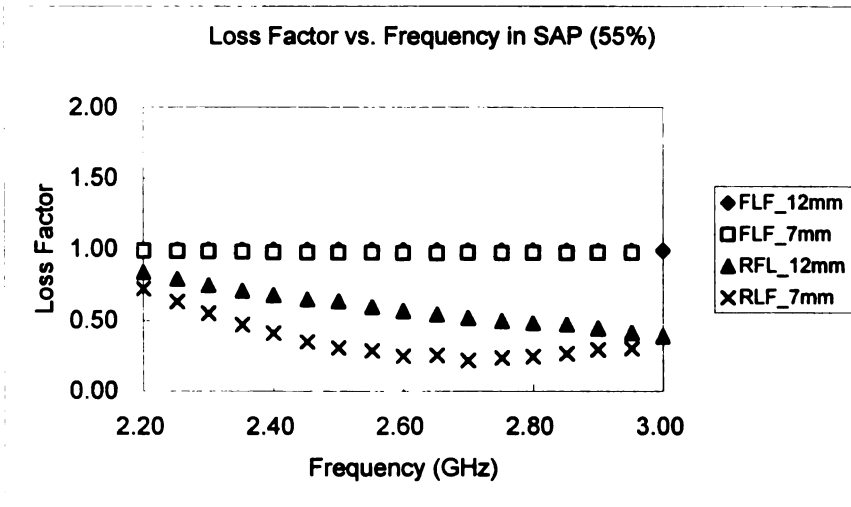


Figure 6.22 Comparison of loss factors in SAP samples (55%)

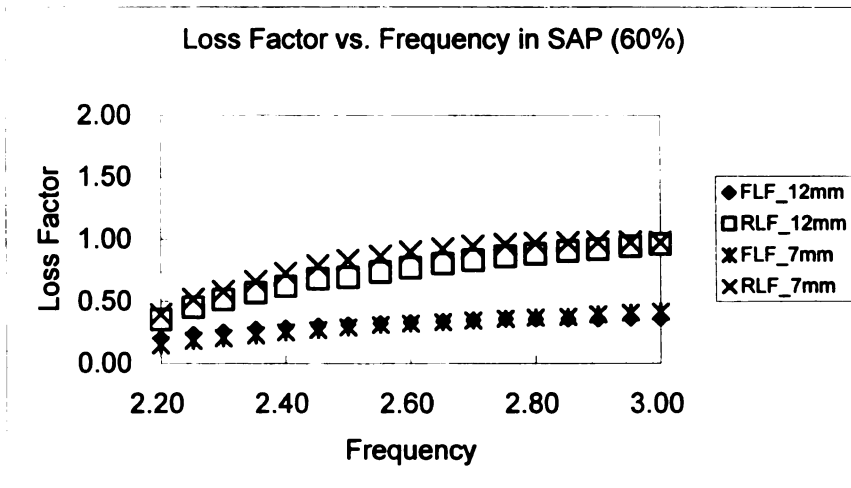


Figure 6.23 Comparison of loss factors in SAP samples (60%)

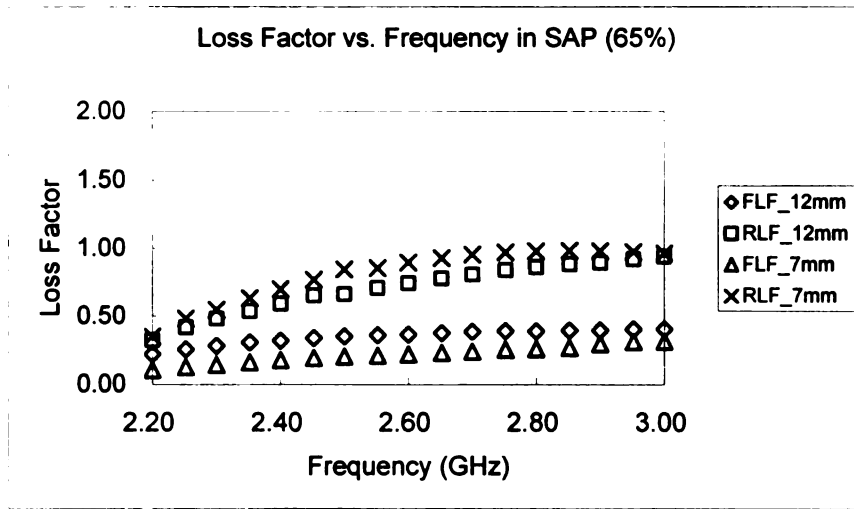


Figure 6.24 Comparison of loss factors in SAP samples (65%)

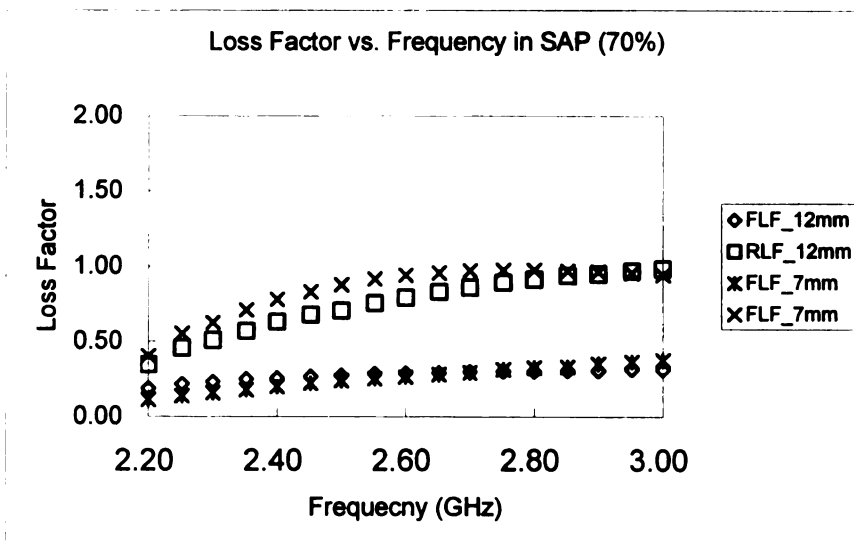


Figure 6.25 Comparison of loss factors in SAP samples (70%)

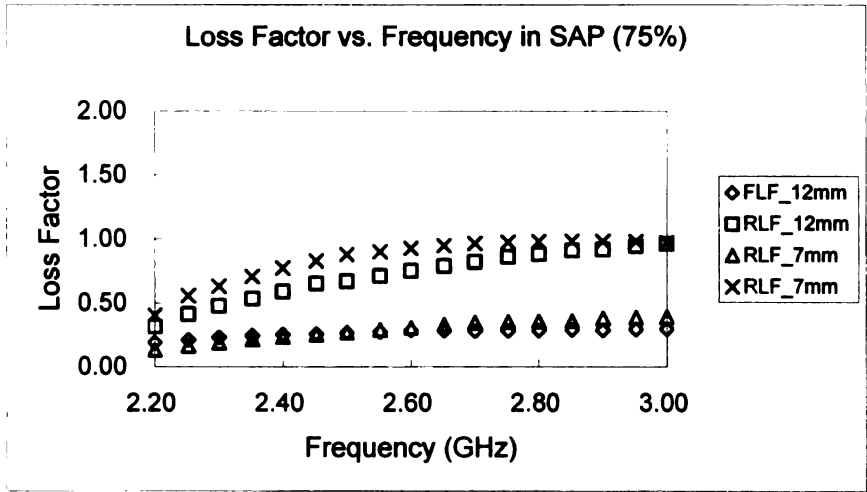


Figure 6.26 Comparison of loss factors in SAP samples (75%)

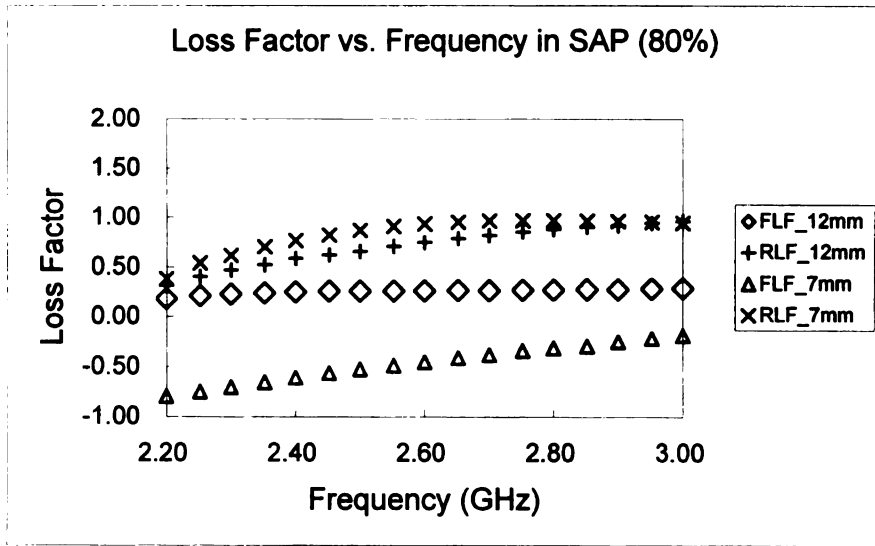


Figure 6.27 Comparison of loss factors in SAP samples (80%)

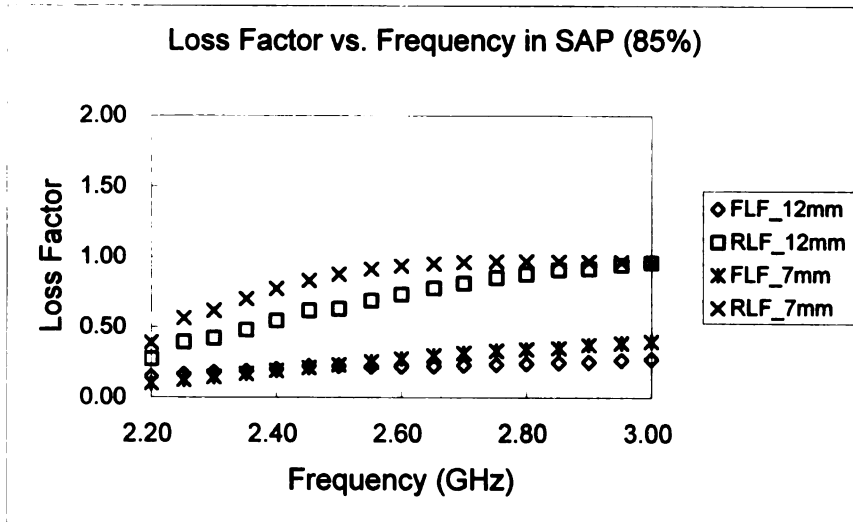


Figure 6.28 Comparison of loss factors in SAP samples (85%)

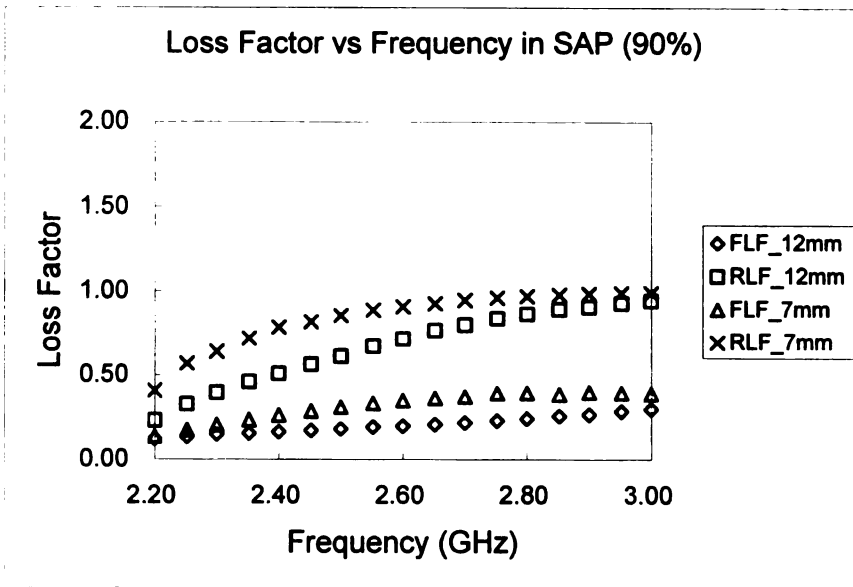


Figure 6.29 Comparison of loss factors in SAP samples (90%)

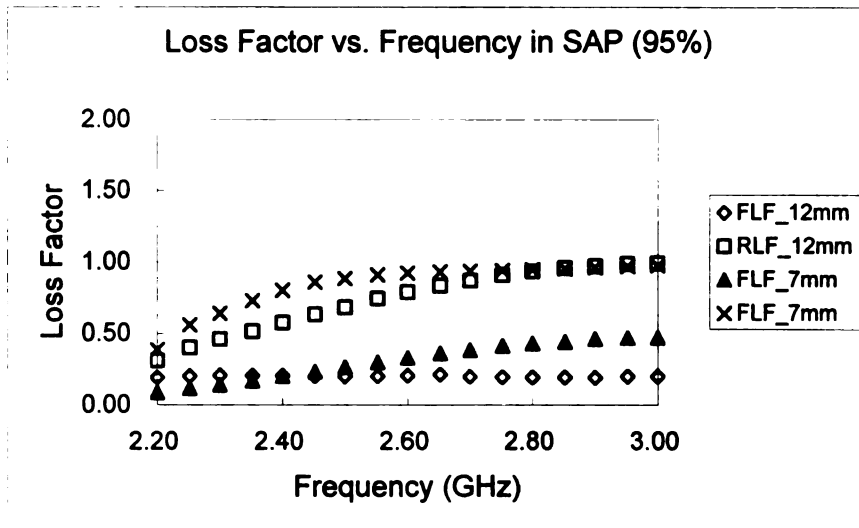


Figure 6.30 Comparison of loss factors in SAP samples (95%)

6.3 Permittivity

Measurement and extraction procedures of material characterization using HP 8510C vector network analyzer with WR340 waveguide were described in Chapter 3 and Chapter 4. The results of the permittivity in term of dielectric constant and loss factor based on the experimental measurement. With a dielectric constant of near 80, water dominates main component of hydrated superabsorbent mixtures due to high concentration of water in the experiment. However, there does not appear to be one widely accepted model for estimation of dielectric constant in water-saturated SAP mixtures. Figure 6.31 showed experimental permittivity and permeability in SAP sample with 5% water content. The graph indicated deviations of experimental permittivity. It showed the thicker sample (12 mm) has a higher permittivity. Obviously, it is not true theoretically. The deviation came from the wave propagation in waveguide. Though the

deviation indicated fluctuation in measurement, the permittivity had good match over the frequency range.

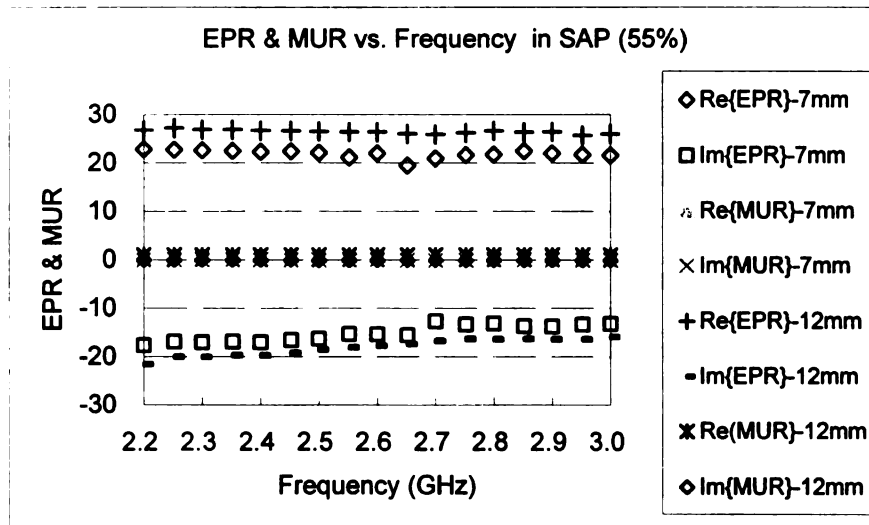


Figure 6.31 Comparison of experimental permittivity (EPR) and permeability (MUR)

Figure 6.32 to Figure 6.35 were created based on extracted permittivity from S-parameters, which showed the real part of permittivity in SAP mixtures with different water content over frequency range 2.2~3.0 GHz. They indicated that dielectric permittivity is fairly stable over frequency range 2.2 GHz to 3.0GHz. However, water content in SAP mixtures is the major influence on fluctuation of permittivity. General, high water content in SAP mixture gained high permittivity. the correlation of relative permittivity and water content was presented in Figure 6.36.

Figure 6.32 and Figure 6.33 showed the real part of relative permittivity (dielectric constant) is relatively stable over the frequency range, it showed a slightly decreasing tendency for thinner samples and relatively low water concentration samples (55%, 60%, 7mm). The permittivity of the rest of samples shows relative invariability or very slight

increase over part of the frequency range. Meanwhile, it showed SAP mixtures with lower water concentration has lower relative permittivity (dielectric constant), the correlation and graphs shows in Figure 6.36 and Figure 6.37. However, Figure 6.34 and Figure 6.35 showed a relative larger fluctuation of permittivity, SAP sample with 95% and 12 mm thickness showed an unexpected result, with so high water content (95%), the permittivity declined quickly over the frequency range, in comparing with the thinner sample but with same amount of water. the unexpected result might be caused by the imperfect of sample. In frequency range 2.6GHz to 2.7GHz, the permittivity of 95% SAP mixture reached near 80 which is almost permittivity of pure water. Generally, the relative permittivity of the saturated SAP mixtures was in the range of 10 to 80. The dielectric constant of pure water is about 80. It showed that the dielectric constant of the SAP mixtures relied on the proportion of two components. With the water content increasing, the dielectric constant of the SAP mixture proportionally increased (see Figure 6.36 and Figure 6.37).

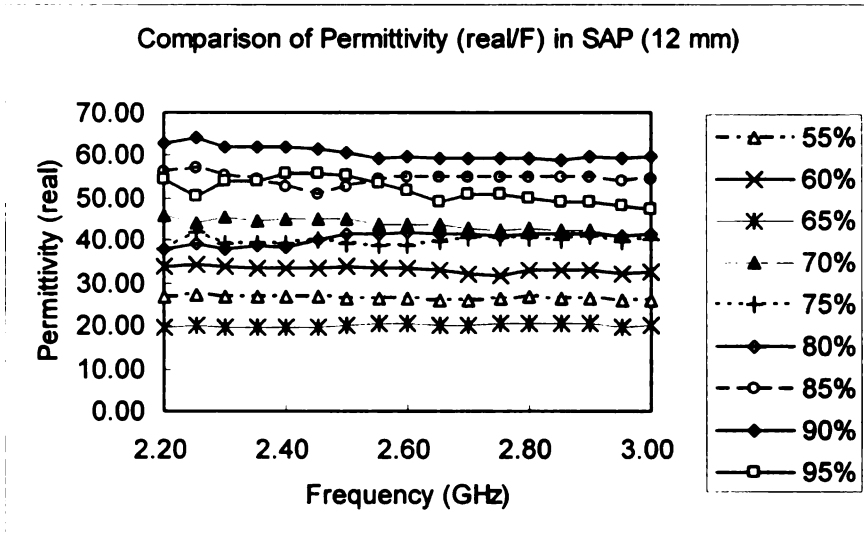


Figure 6.32 Comparison of permittivity in SAP with different water content (12 mm)

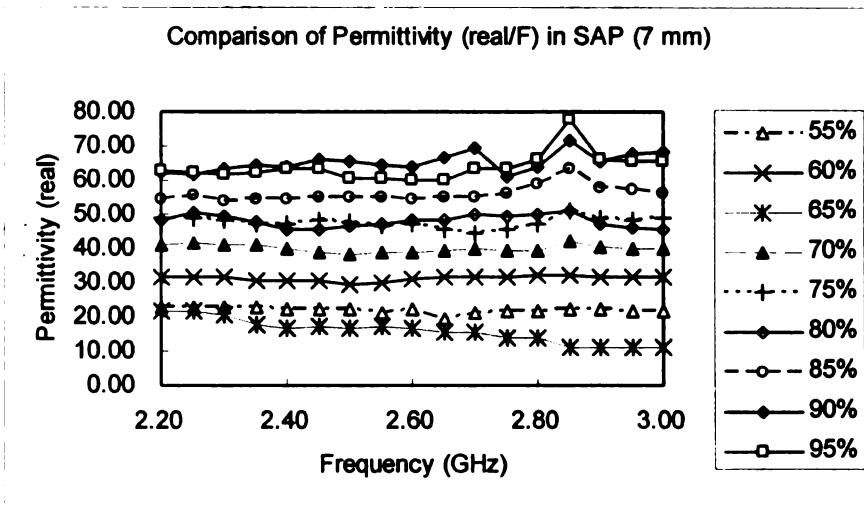


Figure 6.33 Comparison of permittivity in SAP with different water content (7 mm)

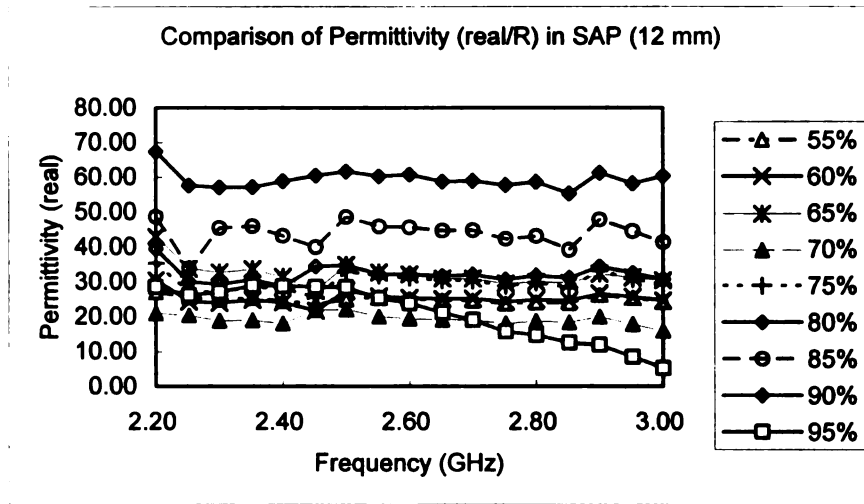


Figure 6.34 Comparison of permittivity in SAP with different water content (12 mm)

Figure 6.36 to Figure 6.38 were created from experimental relative permittivity and standard deviation among 201 points in the range of 2.2 GHz to 3.0 GHz. It was overt that in this range, the permittivity was very sensitive to water content. they presented that the relationship between the relative permittivity and the water content was fit for linear regression from 45% to 95% in SAP mixtures.

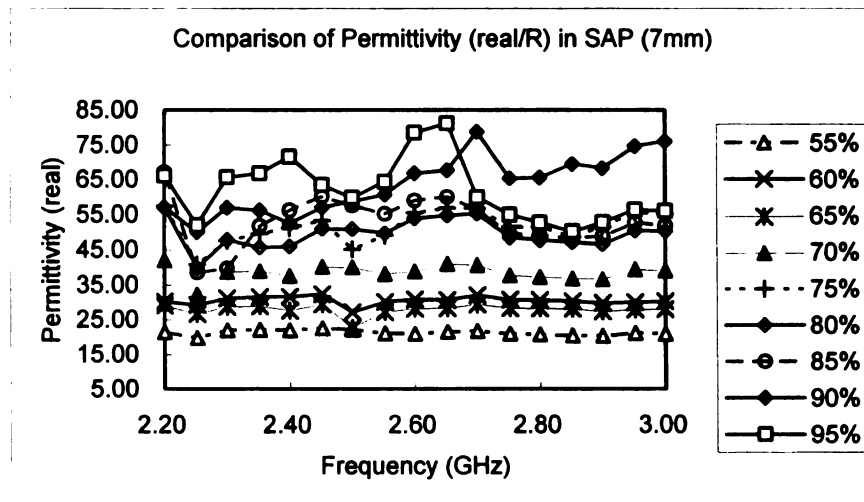


Figure 6.35 Comparison of permittivity in SAP with different water content (7 mm)

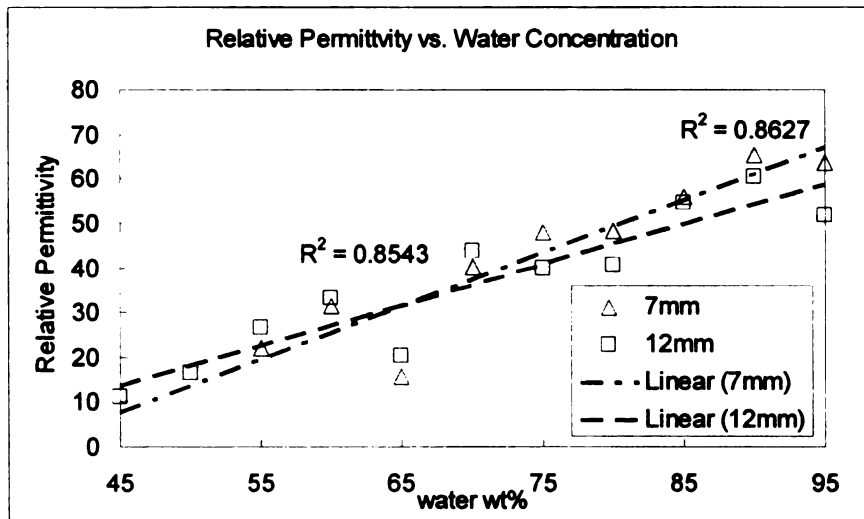


Figure 6.36 Correlation of relative permittivity in different sample thickness

Dependence of the experimental relative permittivity, under RT 68°F at 2.2GHz to 3.0GHz, the permittivity is proportional to the water content in the SAP samples. Two distinct experiments were observed. The result of bivariate correlation analysis showed these variables were highly related to a linear relationship because Pearson's correlation coefficient of water concentration and permittivity were 0.869, 0.932 and 0.966 respectively with their significance levels. (See Table 6.1)

		WATER	2mm	7mm
WATER	Pearson Correlation	1	.869	.932
	Sig. (2-tailed)	.	.002	.000
	N	9	9	9
12mm	Pearson Correlation	.869	1	.966
	Sig. (2-tailed)	.002	.	.000
	N	9	9	9
7mm	Pearson Correlation	.932	.966	1
	Sig. (2-tailed)	.000	.000	.
	N	9	9	9

**Correlation is significant at the 0.01 level (2-tailed).

Table 6.1 Correlations of water concentration and sample relative permittivity

Figure 6.37 showed at 2.45GHz, 12mm and 7mm SAP samples presented a pair of contiguous permittivity curves which were almost superposition with each other. However, loss factor (imaginary part) showed larger deviation in comparing with real part. Figure 6.38 indicated that there were larger deviations in 7 mm SAP samples than 12 mm SAP samples. However, It presented that water content was major influence to deviation, higher water content came higher deviation. However, the sample with higher water content usually has a higher permittivity.

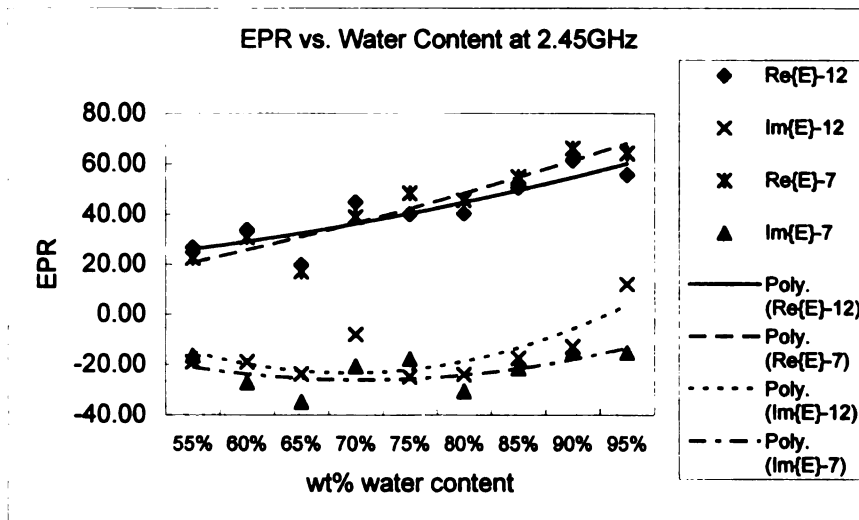


Figure 6.37 Permittivity vs. water concentration at 2.45GHz in different sample thickness

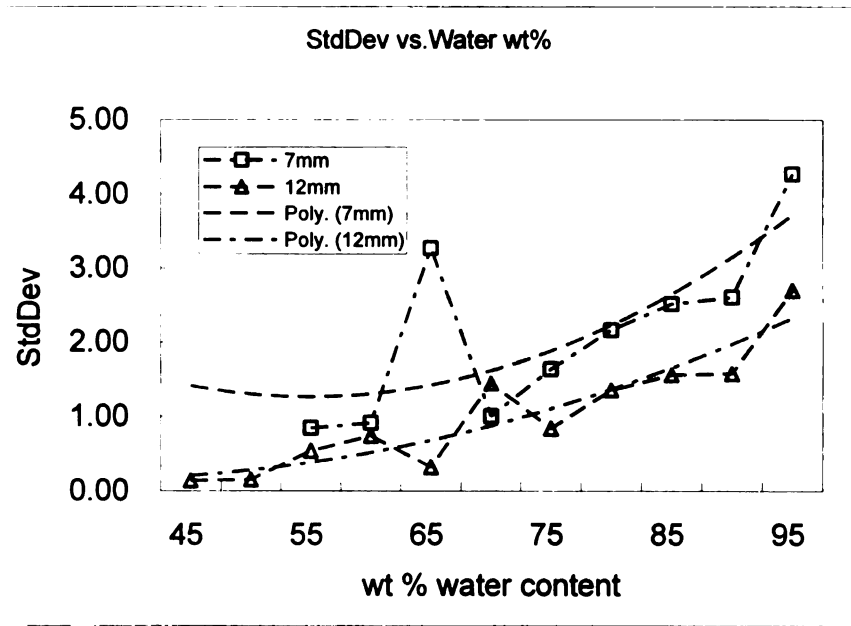


Figure 6.38 Standard deviation of relative permittivity in different sample thickness

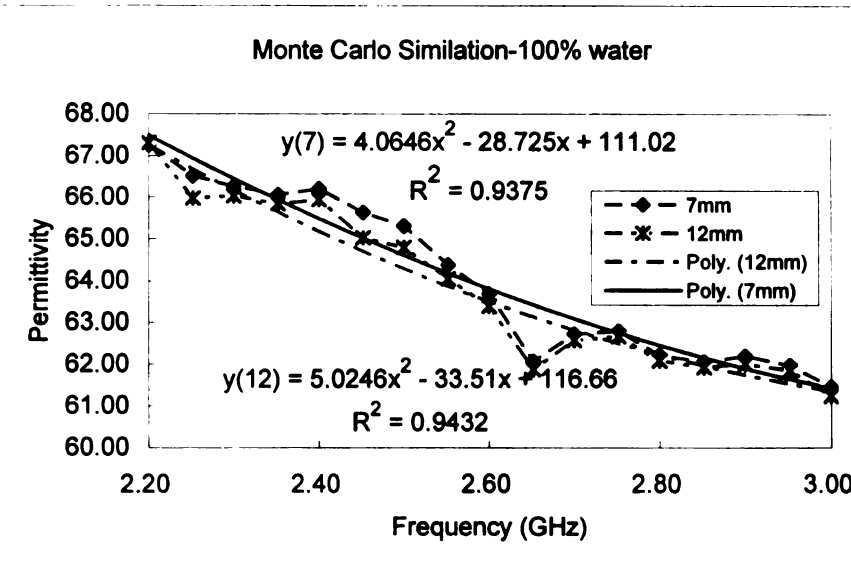


Figure 6.39 Estimated permittivity of 100% water

Figure 6.39 showed a group of estimated permittivity of 100% water using Monte Carlo Simulation. Obvious, the real permittivity value over the frequency range was smaller

than the value in literature. It was hypothesized that the Monte Carlo Simulation software used the right experimental permittivity. However, in the SAP mixtures, part of water molecules were associated with SAP molecules forming part of bounding water. As the water concentration increases, the strength and extent of the hydrogen bonding both increase. This leads to the experimental value lower than theoretical values. Consequently, estimated value was lower than that of 100% pure water in literature. Furthermore, bounding water in SAP would cause a higher loss factor theoretically.

6.4 Loss Factor

The imaginary part of permittivity referred as loss factor in this thesis presented the lossy character of the substance. The loss factor of the SAP specimens slowly increased with increasing frequency at room temperature. Figure 6.40 to Figure 6.41 based on the measurement showed that water content was major influence affecting loss tangent. Lower water content corresponded to a lower loss tangent while higher water content resulted in a higher loss tangent. Loss factor increases slowly and placidly; however, in Figure 6.40, there was different trend in SAP sample with 95 % water. Figure 6.41 showed that loss factor of 7 mm SAP samples was turbulent over the range in comparison with Figure 6.40. Figure 6.43 showed the standard deviations in thinner samples (7mm) were larger than those of in thicker samples (12mm).

As the water concentration increases, the strength and extent of the hydrogen bonding both increase. This elevates the static dielectric permittivity, enhances the difficulty for the movement dipole and so prevents the water molecule to oscillate at higher frequencies and boost up the drag to the rotation of the water molecules, so increasing the

friction and hence the dielectric loss factor increases. Experimental dielectric loss factor of saturated SAP mixtures with 55% to 95% water showed major influence of water content which caused fluctuation of loss factor; however, it did not show simple correlation or linear relationship. The mechanism of loss factor is complicated.

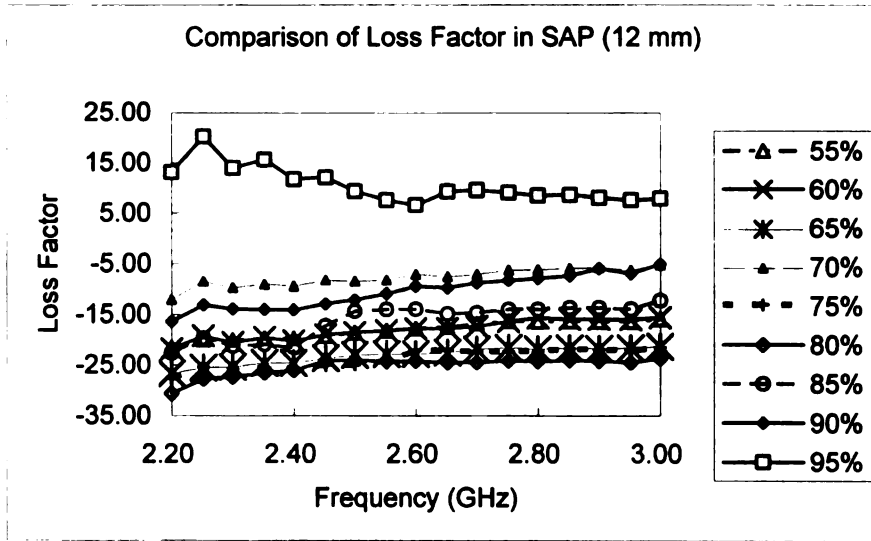


Figure 6.40 Comparison of loss factor in SAP with different water content (12 mm)

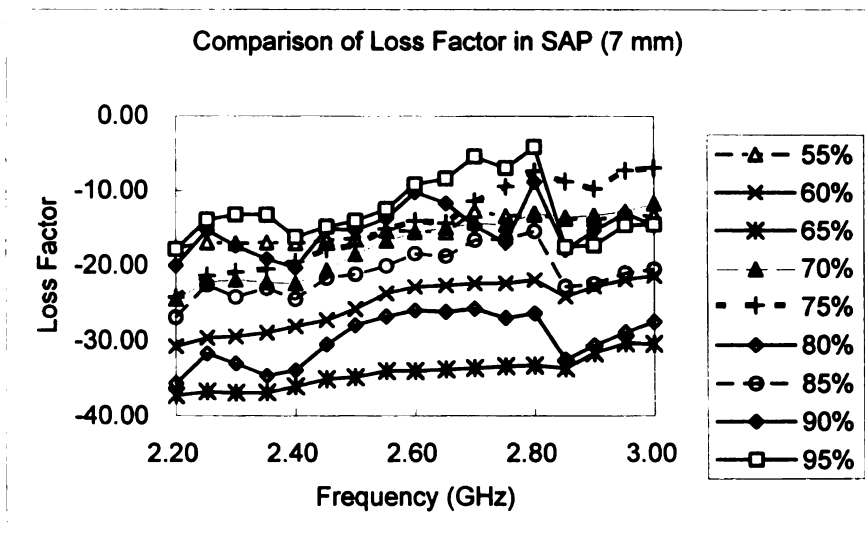


Figure 6.41 Comparison of loss factor in SAP with different water content (7 mm)

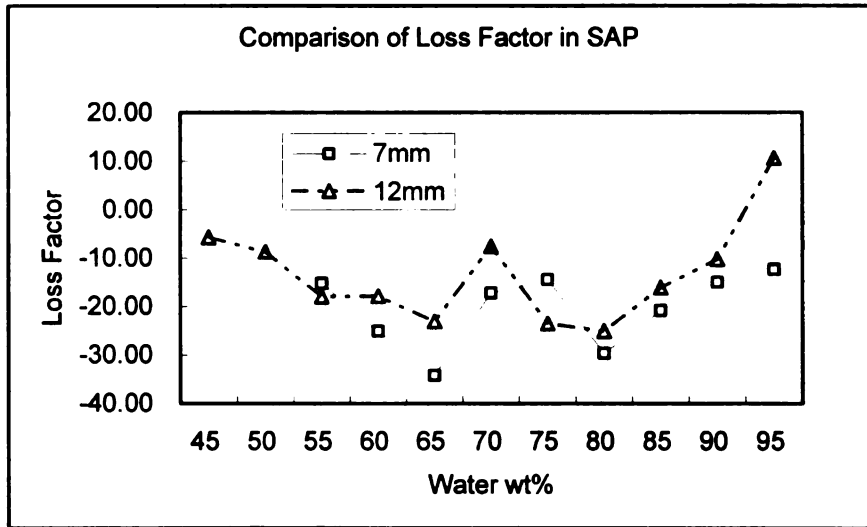


Figure 6.42 Loss factor of different samples

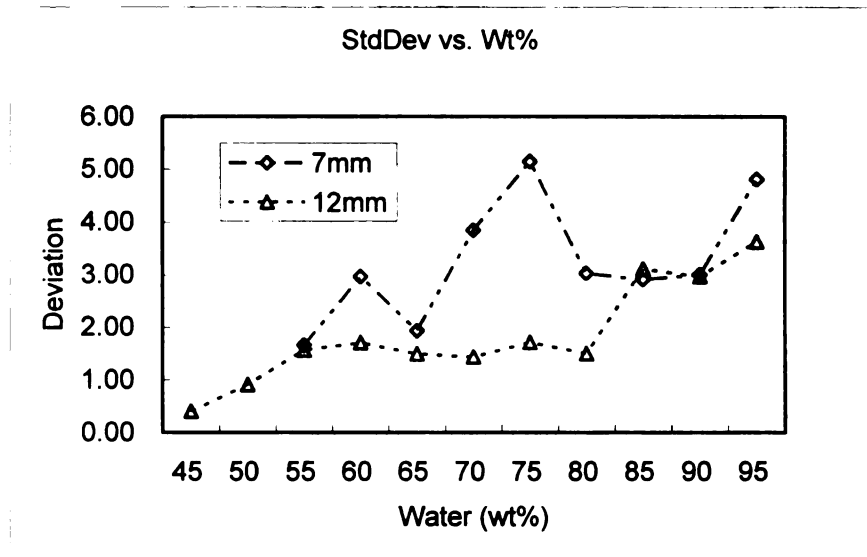


Figure 6.43 Standard deviation of loss factor in different thickness

6.5 Loss Tangent

Figure 6.44 to Figure 6.48 were created based on the measurement. Figure 6.44 and Figure 6.45 showed the loss tangent in 12mm and 7mm SAP samples. The loss tangent

referred to ratio of dielectric loss factor (ϵ_2) to dielectric permittivity (ϵ_1), $\tan \delta = \epsilon_2 / \epsilon_1$. It presented that loss tangent converged while frequency went to high frequency in 12mm SAP samples. However, in 7mm samples, larger undulation of loss tangent occurred over the tested frequency range. Nonetheless, high water content presented larger loss tangent in SAP samples.

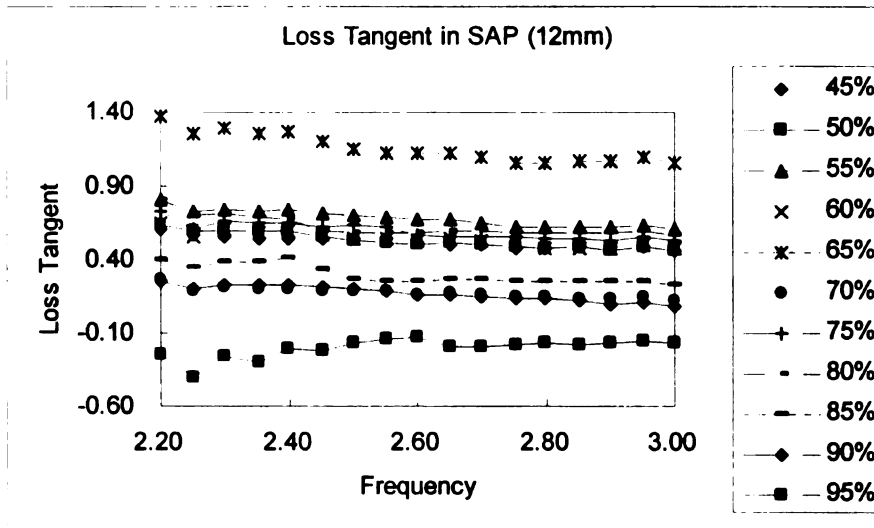


Figure 6.44 Loss tangent in 12 mm SAP samples

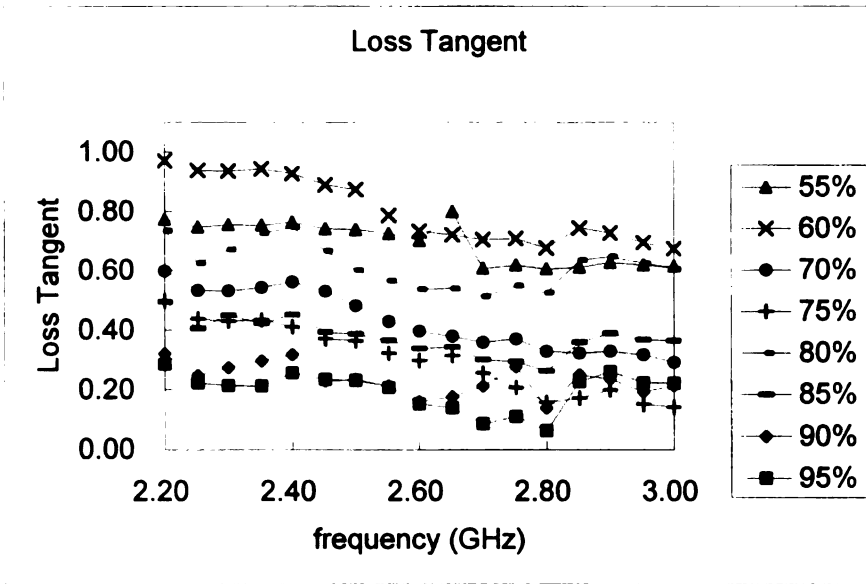


Figure 6.45 Loss tangent in 7 mm SAP samples

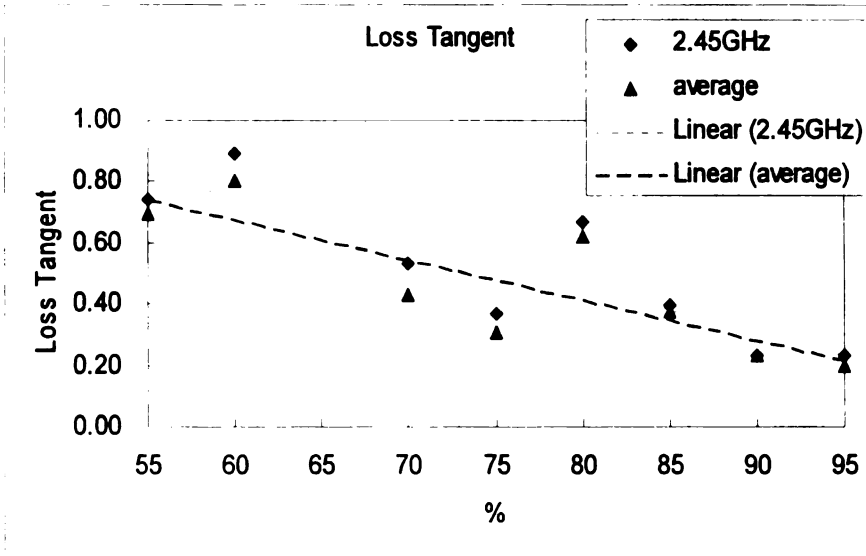


Figure 6.46 Comparison of loss tangent at 2.45 GHz in 7 mm samples

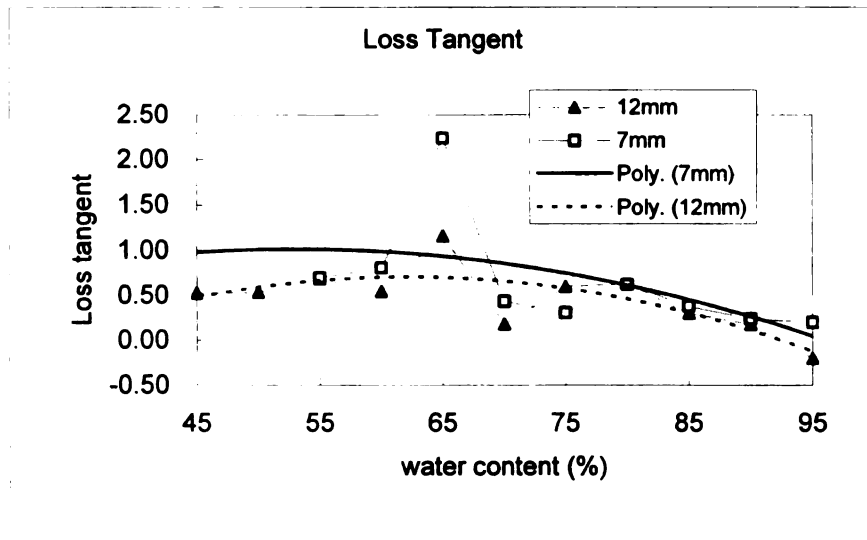


Figure 6.47 Comparison of average loss tangent in SAP samples

Figure 6.46 to Figure 6.48 presented comparison of loss tangent with various conditions.

In Figure 6.46, the loss tangent in 2.45 GHz was really agreed the average loss tangent in SAP samples, loss tangent declines with the water content increasing. Average loss tangent in 7mm and 12 mm were matched pretty well. Figure 6.48 presented that loss tangent in 12mm SAP were stable, however, both of loss tangent in SAP with 65% water content showed a linear correlation over the frequency range.

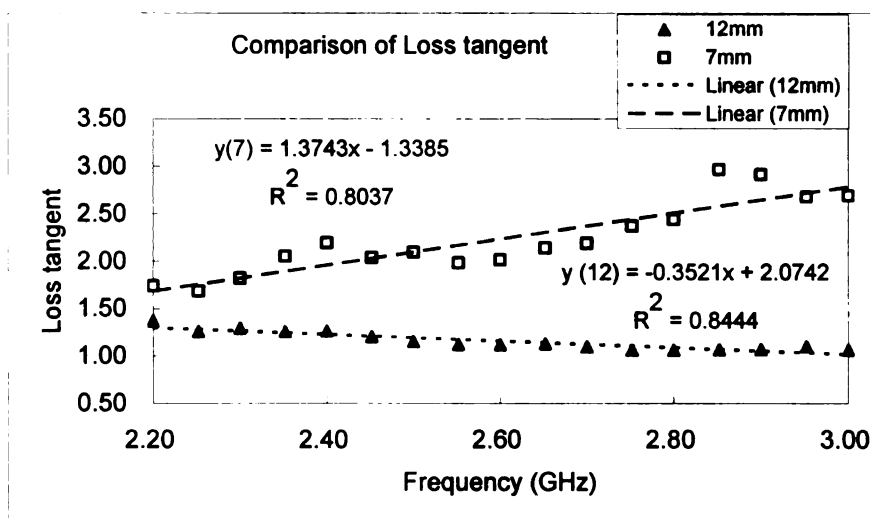


Figure 6.48 Comparison of loss tangent of SAP Mixtures (65%)

6.6 Power Measurement

Amount of power measured by the antenna which was nearly similar to amount of power received by the RFID transponders. The radiated power was measured using the setup shown in Figure 5.7. An RFID interrogator was connected with a linear or circular transmitting antenna at a distance from 1 cm to 65cm. The transponders were placed at a certain distance from the reader antenna oriented in the direction of horizontal and vertical to the transmitting antenna. At each location, the power was measured using the 2-wire dipole antenna placed in the same location and orientation as the transponders. The style of the transmitting antenna, the orientation of transponder (receiving two-wire dipole antennas) and distance were the independent parameters. The power measurement result showed in Figure 6.49 to Figure 6.62. It can be seen that power decaying along with the distance quickly. Figure 6.49 showed as the distance increased, the received power from reader antenna declined quickly. However, Power from linear antenna

declined faster in comparison with circular antenna, Regression analysis showed a small R^2 value (0.7883) in linear antenna in comparison with circular antenna. It implied the radiated power received from linear antenna was unstable in comparison with the circular antenna.

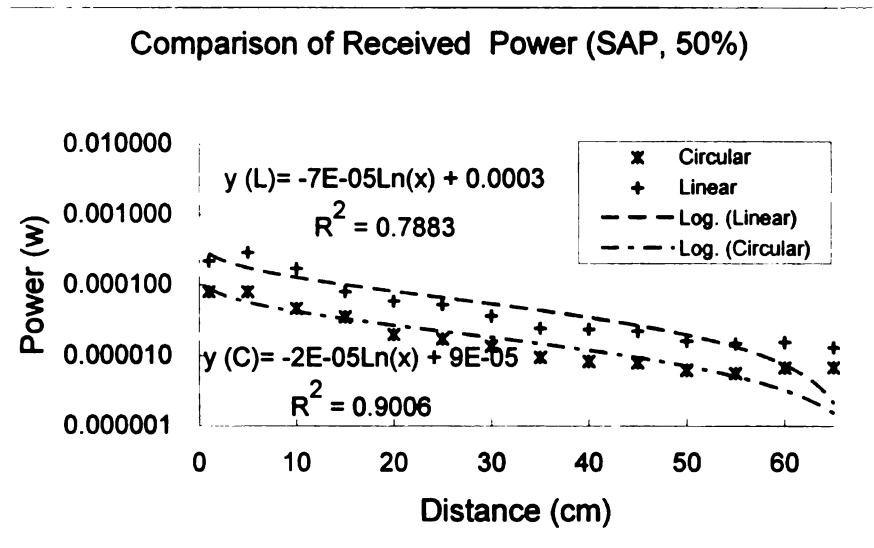


Figure 6.49 Antenna received power between reader antenna and tag

6.6.1 Antenna Style

Figure 6.50 showed the different influence of path loss in open-air with circular antenna and linear antenna. For the circular antenna, changing orientation of the receiving antenna from vertical to horizontal, the average receiving power decline 1.41dB or 30%; however, the power loss is linearly decreasing vs. distance. Figure 6.51 showed in linear antenna, power was rapidly loss vs. distance while changing orientation of the receiving antenna from vertical to horizontal. It presented in free space, linear antenna is serious orientational selectivity. However, circular antenna has less orientational selectivity. but changing the receiving orientation weaken the power transmission.

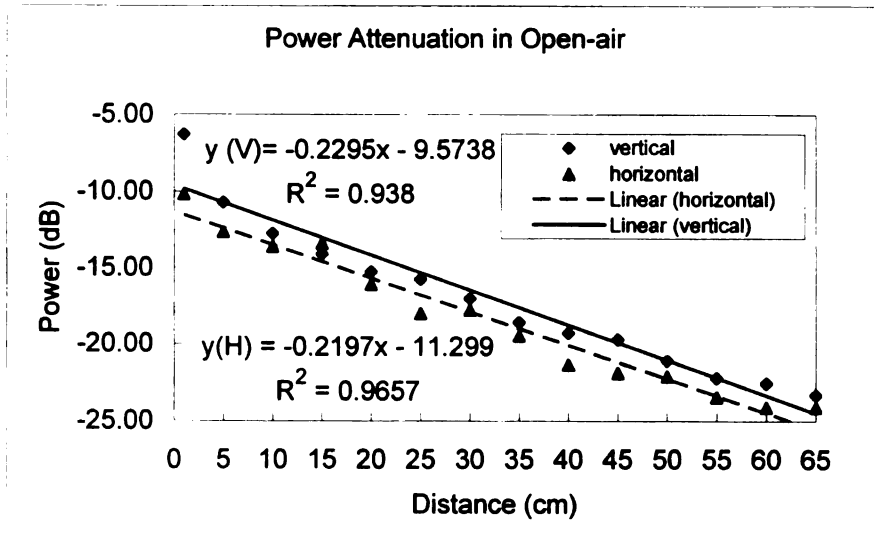


Figure 6.50 Power decaying in open-air with circular antenna

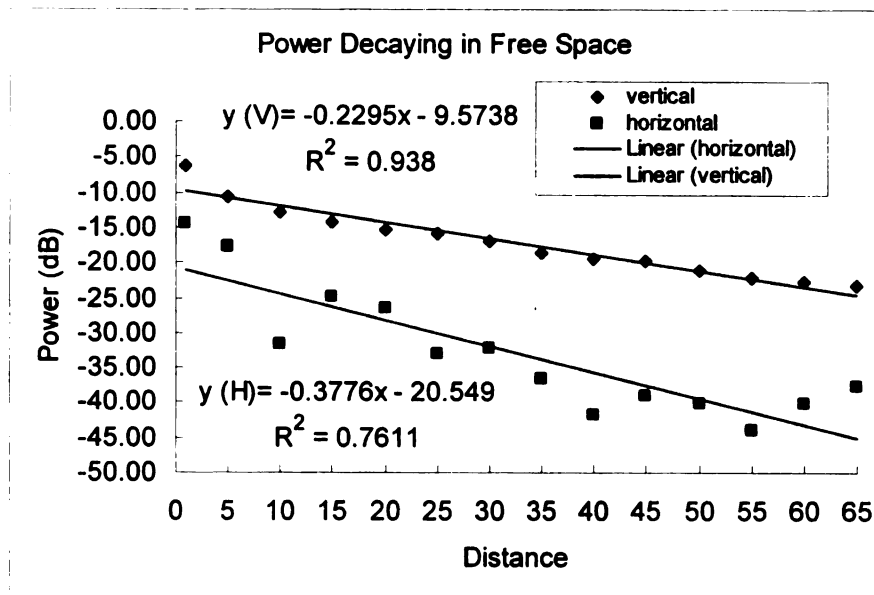


Figure 6.51 Power decaying in open-air with linear antenna

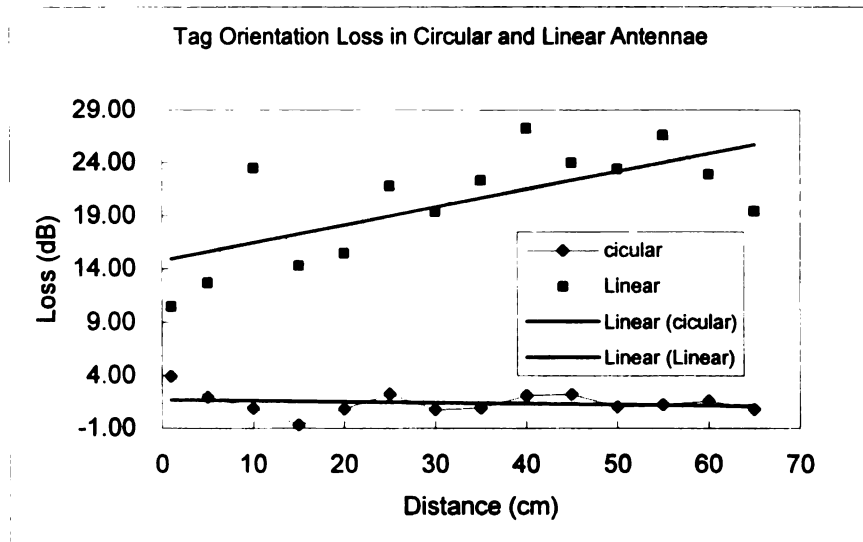


Figure 6.52 Tag orientation loss in different antennas

6.6.2 Shielding

Figure 6.53 showed the power with aluminum shielding. In comparing with power in free space, at the same distance, the power with the shielding decline about 23.92dB or by a factor of 246. Obvious, the Al shielding did good job. Table 6.2 showed a deviation of shielding effect among four configurations. Shielding effect presented the power received by the power sensor was from the sample window only after the RF signal pass through the SAP sample and the measurement was reliable.

V-C	V-L	H-C	H-L	Average
19.71	31.95	28.51	15.51	23.92

Table 6.2 Average shielding power loss (dB)

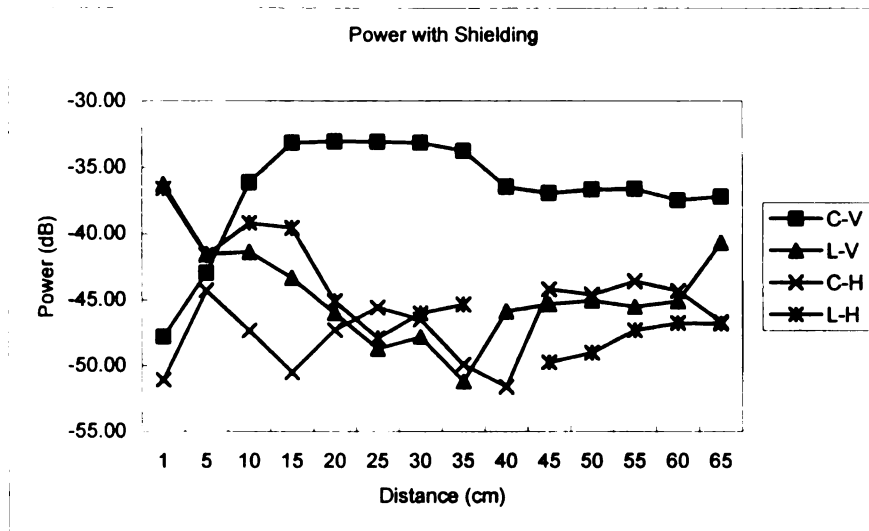


Figure 6.53 Power with Shielding

6.6.3 Circular Antenna

Figure 6.54 and Figure 6.55 were based on the power measurement in circular antenna. It showed water is the major influence of power loss besides path loss. Figure 6.56 presented higher water content has a greater influence in power loss. Figure 6.57 and Figure 6.58 showed that 70% water content has a strong influence to power, the average power loss was 12.08 dB with the largest 14.15dB and smallest 9.85 which occurred in the nearest and farthest location respectively.

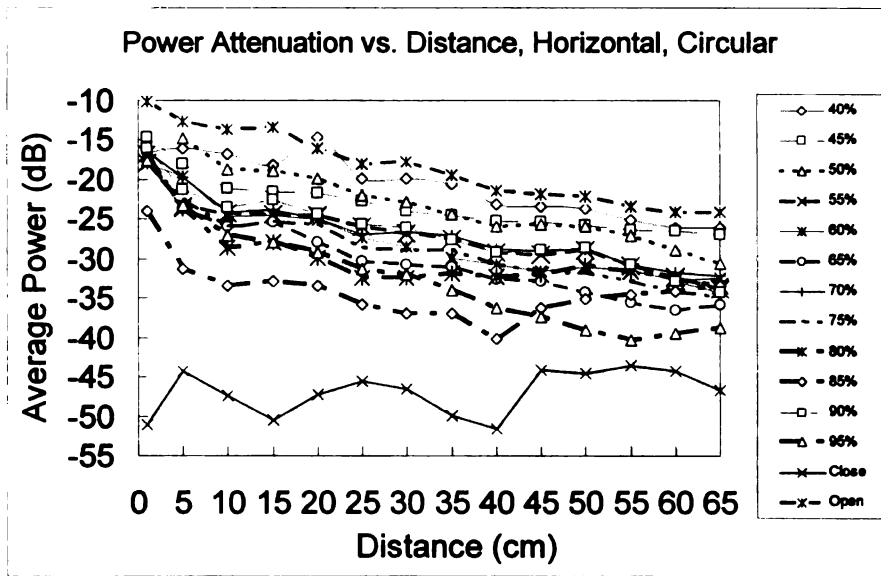


Figure 6.54 Power attenuation of circular antenna (H)

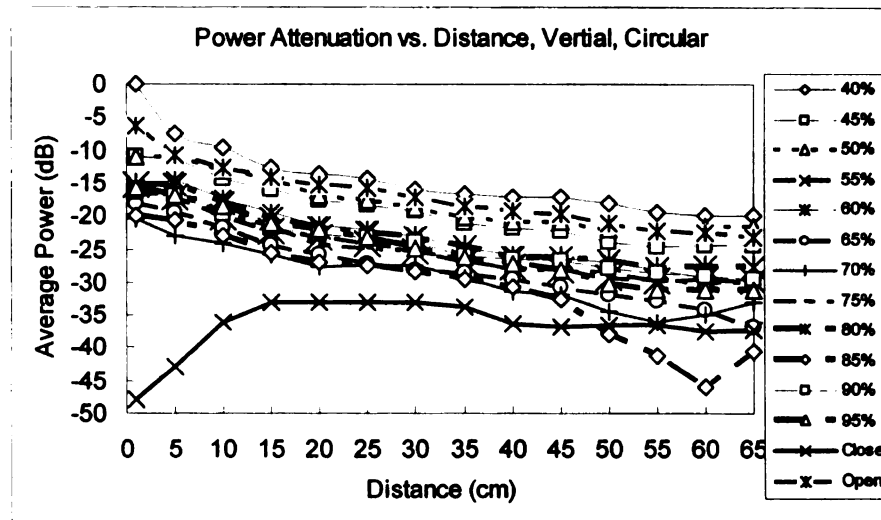


Figure 6.55 Power attenuation of circular antenna (V)

Figure 6.56 showed received power in 50% water SAP sample was much larger than that of with 75 % water SAP. Obvious, Higher water content leads to a lower power

receiving. Figure 6.57 showed in comparing with free space, with a 70% SAP sample, average 15 dB power was lost in the measurement.

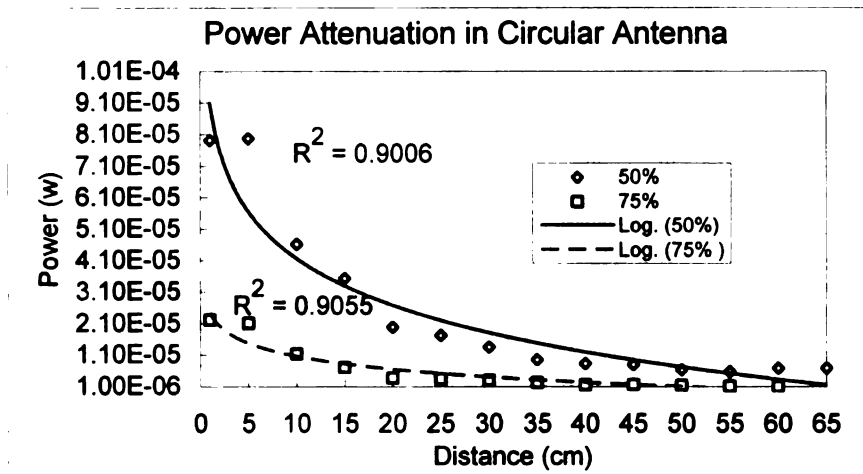


Figure 6.56 Power loss in 50% and 75% SAP

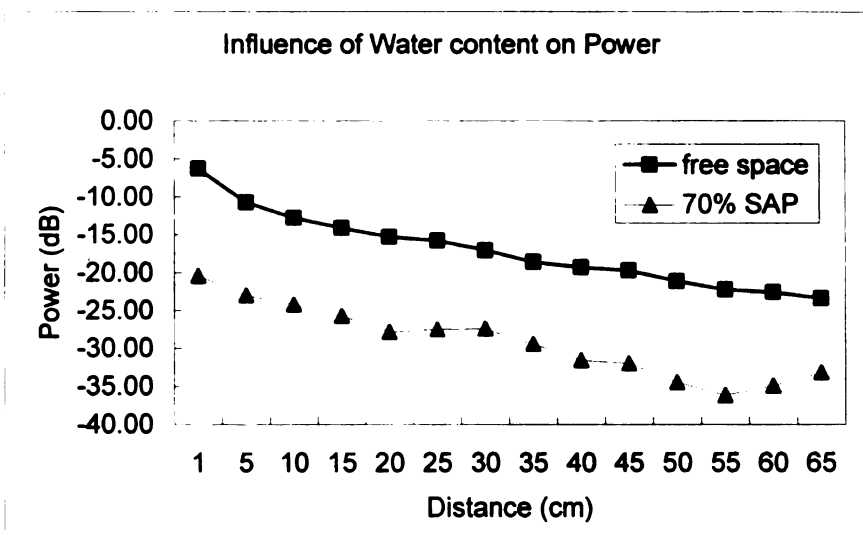


Figure 6.57 Influence of water content on power loss

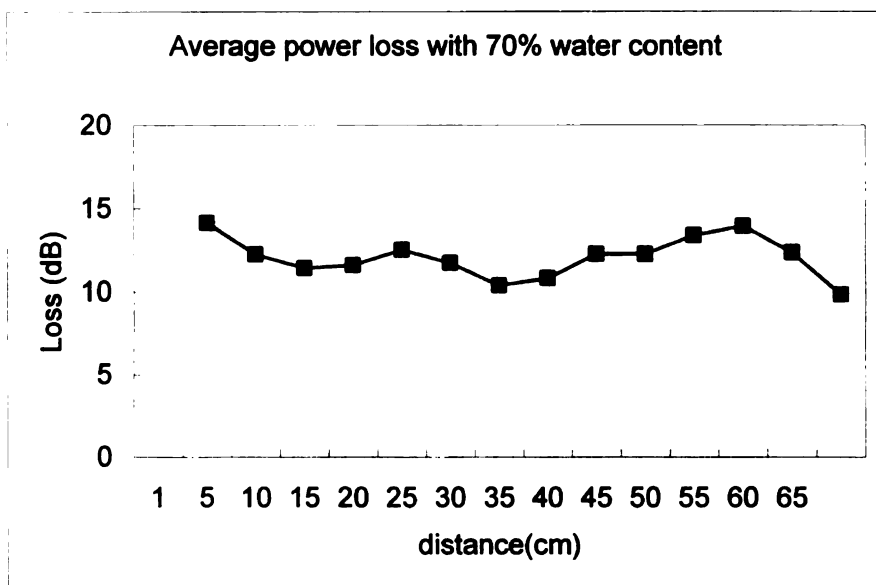


Figure 6.58 Average power loss in 70% SAP specimen

6.6.4 Linear Antenna

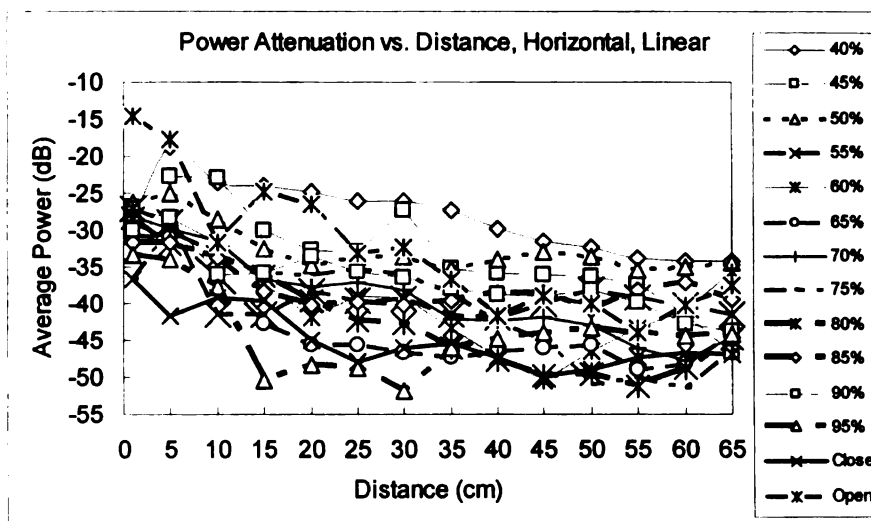


Figure 6.59 Comparison of power attenuation with saturated SAP samples

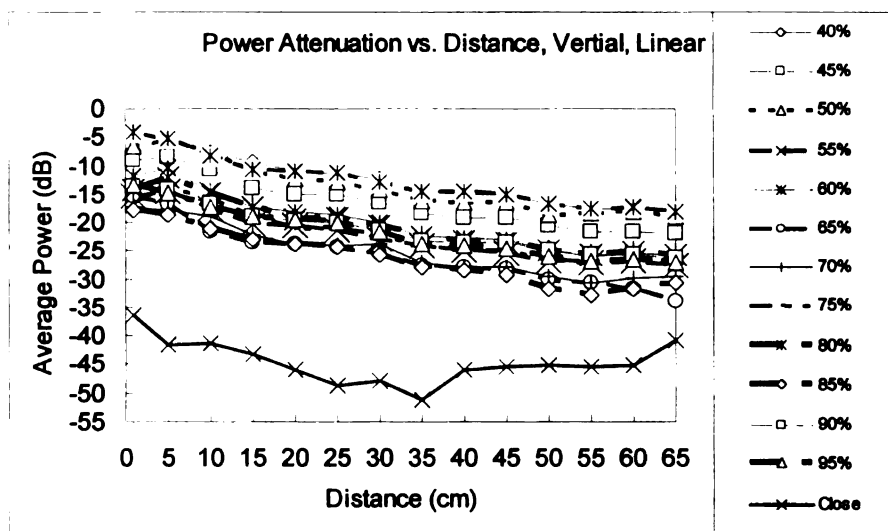


Figure 6.60 Comparison of power attenuation with saturated SAP samples

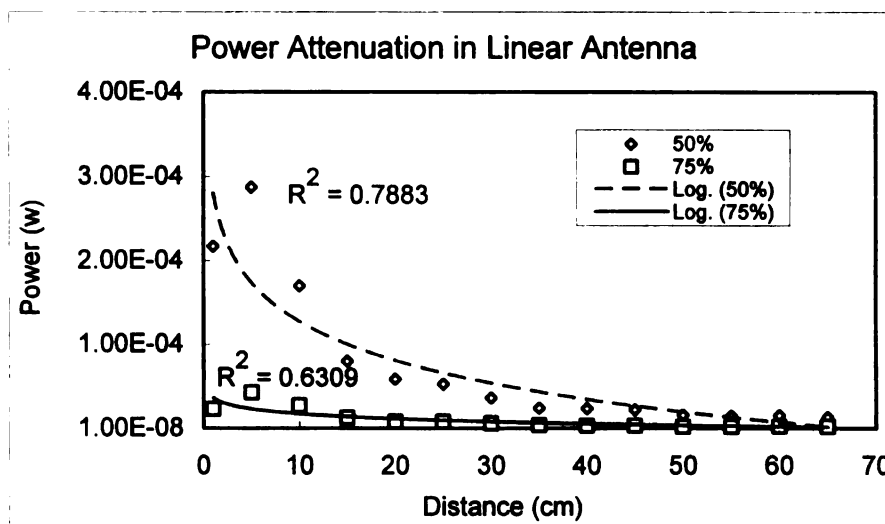


Figure 6.61 Comparison of power attenuation with 50% and 75% water content

Figure 6.61 showed in a linear antenna, receiving power was less in a 50% sample in comparing with in higher water content sample (75%).

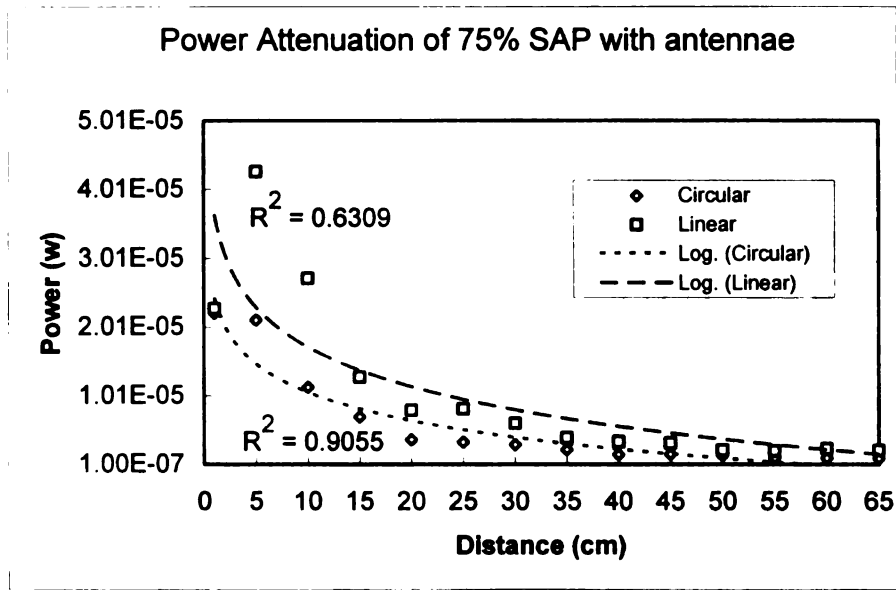


Figure 6.62 Comparison of received power with circular and linear antenna

6.7 Critical Power

Table 6.4 showed the relationship of half decaying rate (HDR) of readability and least power according to the power measurement and readability survey in free space. If the power less than -23.32 dB, the transponders supposedly do not respond to the reader or the reader can not pick up the backscatter signal at all. However, in the power measurement, even if the power was more than -23.32dB, the readability was 0 percent with a high water content SAP sample.

Half decaying rate	100%	50%	25%	12%	6%	3%	0%
Least power (dB)	-8.15	-14.39	-18.34	-18.56	-21.10	-22.23	-23.32

Table 6.3 Half decaying rate of readability and least power in free space

6.8 Readability Survey

When performing the readability survey, the more RFID tags were tested; the average readability data would trend to the reality due to the tag response to critical signal strength may vary, as each of read is crucial to statistically analyze the effect of water content. The following graphs present the readability model in the test. Alien ALL-9238 Squiggle Class1 64 Read/Write UHF tags were used in the test.

6.8.1 Readability Decaying Model in Open-air

Figure 6.63 showed a tag readability decaying model in open-air with four tag and reader combinations:

1. Linear reader antenna with horizontal tag
2. Linear reader antenna with vertical tag
3. Circular reader antenna with vertical tag
4. Circular reader antenna with horizontal tag

The graph really indicates that different reader and tag combination gives different tag readability even if the other conditions are the same. Obvious, Well packaging operation and configuration will create higher readability and system performance. In the combinations, the readability decreased quicker while the tag orientation changed from vertical to horizontal. For circular antenna, the orientation effect is small, however, it still decrease tag readability while the tag orientation has been changed..

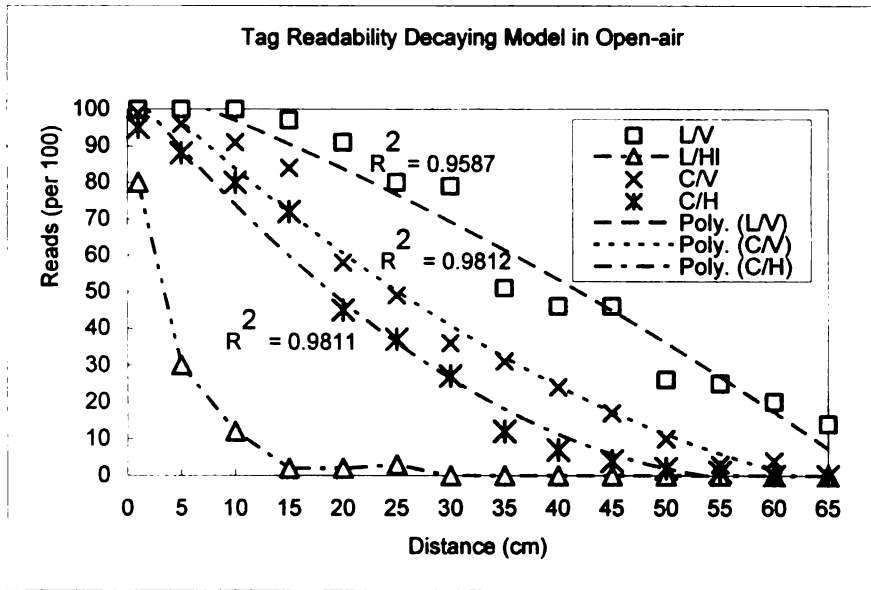


Figure 6.63 Readability decaying in free space

6.8.2 Tag Orientation

Figure 6.64 showed readability decaying model in different tag orientation with 50% water in SAP sample and a linear antenna. Linear antenna had strong polarization, changing antenna polarization caused a 10 time readability declines.

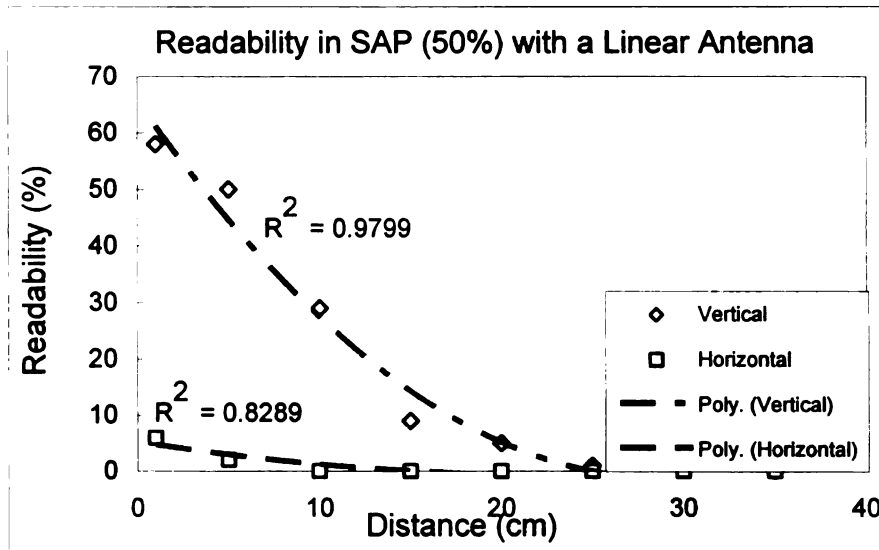


Figure 6.64 Comparison of readability: tag orientation

6.8.3 Water Content

Figure 6.65 to Figure 6.71 showed the major influence of water content on readability, as water content increase, the readability decline fast.

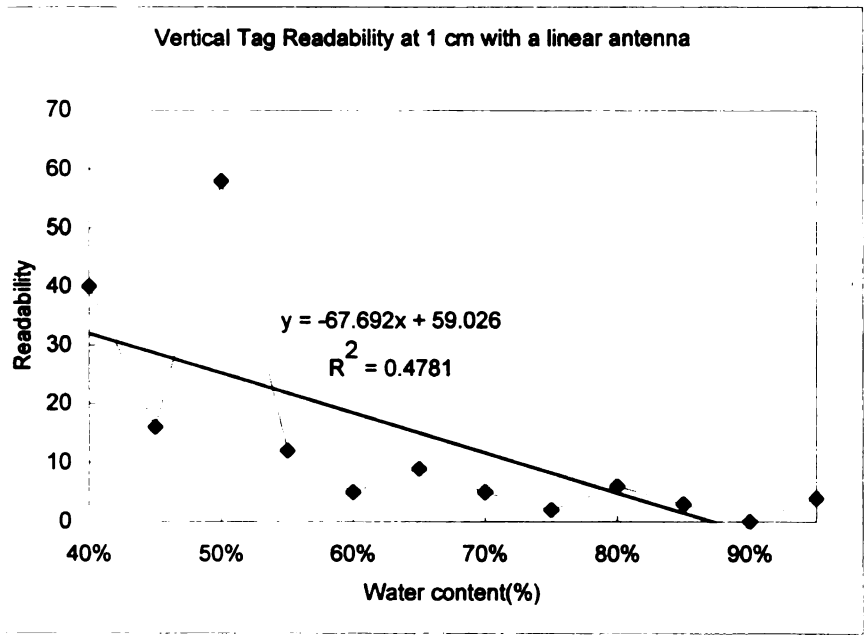


Figure 6.65 Readability fading

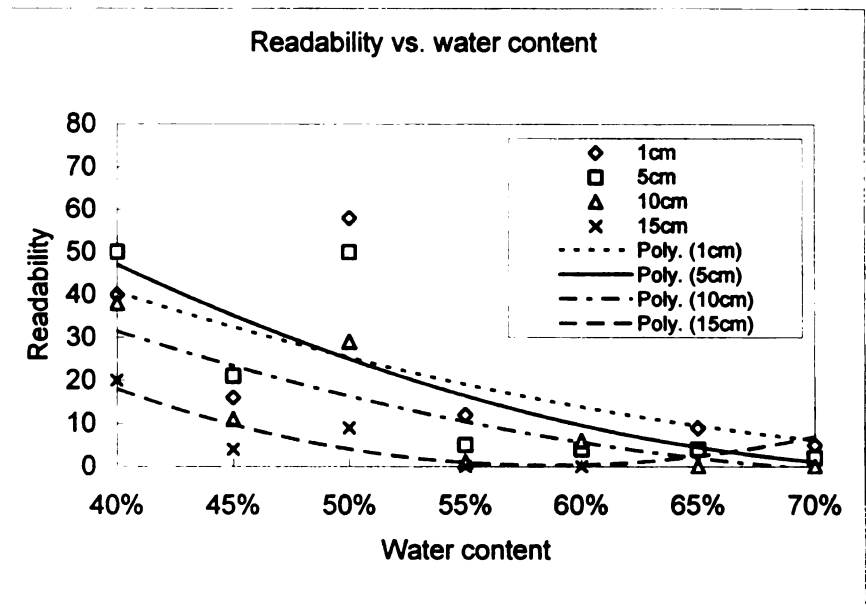


Figure 6.66 Comparison of readability (I)

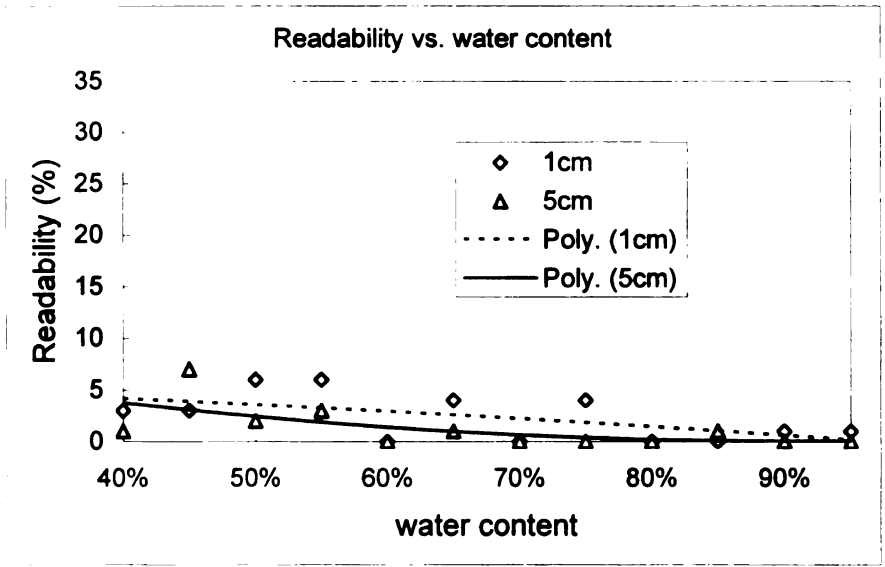


Figure 6.67 Comparison of readability(II)

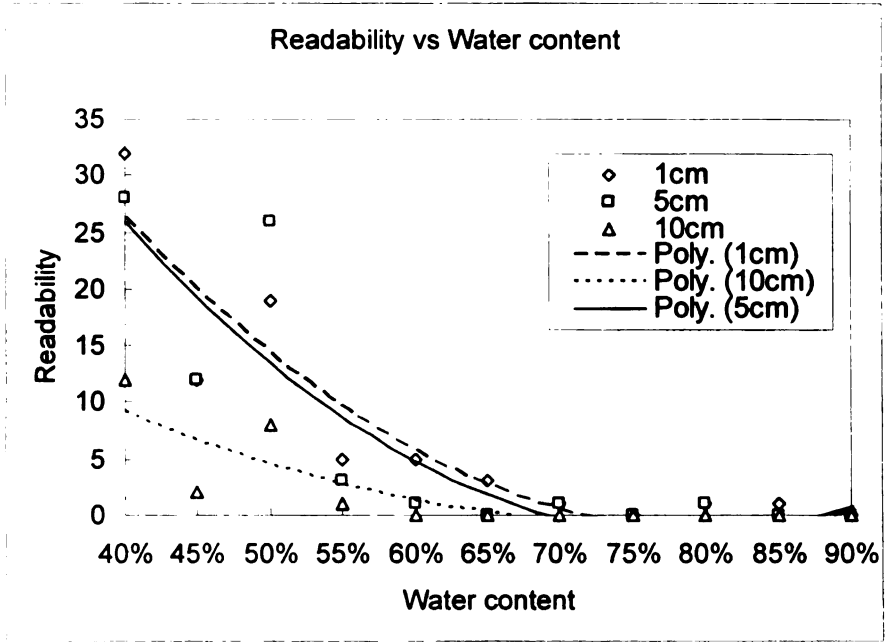
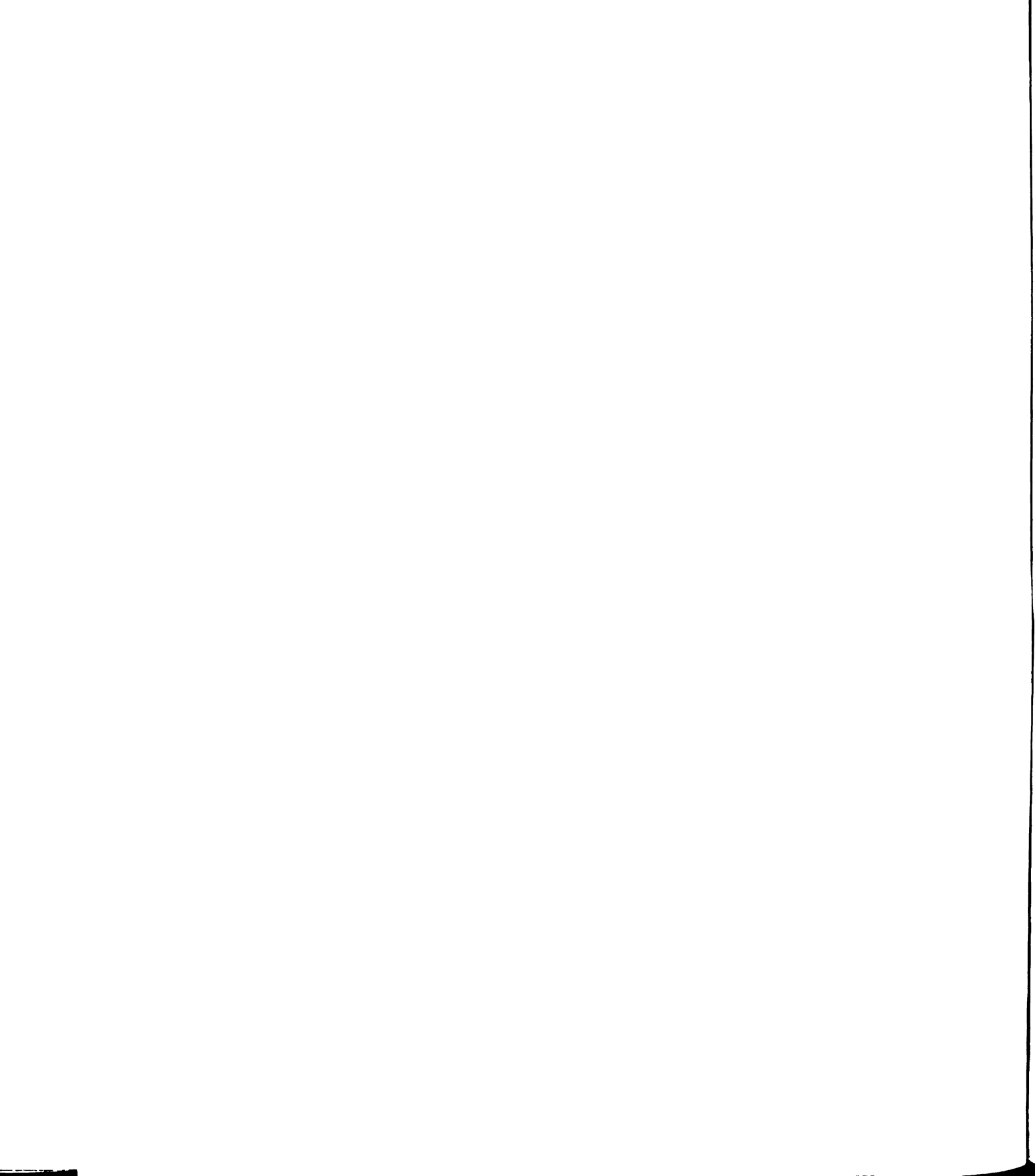


Figure 6.68 Comparison of readability(III)



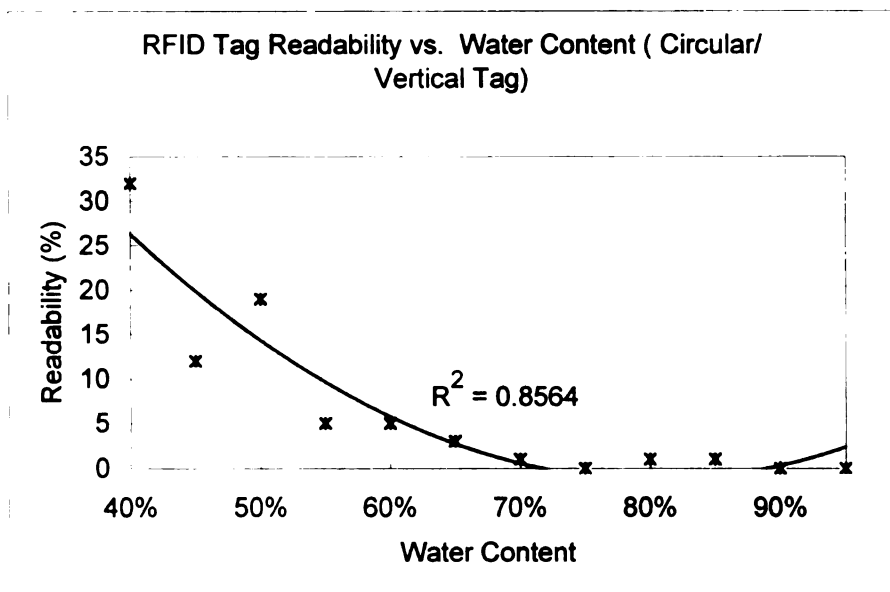


Figure 6.69 Comparison of readability(IV)

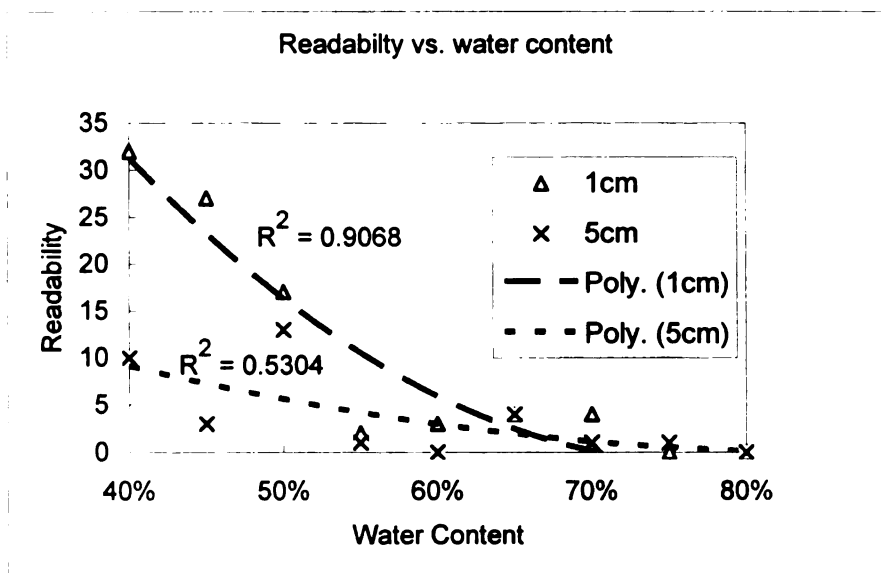


Figure 6.70 Comparison of readability(V)

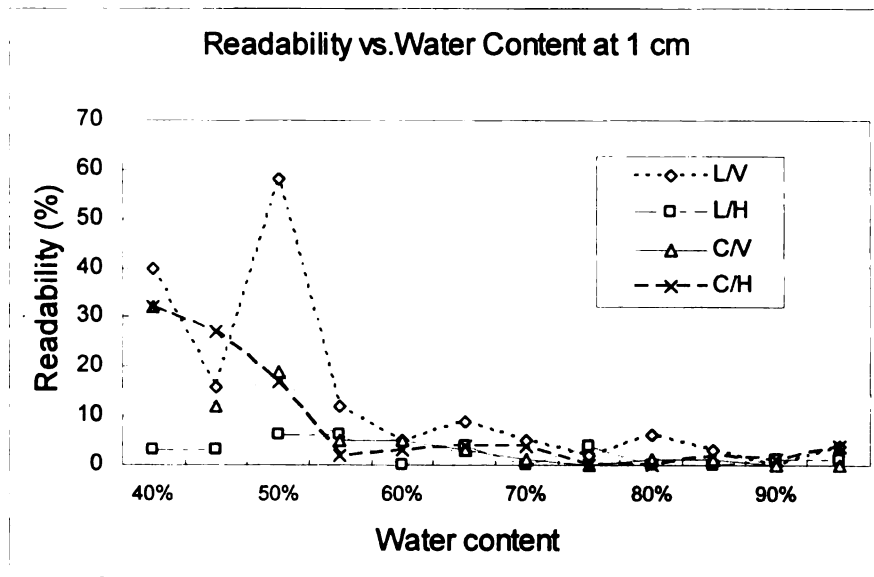


Figure 6.71 Comparison of readability(VI)

Chapter 7

CONCLUSIONS

This thesis provided a material characterization methodology using waveguide and network analyzer for determination of the water contribution in dielectric properties by measuring S-parameters of a serial of saturated superabsorbent polymer with different water content to simulate wide range of real products in supply chain. Further, this thesis described tag readability survey and power measurement methodology using power sensor and a 2-wired folded dipole antenna as receiving antenna to determine the effective receiving power level of RF signal radiated through the SAP specimen from RFID reader. A series of tests and measurements were developed with saturated superabsorbent polymer in the laboratories.

7.1 Material Characterization

The permittivity of hydrated SAP mixtures were extracted by using an iterative complex two dimensional Newton's root-searching algorithm with the experimental S-parameters obtained from a vector network analyzer.

Further statistical and correlation analysis revealed when the water content increased in the hydrated superabsorbent polymer sample, the S-parameters had a slight augment over the frequency range from 2.2GHz to 3.0 GHz. As a result of the extraction, the dielectric properties in term of dielectric constant and loss factor of the hydrated SAP specimens had a distinct influence from water content. The relative permittivity has been raised with

an increasing of water content in saturated superabsorbent polymer. it showed a nearly linear relationship between water content and relative permittivity.

7.2 Received Radiated Power

Power measurement shows major influence from the water content, the higher water content in the sample, the higher power loss measured with the same polarization of receiving antenna at the same location. Nonetheless, the power decay presented logarithm regression with the distance. In comparing with path loss in free space, there were larger fluctuation of power loss in higher water content sample. The power measurement presented that the power level received through high water content sample was far less than the power level received through free space, furthermore, it was less than minimum critical power for RFID tag in the research. Obvious, no tag responding to reader was expected in this situation.

7.3 Readability

Readability study was compared with influence on water content, distance, tag orientation and antenna style. It strongly showed that the tag readability depended on tag orientation, antenna polarization and distance from the RF sources. Orientation or polarization attenuated at least 15 dB power or average 19 dB in linear antenna. The 20dB attenuation with polarization observed agree well with the literature. However, circular antenna attenuated about 1.41dB or about 30% signal loss which reduced the readability with an acceptable level. The tag readability in the different samples also shows this tendency which agreed well with the experimental results. The study also showed that the power level is a necessary condition but not a sufficient condition. With

the same power level, the readability was various. Obvious, other factors may get involved with readability, such as the sensitivity of tags etc.

This scenario showed though there were pretty much undetermined influences from RFID implementation, determination of influences of water content in products and polarization in tag and reader antennas were high priority for successful RFID implementation. Potential influence of product content itself on RFID system performance and stability is not a neglectable factor with RFID application in supply chain. Recognizing the influences of your products and configurations on RFID system is the key to the proper implementation of the RFID system and elimination of negative effects to RFID readability, which meets the bottom line of feasibility RFID solution. It was hypothesized that improving packaging operations in supply chain may enhance the stability and performance of deployed RFID system. However, the influence of product content on tag readability such as, water, salinity, temperature which may cause a low readability is unable to be dispelled completely. Therefore, the system performance and stability will hard to reach the imposed implementation guideline.

7.4 Limitations of This Research

There are several factors that could be limitation for this research. The necessity for further validation and independent analysis of the measurements in this research was emphasized. In material characterization, measurement frequencies, 2.2 GHz to 3.0 GHz were involved, however, the prevalence frequency range of RFID systems in supply chain is 860MHz to 960MHz. Though the tendency of dielectric properties in UHF and VHF are pretty similar, the specific characteristics of the saturated SAP samples at 860MHz to 960MHz in this research was not determined. Power measurement was

conducted in an open area test site (OATS) to simulate a typical supply chain environment. Consequently, the test laboratory is not an anechoic chamber and may get involved with outside interference which may reduce data confidence of power measurement. Furthermore, the hundreds of tested RFID tags showed variety sensitivity to reader and different read ranges though all the tags were passed the single mode readability test. The distinction issue of tag performance was mentioned in literature as well [10], which should be removed in future study if possible.

7.5 Future Research

A number of factors influence the performance and stability of RFID in different application environments. Future work includes material characterization in 860MHz-960MHz to match the 915MHz RFID technology in supply chain. In the range of 0.75GHz to 1.12 GHz, WR975 waveguide can be used for material characterization [57]. However, due to the larger cross-section size in WR975 waveguide (9.75inch *4.875 inch) in comparison with WR340 waveguide, the sample preparation procedure will be a larger challenge for homogeneity and density stability. Therefore, wide bandwidth measurements of the materials using the coaxial probe are recommended for UHF high permittivity materials. Consequently, material characterization of dry SAP powder or particles will be a perfect supplement to describe the undulation of dielectric properties. Simultaneously, the measurement of conductivity (σ) in the material is another interesting area to understand the influence of product content on RFID performance and stability.

According to the results from this research, people may have anxiety whether their products can be "RFID signal compliance", which will give their "peace of mind" or "nightmare" in implementation of the RFID systems. Obviously, the special investigation should be conducted before a reliable RFID solution was deployed in supply chain. Therefore, a research of consummating the "RFID signal compliance" test and procedure for industry will be a perfect project.

Back to this research, in power measurement, determination of receiving antenna specifications will provide more accuracy and reliable correlation to tag response behaviors. Improving sample preparation procedures will provide more converge result. Some error analysis in measurement may also be useful. Tolerances checking on sample thickness, density should be helpful. these aspects are feasible future investigations. Furthermore, dual power sensor measurement will provide simultaneous effect of tag orientation or antenna polarization and reduce the errors due to DUT mobility during the measurement. Again, a better size matched dipole antenna to RFID tags for power sensor will provide vicinal tag status in pallet load test. Certainly, Improving the automatic data acquisition procedures will reduce the human interference in the measurement. These issues and improvements should be nice for future research in RFID.

7.6 Summary Conclusion

This research was of distinct significance as it was the first study concerned on differentiation of influence of water content in products on RFID performance and stability through simulation tests and measurements of saturated SAP mixtures undertaken so far. The methodology provided theoretical accuracy and practical maneuverability through affiliation of material characterization, power attenuation and

readability in the same sample of the saturated material. The results of the research will help us acknowledge the influence of product content and packaging operations on successful implementation of RFID in supply chain. Meanwhile, the methodology in the research will easily be adopted by the RFID project initiative in industry. However, it should be realized that the results of the tests must be reviewed when the set up and test conditions have been altered. Even in the same condition, the difference of homogeneity of the saturated material may lead to a different result due to deviation of the structure, density, salinity in the two phase mixtures. To determine the influence of your special products on RFID implementation, a consistent procedure carried out under the special environment will be appropriate.

Appendix A
S-Parameters in Saturated SAP (90%)

Notes: Respectively, S11, S21, S12, S22. Total points: 201 for one S-parameter.

```
CITIFILE A.01.01
#NA VERSION HP8510C.07.10
NAME MEMORY
#NA REGISTER 1
VAR FREQ MAG 201
DATA S RI
COMMENT YEAR MONTH DAY HOUR MINUTE SECONDS
CONSTANT TIME 2005 05 25 13 56 45.0
BEGIN
-9.27337E-1,0.68634E-1
-9.25018E-1,0.68847E-1
-9.23584E-1,0.68664E-1
-9.21875E-1,0.68450E-1
-9.21600E-1,0.69274E-1
-9.18823E-1,0.68267E-1
...
-7.76092E-1,-0.29541E-1
-7.76153E-1,-0.30456E-1
-7.77221E-1,-0.30883E-1
END
CITIFILE A.01.01
#NA VERSION HP8510C.07.10
NAME MEMORY
#NA REGISTER 2
VAR FREQ MAG 201
DATA S RI
COMMENT YEAR MONTH DAY HOUR MINUTE SECONDS
```

CONSTANT TIME 2005 05 25 13 46 21.0

BEGIN

-7.19642E-2,-7.20443E-2

-7.43408E-2,-7.24372E-2

-7.67822E-2,-7.27310E-2

-1.78955E-1,0.50468E-1

-1.78482E-1,0.52635E-1

-1.78321E-1,0.54206E-1

...

-0.88989E-1,1.58561E-1

-0.87554E-1,1.59149E-1

-0.86158E-1,1.59393E-1

-0.84953E-1,1.60018E-1

END

CITIFILE A.01.01

#NA VERSION HP8510C.07.10

NAME MEMORY

#NA REGISTER 3

VAR FREQ MAG 201

DATA S RI

COMMENT YEAR MONTH DAY HOUR MINUTE SECONDS

CONSTANT TIME 2005 05 25 12 13 47.0

BEGIN

-7.19833E-2,-7.18383E-2

-7.48100E-2,-7.21626E-2

-7.68966E-2,-7.24716E-2

-7.92465E-2,-7.24487E-2

...

-0.87753E-1,1.59141E-1

-0.86448E-1,1.59812E-1

-0.85166E-1,1.60270E-1

END

CITIFILE A.01.01

#NA VERSION HP8510C.07.10

NAME MEMORY

#NA REGISTER 4

VAR FREQ MAG 201

DATA S RI

COMMENT YEAR MONTH DAY HOUR MINUTE SECONDS

CONSTANT TIME 2005 05 25 13 34 30.0

BEGIN

-7.66296E-1,5.41503E-1

-7.60986E-1,5.48919E-1

-7.52807E-1,5.53070E-1

-7.39837E-1,5.59143E-1

...

0.33172E-1,7.83386E-1

0.36315E-1,7.84545E-1

0.38848E-1,7.86224E-1

0.40435E-1,7.85858E-1

0.43823E-1,7.84484E-1

Appendix B

Experimental Permittivity and Permeability

FREQ(GHz), Re{EPR-F}, Im{EPR-F}, Re{MUR-F}, Im{MUR-F}, Re{EPR-R}, Im{EPR-R}, Re{MUR-R}, Im{MUR-R}

0.2200E+01, 0.2286E+02, -1.767E+02, 0.9621E+00, -4.695E-02, 0.2140E+02, -1.821E+02, 0.1029E+01, -2.946E-01

0.2204E+01, 0.2275E+02, -1.758E+02, 0.9619E+00, -1.276E-01, 0.2182E+02, -1.786E+02, 0.1005E+01, -3.703E-01

0.2208E+01, 0.2273E+02, -1.746E+02, 0.9551E+00, -7.811E-02, 0.2200E+02, -1.790E+02, 0.9943E+00, -2.231E-01

0.2212E+01, 0.2277E+02, -1.736E+02, 0.9587E+00, -1.544E-01, 0.2191E+02, -1.844E+02, 0.1020E+01, -7.521E-03

0.2216E+01, 0.2276E+02, -1.720E+02, 0.9582E+00, -1.764E-01, 0.2164E+02, -1.872E+02, 0.1045E+01, 0.8139E-02

0.2220E+01, 0.2275E+02, -1.701E+02, 0.9584E+00, -2.090E-01, 0.2152E+02, -1.919E+02, 0.1062E+01, 0.1152E-01

0.2224E+01, 0.2290E+02, -1.708E+02, 0.9574E+00, -1.260E-01, 0.2182E+02, -1.943E+02, 0.1061E+01, 0.3471E-01

0.2228E+01, 0.2288E+02, -1.695E+02, 0.9580E+00, -1.460E-01, 0.2169E+02, -1.951E+02, 0.1069E+01, 0.3449E-01

0.2232E+01, 0.2291E+02, -1.706E+02, 0.9586E+00, -8.268E-02, 0.2151E+02, -1.944E+02, 0.1071E+01, 0.3024E-01

...

0.2956E+01, 0.2165E+02, -1.350E+02, 0.9159E+00, -6.343E-01, 0.2103E+02, -1.680E+02, 0.9626E+00, 0.3999E-01

0.2960E+01, 0.2165E+02, -1.339E+02, 0.9158E+00, -6.652E-01, 0.2112E+02, -1.690E+02, 0.9606E+00, 0.4482E-01

0.2964E+01, 0.2177E+02, -1.344E+02, 0.9119E+00, -6.212E-01, 0.2108E+02, -1.692E+02, 0.9615E+00, 0.4510E-01

0.2968E+01, 0.2173E+02, -1.345E+02, 0.9148E+00, -6.334E-01, 0.2090E+02, -1.711E+02, 0.9678E+00, 0.5137E-01

0.2972E+01, 0.2164E+02, -1.354E+02, 0.9203E+00, -6.021E-01, 0.2090E+02, -1.713E+02, 0.9680E+00, 0.5263E-01

0.2976E+01, 0.2166E+02, -1.356E+02, 0.9195E+00, -6.088E-01, 0.2079E+02, -1.692E+02, 0.9702E+00, 0.4501E-01

0.2980E+01, 0.2092E+02, -1.413E+02, 0.9501E+00, -5.439E-01, 0.2007E+02, -1.662E+02, 0.1009E+01, 0.3753E-01

0.2984E+01, 0.2171E+02, -1.332E+02, 0.9137E+00, -6.476E-01, 0.2103E+02, -1.705E+02, 0.9656E+00, 0.5034E-01

0.2988E+01, 0.2159E+02, -1.335E+02, 0.9197E+00, -6.740E-01, 0.2098E+02, -1.717E+02, 0.9655E+00, 0.5521E-01

0.2992E+01, 0.2155E+02, -1.335E+02, 0.9201E+00, -6.713E-01, 0.2100E+02, -1.720E+02, 0.9631E+00, 0.5641E-01

0.2996E+01, 0.2155E+02, -1.326E+02, 0.9197E+00, -6.945E-01, 0.2107E+02, -1.708E+02, 0.9609E+00, 0.5305E-01

0.3000E+01, 0.2156E+02, -1.324E+02, 0.9194E+00, -6.928E-01, 0.2087E+02, -1.711E+02, 0.9670E+00, 0.5528E-01

Appendix C

Glossary

Cutoff frequency For a given transmission mode in a nondissipative waveguide, the frequency at which the propagation constant is zero.

Dissipation The power reduction in a transmission path caused by resistive or conductive loss, or both.

Gain The power increase in a transmission path in the mode or form under consideration. It is usually expressed as a positive ratio, in decibels.

Incident wave At a transverse plane in a transmission line or waveguide, a wave traveling in a reference direction.

Loss The power reduction in a transmission path in the mode or modes under consideration. It is usually expressed as positive ratio, in decibels.

Port (for a waveguide component) A means of access characterized by a specified reference plane and a specified propagating mode in a waveguide which permits power to be coupled into or out of a waveguide component.

Reflected wave At a transverse plane in a transmission line or waveguide, a wave returned from a reflecting discontinuity in a direction opposite to the incident wave.

(Compare incident wave)

Reflection coefficient At a given frequency, at a given point, and for a given mode of propagation, the ratio of some quantity associated with the reflected wave to the corresponding quantity in the incident wave.

Reflection loss (gain) The ratio of incident to transmitted power at a reference plane of a network.

Return loss (gain) The ratio of incident to reflected power at a reference plane of a network.

Skin depth Of a conducting material, at a given frequency, the depth at which the surface current density is reduced by one neper.

TE mode (H mode) A waveguide mode in which the longitudinal component of the electric field is everywhere zero and the longitudinal component of the magnetic field is not.

TEM mode A waveguide mode in which the longitudinal component of the magnetic fields is everywhere zero.

TM mode (E mode) A waveguide mode in which the longitudinal component of the magnetic field is everywhere zero and the longitudinal component of the electric field is not.

Waveguide A system of material boundaries or structure for guiding electromagnetic waves. Usually such a system is used for guiding waves in other than TEM modes. Often, and originally, a hollow metal pipe for guiding electromagnetic waves.

References

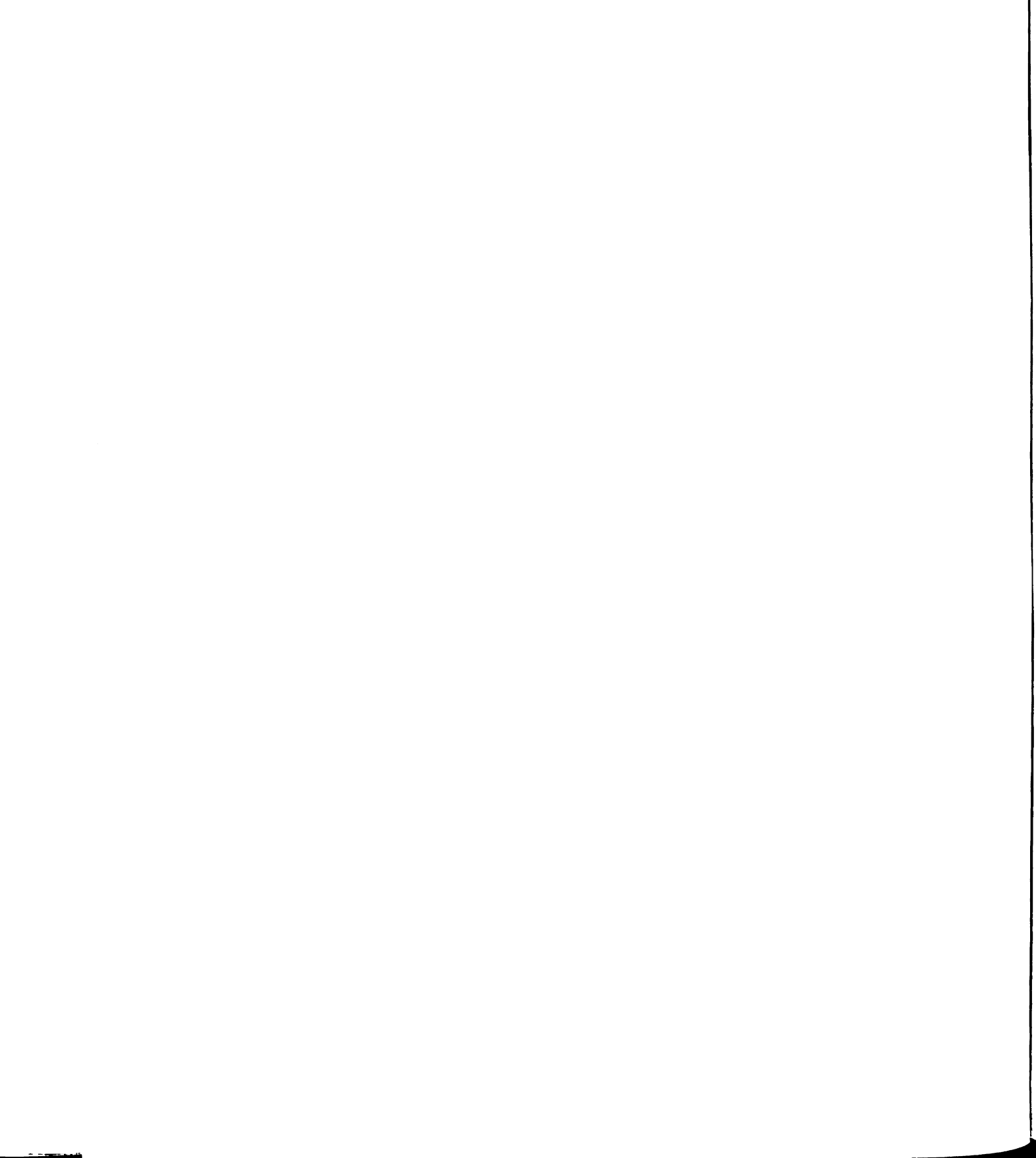
- [1] P. Harrop, *RFID in packaging*. Leatherhead, Surrey, UK: Pira International, 2002.
- [2] R. Clarke, "Radio Frequency Identification: Smart or Intelligent Packaging?," *The Journal of Packaging Science and Technology, Japan*, vol. 10, pp. 233-247, 2001.
- [3] M. Muller, *Essentials of inventory management*. New York: AMACOM, 2003.
- [4] R. Lutter, "Speech in RFID World Conference 2006," presented at RFID World Conference, Dallas, Texas, 2006.
- [5] Philips Semiconductors, Tagsys Inc., and Texas Instruments Inc., "Item-level Visibility in the Pharmaceutical Supply Chain: A Comparison of HF and UHF RFID Technologies," 2004.
- [6] R. Clarke, *Radio Frequency Identification: Will it Work in Your Supply Chain?*, vol. Book 2. Boca Raton, FL: CRC Press, 2002.
- [7] R. Clarke, Tazelaar, Twede, and Boyer, "RFID in the Supply Chain: Separating Fact From Fiction," *Harvard Business Review Supply Chain Strategy*, vol. 2, pp. 9-10, 2006.
- [8] S. Shepard, *RFID : radio frequency identification*. New York: McGraw-Hill, 2005.
- [9] S. Garfinkel and B. Rosenberg, *RFID : applications, security, and privacy*. Upper Saddle River, NJ: Addison-Wesley, 2006.
- [10] J. R. Tazelaar, "The effect of tag orientation and package content on the readability of radio frequency identification (RFID) transponders," Michigan State University. School of Packaging, 2004., 2004, pp. xvi, 166 leaves.
- [11] J. C. Onderko, "Radio frequency identification transponder performance on refrigerated and frozen beef loin muscle packages," Michigan State University. School of Packaging, 2004., 2004, pp. viii, 44 leaves.
- [12] M. R. Ryan, "A model for the implementation of a radio frequency identification system into a warehouse environment," Michigan State University. Dept. of Packaging, 2002., 2002, pp. vi, 117 leaves.

- [13] M. D. Jonson, "Determination of class 0 radio frequency identification tag failure modes," Michigan State University. School of Packaging, 2005., 2005, pp. xii, 87 leaves.
- [14] R. Clarke and Tanprasert, "Packaging and International RFID Operations," presented at The Society of Packaging Science & Technology, Japan, 2005.
- [15] S. Rao, P. Nikitin, and S. Lam, "Antenna Design for UHF RFID Tags: a Review and a Practical Application," *IEEE Transactions on Antennas and Propagation*, vol. 53, pp. 3870-3876, 2005.
- [16] H. Stockman, "Communication by Means of Reflected Power," in *Proceeding of the IRE*, 1948, pp. pp1196-1204.
- [17] K. Finkensteller, *RFID handbook: fundamentals and applications in contactless smart cards and identification*, 2nd ed. Chichester, England ; Hoboken, N.J.: Wiley, 2003.
- [18] R. Clarke, Tazelaar, Twede, and Boyer, "Radio Frequency Identification (RFID) Performance: The Effect of Tag Orientation and Package Contents," *Packaging Technology and Science*, vol. 19, pp. 45-54, 2005.
- [19] S. A. Weis, "Security and privacy in radio-frequency identification devices," in *Dept. of Electrical Engineering and Computer Science*, vol. MS: Massachusetts Institute of Technology, 2003, pp. 79 p.
- [20] Matrics Inc., "Stationary Reader User's Manual," <http://www.matrics.com>, 2002.
- [21] Y. Lee, "RFID Coil Design," vol. AN678: Microchip Technology Inc., 1998.
- [22] J. D. Kraus, *Electromagnetics*, 3rd ed. New York: McGraw-Hill, 1984.
- [23] L. Lewin, *Theory of waveguides; techniques for the solution of waveguide problems*. New York,: Wiley, 1975.
- [24] P. Nikitin, S. Rao, S. Lam, V. Pillai, R. Martinez, and H. Heinrich, "Power Reflection Coefficient Analysis for Complex Impedances in RFID Tag Design," *IEEE Transactions on Microwave Theory and Techniques*, vol. 53, pp. 2721-2725, 2005.

- [25] Matrics Inc, "Passive RFID- A primer for New RF regulations," <http://www.matrics.com>, 2004.
- [26] FCC, "Radio Frequency Identification: Short Range Device regulation," *CFR15*, vol. 47, 2004.
- [27] S. Tedjini, "Antennas for RFID Tags," presented at Joint sOc-EUSAI conference, Greboble, 2005.
- [28] E. C. Ifeachor and B. W. Jervis, *Digital signal processing : a practical approach*, 2nd ed. Harlow, England ; New York: Prentice Hall, 2002.
- [29] H. Frèohlich, *Theory of dielectrics; dielectric constant and dielectric loss*, 2d ed. Oxford,: Clarendon Press, 1958.
- [30] A. R. Von Hippel, *Dielectric materials and applications; papers by twenty-two contributors*. Cambridge, New York: Published jointly by the Technology Press of M.I.T. and Wiley, 1954.
- [31] V. V. Daniel, *Dielectric relaxation*. London, New York,: Academic Press, 1967.
- [32] N. Tran, "Microwave Technology," <http://microwaveprocessing.com/water.html>.
- [33] T. M. Hardman, *Water and food quality*. London ; New York: Elsevier Applied Science, 1989.
- [34] R. R. Ruan and P. L. Chen, *Water in foods and biological materials : a nuclear magnetic resonance approach*. Lancaster, Pa.: Technomic Pub. Co., 1998.
- [35] J. McClements, "Analysis of Food Products," <http://www-unix.oit.umass.edu/~mcclemen/581Toppage.html>, 2003.
- [36] Y. Pomeranz and C. E. Meloan, *Food analysis : theory and practice*, 3rd ed. New York: Chapman & Hall, 1994.
- [37] H. Levine and Churchill College., *Amorphous food and pharmaceutical systems*. Cambridge, UK: Royal Society of Chemistry, 2002.
- [38] S. Sacharow and R. F. Schiffmann, *Microwave packaging*. Leatherhead, [Eng.]: Pira International, 1992.

- [39] E. Pytlik, "Superabsorbent Polymers," <http://www.eng.buffalo.edu/Courses/ce435/Diapers/Diapers.html>.
- [40] F. Buchholtz and N. Peppas, *Superabsorbent polymers : science and technology*. Washington, DC: American Chemical Society, 1994.
- [41] M. Elliott, "Superabsorbent Polymers," <http://www.basf.com>, 2004.
- [42] K. Vorst, A. Booren, and R. Clarke, "Evaluation of Radio Frequency Transponders Effects on Quality and Consumer Acceptance of Perishable Food Products," presented at International Association of Packaging Research Institutes/Worldpak 2002, East Lansing, MI, 2002.
- [43] A. Booren, K. Vorst, R. Clarke, and Allison, "Radio Frequency Transponder Effects on Bloom of Beef Muscle," *Meat Science, The Official Journal of the American Meat Science Association*, 2003.
- [44] K. Ramakrishnan, "Performance Benchmarks for Passive UHF RFID Tags," in *Department of Electrical Engineering and Computer Science*, vol. Master Kansas City: University of Kansas, 2005, pp. 100.
- [45] A. R. Ramchandran, "Plant scanner a handheld PDA using RFID tags for child visitors to the Michigan 4-H Children's Garden," Michigan State University. Dept. of Telecommunication, Information Studies and Media, 2004., 2004, pp. vi, 50 leaves.
- [46] B. Hardgrave, M. Waller, and R. Miller, "Does RFID Reduce Out of Stocks? A preliminary Analysis," University of Arkansas 11/1/2005.
- [47] M. D. Janezic, "Nondestructive relative permittivity and loss tangent measurements using a split-cylinder resonator," 2003, pp. xviii, 130 leaves.
- [48] A. E. Bogle, "Electromagnetic material characterization using a partially filled rectangular waveguide," Michigan State University. Dept. of Electrical and Computer Engineering, 2004., 2004, pp. viii, 106 leaves.
- [49] J. J. Meeusen, "Error analysis of material characterization using a wave guide applicator," Michigan State University. Dept. of Electrical and Computer Engineering, 2004., 2004, pp. xi, 165 leaves.

- [50] D. S. Killips, "Classical mixing approaches to determine effective permittivity and permeability of a two-phase mixture," Michigan State University. Dept. of Electrical and Computer Engineering, 2004., 2004, pp. x, 76 leaves.
- [51] T. P. Hoepfner, "The influence of the microstructure of sintered hydroxyapatite on the properties of hardness, fracture toughness, thermal expansion and the dielectric permittivity," Michigan State University. Dept. of Materials Science and Mechanics, 2001., 2001, pp. xv, 161 leaves.
- [52] A. M. Nicholson and G. Ross, "Measurement of the intrinsic properties of material by time domain techniques," *IEEE Trans. Instrum. Meas.*, vol. IM-19, pp. 377-382, 1970.
- [53] W. B. Weir, "Automatic measurement of complex dielectric constant and permeability at microwave frequencies," *Proc. IEEE*, vol. 62, pp. 33-36, 1974.
- [54] J. Baker-Jarvis, "Transmission / Reflection and short-circuitline permittivity measurements," *NIST Technical Notes 1341*, 1990.
- [55] Grain Processing Corporation, "Material Safety Data Sheet for Water Lock superabsorbent polymer A-100," Iowa 2001.
- [56] Agilent Technologies, "8510C Network Analyzer System Operation Manual," <http://www.agilent.com>, 1994.
- [57] N. Marcuvitz, *Waveguide handbook*, 1st ed. New York,: McGraw-Hill, 1951.
- [58] Agilent Technologies, "Applying Error Correction to Network Analyzer Measurements," <http://www.agilent.com>, 2001.
- [59] T. W. J. Capwell, D. Markell, L. Dunleavy, "Automation and Real-time Verification of Passive Component S-parameter Measurements Using Loss Factor Calculations," *Microwave Journal*, 2004.
- [60] Agilent Technologies, "Fundamentals of RF and Microwave Power Measurements," <http://www.agilent.com>, 2003.
- [61] Rohde&Schwarz, *Manual: Average Power Sensor R&S NRP-Z22*, 2004.
- [62] R. H. Bishop, *Learning with LabVIEW*. Menlo Park, Calif. ; Harlow, England: Addison-Wesley, 1999.



- [63] D. Anderson, "S-Parameter Techniques for faster, more accurate network design," in *Hewlett-Packard Journal*, 1997.

MICHIGAN STATE UNIVERSITY LIBRARIES



3 1293 03062 6794